

CORRELATION OF DEFORMATION DEMANDS
WITH GROUND MOTION INTENSITY

A THESIS SUBMITTED TO
THE GRADUATE SCHOOL OF NATURAL AND APPLIED SCIENCES
OF
MIDDLE EAST TECHNICAL UNIVERSITY

BY

HAZIM YILMAZ

IN PARTIAL FULFILLMENT OF THE REQUIREMENTS
FOR
THE DEGREE OF MASTER OF SCIENCE
IN
CIVIL ENGINEERING

AUGUST 2007

Approval of the Thesis

**CORRELATION OF DEFORMATION DEMANDS
WITH GROUND MOTION INTENSITY**

Submitted by **HAZIM YILMAZ** in partial fulfillment of the requirements for the degree of **Master of Science in Civil Engineering** by,

Prof. Dr. Canan Özgen
Dean, Graduate School of **Natural and Applied Sciences** _____

Prof. Dr. Güney Özcebe
Head of Department, **Civil Engineering** _____

Assoc. Prof. Dr. Ahmet Yakut
Supervisor, **Civil Engineering Dept., METU** _____

Examining Committee Members:

Prof. Dr. Haluk Sucuoğlu (*)
Civil Engineering Dept., METU _____

Assoc. Prof. Dr. Ahmet Yakut (**)
Civil Engineering Dept., METU _____

Assoc. Prof. Dr. Sinan Akkar
Civil Engineering Dept., METU _____

Assist. Prof. Dr. Altuğ Erberik
Civil Engineering Dept., METU _____

Assist. Prof. Dr. Tolga Yılmaz
Engineering Sciences Dept., METU _____

Date: _____

(*) Head of Examining Committee

(**) Supervisor

I hereby declare that all information in this document has been obtained and presented in accordance with academic rules and ethical conduct. I also declare that, as required by these rules and conduct, I have fully cited and referenced all material and results that are not original to this work.

Name, Last name: Hazım Yılmaz

Signature:

ABSTRACT

CORRELATION OF DEFORMATION DEMANDS WITH GROUND MOTION INTENSITY

YILMAZ, Hazım

M.S., Department of Civil Engineering

Supervisor: Assoc. Prof. Dr. Ahmet YAKUT

August 2007, 128 pages

A comprehensive study has been carried out to investigate the correlation between deformation demands of frame structures and a number of widely cited ground motion intensity parameters. Nonlinear response history analyses of single-degree-of-freedom (SDOF) and multi-degree-of-freedom (MDOF) models derived from sixteen reinforced concrete frames were carried out under a set of eighty ground motion records. The frames were selected to portray features of typical low-to-mid rise reinforced concrete structures. The records contained in the ground motion database were compiled from the recorded ground motions with the intention to possess a broad range of amplitude, frequency content and duration characteristics that shift selected frames into various degrees of elastic as well as inelastic response. Maximum deformation demands of SDOF models and the maximum interstory drift ratios of MDOF models, response parameters of interest, were computed employing 1280 nonlinear response history analyses. Computed response parameters were compared with the ground motion intensity parameters employed and correlation between them were quantified through coefficients of correlation and determination.

The results revealed that the spectral intensity parameters including spectral amplitudes over a range of period covering the frame structures have the strongest correlation and present better relationship with the deformation demands compared to the intensity parameters that are based on a single amplitude such as PGA, PGV and spectral acceleration. Besides analytical study, association of ground motion parameters with observed damage has been investigated and no clear trend has been observed between the performance of the buildings and the seismic indices.

Keywords: Ground motion intensity, seismic damage, deformation demand, reinforced concrete

ÖZ

DEFORMASYON TALEPLERİ İLE YER HAREKETİ ŞİDDETİNİN KORELASYONU

YILMAZ, Hazım

Yüksek Lisans, İnşaat Mühendisliği Bölümü

Tez Yöneticisi: Doç. Dr. Ahmet YAKUT

Ağustos 2007, 128 pages

Çerçeve yapıların deformasyon talepleri ile yer hareketi şiddet paramaterleri arasındaki korelasyonun incelenmesi amacıyla kapsamlı bir çalışma yürütülmüştür. 16 betonarme çerçeveden elde edilen tek serbestlik dereceli ve çok serbestlik dereceli modellerin zaman ortamında doğrusal olmayan analizleri 80 yer hareketi kullanılarak yapılmıştır. Çerçeveler, az ve orta katlı betonarme binalarının tipik özelliklerini yansıtabilecek şekilde seçilmişlerdir. Yer hareketi veri tabanında bulunan kayıtlar, çerçeveleri elastik ve elastik olmayan davranışa çeşitli derecelerde itecek yeterlikte genlik, frekans içeriği ve süreye sahip olmaları maksadıyla seçilmiştir. Tek serbestlik dereceli sistemlerin maksimum deformasyon talepleri ve çok serbetlik dereceli sistemlerin maksimum kat arası ötelenme talepleri 1280 zaman ortamında doğrusal olmayan analiz sonucu elde edilmiştir. Hesaplanan tepki parametreleri, yer hareketi şiddet parametreleri ile karşılaştırılmış ve aralarındaki korelasyon regresyon katsayısı ve Pearson korelasyon katsayısı baz alınarak değerlendirilmiştir. Sonuçlar, çerçeve yapıların periyot aralıklarındaki spektral genliklerini kapsayan spektral şiddet parametrelerinin en güçlü korelasyona sahip olduğunu açığa çıkarmaktadır ve

bu parametreler tek genlike bađlı olan MYİ, MYH ve spektral ivmeye gre deformasyon talepleri ile daha iyi bir iliřki gstermektedir. Bunun yanında, yer hareketi parametreleri ile gzlemlene hasar arasında ki iliřki de incelenmiřtir ve bina performansları ile sismik endeksler arasında belirgin bir eđilim grlmemiřtir.

Anahtar Szckler: Yer hareketi řiddeti, sismik hasar, deformasyon talebi, betonarme

To Nurhayat, Cevdet, Atilla Yılmaz and Burcu Gürsaf

ACKNOWLEDGMENT

It is a pleasure to thank the many people who made this thesis possible. I am very grateful for my years at Civil Engineering Department, METU.

I would like to express my gratitude to my supervisor, Assoc. Prof. Dr. Ahmet Yakut, whose expertise, understanding, and patience, added considerably to my graduate experience. I appreciate his vast knowledge and skill in many areas.

I want to thank Bekir Özer Ay and his crew, Sami Demiroglu, Zerrin Ardic and Bilge Küçükdoğan (she knows what she stands for me) for their support and friendship throughout my study. I also want to thank Bülent Ortaçgil, Erkan Oğur and Aleksi Zorba for feeding my soul.

My grand ortis Gökhan Marım and Serkan Yılmaz have been a great source of my strenght through my years in Ankara and deserve special thanks. We know each other, you mean a lot to me.

This acknowledgment is for a 15 years friendship. My sensitive friend F.Onur Bağlan, thank you for being the man who undestands me the most.

There are too many words to say for you my dear Burcu. I owe you everything in return. As the song tells, I can not live with or without you.

Finally, I am forever indebted to my family Nurhayat, Cevdet and Atilla Yılmaz. I can not imagine a life without you. I love you...

TABLE OF CONTENTS

ABSTRACT	iv
ÖZ	vi
ACKNOWLEDGMENTS	ix
TABLE OF CONTENTS	x
LIST OF TABLES	xiii
LIST OF FIGURES	xv
CHAPTER	
1. INTRODUCTION	1
1.1 GENERAL	1
1.2 GROUND MOTION INTENSITY PARAMATERS	2
1.2.1 Response Spectrum Concept.....	3
1.2.2 Ground Motion Intensity Parameters Used in This Study	3
1.2.3 Engineering Demand Measure	7
1.3 LITERATURE SURVEY	8
1.4 OBJECTIVE AND SCOPE	12
2. GROUND MOTIONS AND FRAMES.....	14
2.1 GENERAL	14
2.2 GROUND MOTIONS	15
2.2.1 Correlation Among Ground Motion Paramaters.....	22
2.3 DESCRIPTION OF FRAMES.....	23
3. ANALYSIS OF FRAMES.....	27
3.1 GENERAL	27
3.2 MODELING	28
3.3 NONLINEAR STATIC (PUSHOVER) ANALYSIS.....	30
3.3.1 Idealization of Pushover Curves	35

3.4	NONLINEAR RESPONSE HISTORY ANALYSIS	36
3.4.1	SDOF Response History Analysis	37
3.4.2	MDOF Response History Analysis.....	40
3.4.3	Comparison of SDOF and MDOF Results	46
3.5	DISCUSSION OF RESULTS.....	47
4.	CORRELATION STUDY	48
4.1	GENERAL	48
4.2	CORRELATION WITH ANALYTICAL RESULTS	49
4.2.1	Correlation Measures	49
4.2.2	Demand Measures.....	50
4.2.3	Correlation Study for SDOF Response	51
4.2.4	Comparison with Other Studies (SDOF)	56
4.2.5	Correlation Study for MDOF Response.....	58
4.2.6	Comparison with Other Studies (MDOF).....	69
4.3	CORRELATION WITH OBSERVED DAMAGE	70
4.3.1	Damage States.....	71
4.3.2	Strong Motion Data.....	72
4.3.3	Building Survey Data.....	72
4.3.4	Correlation Study	75
5.	SUMMARY AND CONCLUSIONS	79
5.1	SUMMARY	79
5.2	CONCLUSIONS.....	1
5.3	FUTURE RECOMMENDATIONS	1
	REFERENCES.....	83
	APPENDIX	
A.	FRAME DETAILS	88
A.1	F1-2S3B	88
A.2	F2-3S3B	90
A.3	F3-3S2B	92
A.4	F4-3S3B	94
A.5	F5-4S3B	96

A.6	F6-4S3B	98
A.7	F7-4S3B	100
A.8	F8-5S4B	102
A.9	F9-5S3B	105
A.10	F10-5S4B	108
A.11	F11-5S3B	111
A.12	F12-6S4B	114
A.13	F13-6S3B	117
A.14	F14-6S3B	120
A.15	F15-7S3B	123
A.16	F16-9S3B	126

LIST OF TABLES

Table 2.1 Ground motions	16
Table 2.2 Computed ground motion parameters.....	21
Table 2.3 Correlation among seismic parameters	23
Table 2.4 Properties of the frames	25
Table 3.1 Total weight and height of the selected frames.....	31
Table 3.2 Idealized pushover curve parameters.....	36
Table 3.3 Properties of the equivalent SDOF systems.....	38
Table 3.4 Yield MIDR values of the selected frames	41
Table 4.1 Pearson's coefficient results for overall response (SDOF).....	52
Table 4.2 Coefficient of determination values for three ranges (SDOF).....	53
Table 4.3 Average correlation of ground motion parameters with roof disp.....	54
Table 4.4 Coefficient of determination values for three ranges (MDOF).....	59
Table 4.5 Pearson's coefficient results for overall response (MDOF).....	60
Table 4.6 Average correlation of ground motion parameters with MIDR.....	61
Table 4.7 Average correlation results for exponential and linear fit.....	63
Table 4.8 Pearson's correlation coefficient for ASI for different c values	67
Table 4.9 Pearson's correlation coefficient for VSI for different c values	67
Table 4.10 Averaged Pearson's results for ASI and VSI.....	68
Table 4.11 Comparison of Pearson' correlation coefficient results.....	70
Table 4.12 Structural damage states.....	72
Table 4.13 Surveyed damage states of the selected buildings	74
Table 4.14 Coefficient of determination values for observed damage	75
Table A.1 Column properties (F1-2S3B).....	88
Table A.2 Beam properties (F1-2S3B)	89
Table A.3 Column properties (F2-3S3B).....	90

Table A.4 Beam properties (F2-3S3B)	91
Table A.5 Column properties (F3-3S2B).....	92
Table A.6 Beam properties (F3-3S2B)	93
Table A.7 Column properties (F4-3S3B).....	94
Table A.8 Beam properties (F4-3S3B)	95
Table A.9 Column properties (F5-4S3B).....	96
Table A.10 Beam properties (F5-4S3B)	97
Table A.11 Column properties (F6-4S3B).....	98
Table A.12 Beam properties (F6-4S3B)	99
Table A.13 Column properties (F7-4S3B).....	100
Table A.14 Beam properties (F7-4S3B)	101
Table A.15 Column properties (F8-5S4B).....	103
Table A.16 Beam properties (F8-5S4B)	104
Table A.17 Column properties (F9-5S3B).....	106
Table A.18 Beam properties (F9-5S3B)	107
Table A.19 Column properties (F10-5S4B).....	109
Table A.20 Beam properties (F10-5S4B)	110
Table A.21 Column properties (F11-5S3B).....	112
Table A.22 Beam properties (F11-5S3B)	113
Table A.23 Column properties (F12-6S4B).....	115
Table A.24 Beam properties (F12-6S4B)	116
Table A.25 Column properties (F13-6S3B).....	118
Table A.26 Beam properties (F13-6S3B)	119
Table A.27 Column properties (F14-6S3B).....	121
Table A.28 Beam properties (F14-6S3B)	122
Table A.29 Column properties (F15-7S3B).....	124
Table A.30 Beam properties (F15-7S3B)	125
Table A.31 Column properties (F16-9S3B).....	127
Table A.32 Beam properties (F16-9S3B)	128

LIST OF FIGURES

Figure 2.1 PGA and PGV distribution of the records	15
Figure 2.2 Moment magnitude vs. closest distance	18
Figure 2.3 Moment magnitude distribution of data set	18
Figure 2.4 Closest distance distribution of data set	18
Figure 2.5 Mean and 84-th percentile 5% damped pseudo acceleration spectra ...	19
Figure 2.6 Mean and 84-th percentile 5% damped pseudo velocity spectra.....	19
Figure 2.7 Distributions of ground motion parameters.....	20
Figure 2.8 Story-wise distributions of frames.....	23
Figure 2.9 Computed and approximated periods	26
Figure 3.1 Bilinear hysteretic model (Valles et al., 1996)	29
Figure 3.2 Confinement effectiveness (Valles et al., 1996).....	30
Figure 3.3 Pushover curves for frames F1-F6.....	32
Figure 3.4 Pushover curves for frames F7-F12.....	33
Figure 3.5 Pushover curves for frames F11-F16.....	34
Figure 3.6 Original and idealized force-displacement curves.....	35
Figure 3.7 Equivalent SDOF system with mass M^* and stiffness K^*	37
Figure 3.8 Force-displacement relationship of equivalent SDOF model.....	38
Figure 3.9 Elastic ductility demands	39
Figure 3.10 Inelastic ductility demands	39
Figure 3.11 Computation of yield MIDR.....	41
Figure 3.12 MIDR distribution of results.....	42
Figure 3.13 Relationship between average and maximum interstory drift ratio....	42
Figure 3.14 Displacement profiles of frames F1-F6	43
Figure 3.15 Displacement profiles of frames F7-F12	44
Figure 3.16 Displacement profiles of frames F13-F16	45

Figure 3.17 Comparison of SDOF and MDOF results	46
Figure 4.1 Fitted lines for overall, linear and nonlinear response.....	52
Figure 4.2 Correlation of acceleration related parameters (SDOF)	55
Figure 4.3 Correlation of velocity related parameters (SDOF).....	55
Figure 4.4 Distribution of PGA and PGV used in Akkar and Ozen (2005)	57
Figure 4.5 Distribution of PGA and PGV used in Riddell (2007).....	58
Figure 4.6 Correlation of acceleration related parameters (MDOF).....	62
Figure 4.7 Correlation of velocity related parameters (MDOF)	62
Figure 4.8 Correlation of existing and designed frames (PGA, ASI, CAV, I_c , AI, EPA).....	64
Figure 4.9 Correlation of existing and designed frames (VSI, HI, I_F , PGV, S_a)....	65
Figure 4.10 Average Pearson's results for revised ASI and VSI.....	68
Figure 4.11 Comparison of SDOF and MDOF results	69
Figure 4.12 Story-wise distribution of surveyed buildings.....	73
Figure 4.13 Damage state versus CAV, ASI, AI and I_c	76
Figure 4.14 Damage state versus PGV, I_F , VSI and HI	77
Figure 4.15 Damage state versus PGV, I_F , VSI and HI	78
Figure A.1 Frame F1-2S3B.....	88
Figure A.2 Frame F2-3S3B.....	90
Figure A.3 Frame F3-3S2B.....	92
Figure A.4 Frame F4-3S3B.....	94
Figure A.5 Frame F5-4S3B.....	96
Figure A.6 Frame F6-4S3B.....	98
Figure A.7 Frame F7-4S3B.....	100
Figure A.8 Frame F8-5S4B.....	102
Figure A.9 Frame F9-5S3B.....	105
Figure A.10 Frame F10-5S4B.....	108
Figure A.11 Frame F11-5S3B.....	111
Figure A.12 Frame F12-6S4B.....	114
Figure A.13 Frame F13-6S3B.....	117
Figure A.14 Frame F14-6S3B.....	120

Figure A.15 Frame F15-7S3B.....	123
Figure A.16 Frame F16-9S3B.....	126

CHAPTER 1

INTRODUCTION

1.1 GENERAL

One of the key research areas of earthquake engineering field is the assessment of the capacity of a strong ground motion to damage structures, thus establishing a proper and objective measure of earthquake intensity. Defining the severity of a seismic excitation has become an important task in earthquake engineering field. Many ground motion intensity parameters have been proposed to relate the seismic damage to the intensity of the ground motions. Recently, evaluation of the seismic performance of structures under seismic excitations, where excitation is represented by a ground motion intensity parameter, has gained a wide popularity.

Previous studies investigated some ground motion intensity indices that provide a relation between the seismic excitation and the damage sustained. However there is not an agreement on which ground motion intensity to use. Hence, establishing a consistent measure of earthquake damage potential proposing a ground motion intensity parameter will definitely contribute to following areas;

- Seismic design/rehabilitation
- Seismic hazard analysis
- Ground motion scaling for analysis and design
- Early warning systems
- Performance based vulnerability assessment

It is well known that reinforced concrete structures are common systems all over the world in construction practice. Observations from past earthquakes have revealed that reinforced concrete structures are vulnerable to strong ground motions. Previous earthquakes in Turkey, where majority of the structures are reinforced concrete, resulted in huge life and monetary losses. Thus, seismic design and assessment issues of reinforced concrete systems require proper measures of earthquake damage potential to be well correlated with structural response.

This study is aimed at investigating the adequacy of salient ground motion parameters to portray the severity of seismic events using a comprehensive frame and ground motion database. The preferred methodology is to perform nonlinear response history analyses to obtain the response parameters of the models derived from reinforced concrete frames and investigate the correlation of computed response with the ground motion intensity parameters through correlation coefficients.

1.2 GROUND MOTION INTENSITY PARAMETERS

Ground motion time history records of acceleration, velocity and displacement are the central elements of earthquake engineering field and structural dynamics. Those time series comprise a great deal of information about the strong ground motion. Among those information embedded in time history record, amplitude, frequency content and duration characteristics of the strong ground motion rank first for engineering purposes (Kramer, 1996). Many ground motion parameters, as an intensity measure, have been proposed in the literature to reflect these characteristics. While some of them can be directly extracted from ground motion time series, others require some computational effort.

1.2.1 Response Spectrum Concept

Response spectrum concept is the key component of the earthquake engineering field and used in the evaluation of some ground motion parameters. It is a well integrated and a practical approach in structural dynamics. Maximum response of elastic/inelastic single-degree-of-freedom (SDOF) systems within the period range of interest for preferred damping ratios can be observed in a response spectrum. Acceleration, velocity and displacement response spectra are the primary response spectra used in structural dynamics. Lateral forces defined in many codes are based on response spectrum concept.

Response spectrum is divided into three period ranges: acceleration-sensitive region (short periods), velocity-sensitive region (intermediate periods) and displacement-sensitive region (long periods) since the dynamic structural response of structures in these regions are related to the peak values of acceleration, velocity and displacement respectively (Chopra, 2000). This relation is used in the construction of smoothed elastic design spectra using peak values of ground acceleration, velocity and displacement. Riddell (2007) designated that ground acceleration related ground motion intensity parameters show better correlation in the acceleration-sensitive region and indices related to ground velocity correlate better in the velocity-sensitive region with the structural demand measures. Sensitivity of ground motion parameters used in this study in different period ranges (short and intermediate periods) will be further discussed in detail.

1.2.2 Ground Motion Intensity Parameters Used in This Study

Among the parameters defined in the literature, promising eleven ground motion parameters were selected and employed in the correlation study. These parameters are peak ground acceleration, peak ground velocity, effective peak acceleration, Arias intensity, cumulative absolute velocity, acceleration spectrum intensity,

Housner intensity, velocity spectrum intensity, Fajfar intensity and characteristic intensity. A brief description of these parameters is given as follows;

Peak Ground Acceleration (PGA) is one of the simplest and most widely used ground motion parameters. PGA is the maximum absolute amplitude of the acceleration time history of a ground motion. In terms of structural response, it is the peak value of absolute acceleration of an infinitely stiff SDOF system. PGA is sensitive to high frequency components of the ground motion. Many attenuation relationships are readily available in literature for PGA (Douglas, 2001). Popularity of PGA comes from the relationship between the inertial forces and acceleration in seismic design. The information hidden in PGA is only the amplitude of the ground motion. Frequency content or duration of the ground motion is not presented in PGA.

Peak Ground Velocity (PGV) is the largest absolute value of velocity trace and has recently gained an increasing popularity. PGV is less sensitive to higher frequency components of the ground motion and may provide more accurate damage measures than PGA at the intermediate frequencies. Prediction equations for PGV are presented in the literature (Akkar and Bommer 2007). However, those equations do not fill too much space in literature when the prediction equations for PGA and spectral ordinates are considered. PGA and PGV are frequently employed in fragility curves.

Definition of *Effective Peak Acceleration (EPA)* was first introduced in ATC-3 (Applied Technology Council, 1978) report. It is computed as the average of spectral acceleration values of elastic response spectrum between 0.1 s and 0.5 s divided by a constant value of 2.5 for 5% damping. Considering an acceleration trace with a single cycle of high amplitude and lower amplitudes in the other cycles, PGA value of that trace may give insufficient information about the damage potential. As an alternative to PGA, EPA is introduced by averaging the spectral values in the period range of 0.1-0.5 s divided by 2.5 as defined earlier to mitigate the effect of local spikes. EPA is not necessarily same or proportional to PGA and its relation with

PGA is strongly dependent on the frequency content of the ground motion. EPA gives information about the frequency content and the amplitude of ground motion and is used in the construction of smoothed design response spectra.

Arias Intensity (AI) was proposed by Arias (Arias, 1970) as ground motion intensity related to the energy content of the ground motion. Square of the acceleration is integrated over the entire length of the ground motion record (Equation 1.1). The assumption behind the formulation of AI is that the energy dissipated by the structure per unit weight is related to the damage occurred in that structure. AI is a cumulative representation of energy dissipated per unit weight by undamped SDOF oscillators having frequencies uniformly distributed between $(0, \infty)$. Amplitude, frequency content and the duration characteristics of the ground motion are reflected in AI. Empirical attenuation relationship for AI is presented in Travararou et al. (2003).

$$AI = \frac{\pi}{2g} \int_0^{t_d} a(t)^2 dt \quad (1.1)$$

As part of an extensive study, Sucuoğlu and Nurtuğ (1995) studied the sensitivity of AI for two different excitation types, an acceleration pulse and a sinusoidal harmonic excitation. They concluded that AI amplifies the short duration pulses and is not sensitive to the frequency of the harmonic excitation.

Cumulative Absolute Velocity (CAV) is the absolute area under the ground motion trace and was introduced in Electrical Power Research Institute (EPRI, 1988). Amplitude, frequency content and the duration characteristics of ground motion are reflected in CAV. This quantity is computed using Equation 1.2 where t_d is the total duration of the record.

$$CAV = \int_0^{t_d} |a(t)| dt \quad (1.2)$$

Acceleration Spectrum Intensity (ASI) is defined as the area under the elastic acceleration spectrum between the periods 0.1-0.5 s (Von Thun et al., 1988). This parameter was introduced to characterize strong ground motion for analysis and design of concrete dams, which generally have fundamental periods less than 0.5 s. Von Thun et al. (1988) stated that scaling design ground motions using ASI for concrete dams takes frequency content into consideration. Attenuation relationships were developed for ASI using 30 strong ground motion records from rock sites (Von Thun et al., 1988).

Housner (1952) defined the *Housner Intensity* (HI) as a measure of earthquake intensity as the area under the pseudo velocity spectrum between periods of 0.1 and 2.5 s. Housner (1952) used pseudo-velocity to relate the earthquake intensity to the maximum stresses (F_{\max}) occurred in the structure using Equation 1.3 where m is the total mass and k is the stiffness of the SDOF system. As long as m and k are known, maximum force is directly related to S_v (pseudo spectral velocity). If this dependence of maximum stresses on S_v , given m and k , is averaged over a period range (0.1-2.5 s), Housner stated that this averaged value is a measure of earthquake intensity. Period range is set considering fundamental periods of most of the structures in a population that fall in 0.1-2.5 s. 5% damping is used in the computation of HI in this study.

$$F_{\max} = (mk)^{1/2} \cdot S_v \quad (1.3)$$

Formulation of *Velocity Spectrum Intensity* (VSI) is similar to that of HI. Actual velocity spectrum is used instead of pseudo velocity in computation of VSI. VSI was defined by Von Thun et al. (1988) in order to form a compatible platform for the selection of ground motions for seismic design and analysis of dams considering natural periods of earth-fill and rock-fill dams ranging between 0.6 and 2.0 s. This range is extended to 0.1-2.5 s in the formulation to effectively cover the possible natural periods of the earth-fill and rock-fill dams.

Fajfar et al. (1990) defined the I_F (Equation 1.4) as a measure of earthquake damage potential to medium-period structures and as a scaling parameter as well. As shown in Equation 1.4, two basic parameters are involved in the formulation of I_F ; peak ground velocity and effective strong motion duration, respectively. Effective strong motion duration t_e is defined as the time interval between 5% and 95% of AI. Fajfar et al. (1990) used a total of 40 ground motion records in order to propose I_F and defined the bounding periods of the medium-period range in their study.

$$I_F = PGV.t_e^{0.25} \quad (1.4)$$

Park et al. (1985) conducted the damage analysis of SDOF and MDOF reinforced concrete buildings and proposed an explicit relationship between sustained damage and destructiveness of ground motions as a function of the strong motion intensity and duration. *Characteristic Intensity* (I_c) was defined as a reasonable representation of the destructiveness of earthquakes (Equation 1.5). I_c is related to acceleration root mean square (a_{rms}) and t_d (total duration of the record).

$$I_c = (a_{rms})^{3/2} \sqrt{t_d}, \quad a_{rms} = \sqrt{\frac{1}{t_d} \int_0^{t_d} a(t)^2 dt} \quad (1.5)$$

To conclude, PGA, PGV, EPA, S_a (pseudo spectral acceleration at the fundamental period), ASI, VSI, I_c , I_F , CAV, AI, HI are the eleven ground motion intensity parameters selected and employed in this study.

1.2.3 Engineering Demand Measure

For evaluating the correlation of ground motion parameters with structural response, a suitable demand measure must be set for reinforced concrete frames. Roof displacement, interstory drift, concrete and steel strain, curvature ductility, plastic

rotation, hysteretic energy dissipated can be listed among engineering demand measures. Maximum interstory drift and global drift are commonly used demand parameters in reinforced concrete building type of structures and are deemed to be a measure of structural damage in earthquake engineering field. Due to the interdependency between lateral deformation and structural damage, maximum interstory drift and global drift have been used by many researchers (Algan, 1982; Moehle, 1994; Moehle, 1992; Miranda, 1999; Gulkan and Sozen, 1999) as a damage inducing parameter. Hence, maximum displacement demand was taken as the demand parameter in SDOF analysis and correspondingly maximum interstory drift ratio was taken as the demand parameter for MDOF analysis in this study.

1.3 LITERATURE SURVEY

Selected studies from the literature investigating the adequacy of ground motion parameters to reflect the severity of ground shaking through analytical analyses as well as investigating the observed damage after earthquakes are briefly described below.

Uang and Bertero (1988) investigated the adequacy of the parameters that have been used to identify the damage potential of an earthquake and stated that the destructiveness of a ground motion record at the foundation of a structure depends on the intensity, frequency content, duration and the dynamic characteristics of the structure. They concluded that the most reliable parameter for assessing the damage potential is earthquake energy input

Cabanas et al. (1997) studied the correlation of AI and CAV with the observed damage represented through local intensity (MSK intensity) proposing relationships for these intensity measures. A total of 25 strong motion records were selected from the Campano Lucano, Umbria and Lazio-Abruzzo earthquakes. Damage data were gathered from the buildings (more than 100 buildings) in the vicinity of the recording

stations where the maximum distance between the station and the observed building is 300 m (local intensity ranging between 5.5 and 7.5). AI and CAV are found to have an exponential relation with the local intensity. Damage data consists of three types of buildings: rural structures, ordinary brick buildings and precast concrete skeleton structures. Besides the local intensity, correlation of both parameters with damage is investigated using the damage data of different building types. Among those aforementioned three types, rural structures show a clear exponential trend.

Sucuoglu (1997) discussed the outcomes of the study performed by Cabanas et al. (1997) and concluded that PGA and PGV have stronger correlations than AI and CAV contrary to the priority given to AI and CAV.

Correlation of seven intensity parameters with surface wave magnitude (M_s) was investigated by Sucuoğlu et al. (1999). Fifteen pairs of near-fault ground motion records with magnitudes ranging from 4.6 to 7.1 were used. The objective behind the selection of near-fault records is to decrease the effect of site-to-source distance and site response on magnitude. Results of the above mentioned study indicate that spectral parameters show stronger correlation with magnitude and effect of magnitude on response spectrum shows itself in the medium period range.

Wu et al. (2004) studied the relationship of some ground motion parameters with earthquake loss and intensity using 1999 Chi-Chi, Taiwan earthquake data. Earthquake loss is defined in two different ways as the number of fatalities and totally collapsed households, respectively. Among the ground motion parameters considered in the study, PGA and S_a at 1 s. are the two parameters that have the highest correlation with earthquake damage. Nevertheless, authors do not suggest using PGA as a damage assessment parameter since a single spike with high frequency may give misleading impression about the damage potential. As a second part of the study, Wu et al. (2004) investigated the correlation between ground motion parameters and intensity and stated that PGV and S_a at 1 s. are consistent parameters with intensity. Working on earthquake loss and intensity separately, Wu

et al (2004) concluded that PGV and S_a at 1 s. are more stable parameters in earthquake loss assessment and intensity estimation.

Cordova et al. (2000) proposed a two-parameter seismic intensity measure that considers period softening encountered in inelastic time-history analysis. Authors stated that linear response spectrum quantities are insufficient to reflect the inelastic behavior and corresponding period softening as the structure deforms into inelastic range. This new intensity measure is formulated as follows in Equation 1.6.

$$S^* = S_a(T_1) \cdot \left[\frac{S_a(cT_1)}{S_a(T_1)} \right]^\alpha \quad (1.6)$$

Parameters c and α were determined by a calibration process as 2 and 0.5 respectively. Three six-story and one twelve-story moment frames (fundamental periods ranging from 1.3 to 2.1 s) were used in the calibration process. Two sets of; general and near-fault records, eight ground motions were employed in the study. This new intensity measure accounts for both spectral intensity and spectral shape. Since there are attenuation relations available for spectral ordinates, S^* can easily be calculated for a given $S_a(T_1)$ and $S_a(cT_1)$.

Elenas (2000) investigated the interdependency between seismic parameters and structural response, in terms of overall structural damage indices, using an eight story reinforced concrete frame building (having a fundamental period of 1.18 s) designed according to Eurocode 8 (2003). A total number of 20 ground motions were used in the analyses. Hysteretic behavior of the model is formed using the results of an experimental study conducted on the typical members of the analyzed frame. S_a was found to be the parameter that has the highest correlation with the overall structural damage. The same frame and ground motion data set were used in Elenas and Meskouris (2001) in order to conduct a correlation study between the maximum interstory drift demand and floor acceleration with ground motion parameters and concluded that S_a has the highest correlation with both demand parameters. The

results of Elenas (2000) and Elenas and Meskouris (2001) can not be generalized due to the use of limited number of records and a single frame in the analyses.

Liao et al. (2001) studied the response of two concrete moment resisting frames (twelve-storey and five-storey) subjected to near-fault ground motions. Using 22 near-fault ground motions, Liao et al. observed that maximum interstory drift increases as PGV/PGA, S_v and input energy increase for the analyzed frames. Results of this study are limited to the number of records and frames.

Akkar and Özen (2005) highlighted PGV as a potential ground motion intensity measure for earthquake hazard analysis, after investigating the effect of PGV on SDOF response and interdependency between PGV and some ground motion features. 60 soil site records having moment magnitudes between 5.5 and 7.6 with maximum source-to-site distance being 23 km are used in the study. Records do not contain pulse signals that may have remarkable effects on response. The study by Akkar and Ozen (2005) concluded that PGV shows a good correlation with the earthquake magnitude, effective ground motion duration and frequency content of ground motions, and confirmed that PGV correlates better with SDOF response than PGA, PGV/PGA and S_a when different constant μ (ductility ratio) and R (normalized lateral strength ratio) levels are considered.

The study of Riddell (2007) exhibits the result of a correlation study between 23 ground motion parameters and SDOF response. SDOF response was defined in four distinct ways; elastic and inelastic deformation demands, input energy and hysteretic energy respectively. Elastoplastic, bilinear and bilinear with stiffness degradation models subjected to 90 ground motions were used in the analysis. Ground motion data was gathered in a way that all records have PGA larger than 0.25 g and PGV larger than 25 cm/s. Riddell (2007) found that no intensity parameter is sufficient over the three spectral regions. Ground acceleration related parameters have higher correlation in the acceleration-sensitive region, parameters related to the ground velocity are more satisfactory in the velocity-sensitive region and the same situation

is valid for displacement-sensitive region. Considering average response for four distinct responses, for stiff structures PGA, AI and I_c are promising parameters and for intermediate periods PGV, HI and I_F show higher correlation with response.

1.4 OBJECTIVE AND SCOPE

The main objective of this thesis is to identify the correlation between deformation demands of reinforced concrete frames and salient ground motion intensity parameters employing SDOF and MDOF models. An inclusive study has been carried out performing nonlinear response history analyses of sixteen reinforced concrete frames under a set of eighty ground motion records presenting various levels of seismic intensity. Association of ground motion intensity parameters with observed damage using the survey data presented in ATC-38 (2000) has been examined as a second objective.

This study is composed of five chapters and an appendix. Introductory remarks and a brief description of ground motion intensity parameters and related previous studies are presented in Chapter 1.

Chapter 2 presents the description of ground motion records and frames used in the analyses. The chapter starts with the description of the important features of the ground motion records and this is followed by the numerical and graphical representation of ground motion intensity parameters utilized in this thesis and evaluation of correlation among them. Description of the selected sixteen reinforced concrete frames is presented at the end of the chapter.

Chapter 3 contains the details of nonlinear static and nonlinear response history analyses of the SDOF and MDOF models derived from the selected reinforced concrete frames. Firstly, nonlinear static analyses of the frames were performed and MDOF systems were reduced to equivalent SDOF systems accordingly. Nonlinear

response history analyses of equivalent SDOF models and MDOF models are than performed and discussed. The chapter concludes with the comparison of the equivalent SDOF and MDOF system roof displacement results and discussion.

Chapter 4 is devoted to the correlation study. Degree of correlation between the response parameters with ground motion intensity indices are evaluated through correlation coefficients for SDOF and MDOF nonlinear response history analyses results respectively and presented. Chapter 4 also surveys the relationship between observed damage and seismic parameters.

Finally, Chapter 5 includes the summary and conclusions of this thesis and presents future recommendations.

Appendix A includes the size, configuration and detailing of the members of the frames.

CHAPTER 2

GROUND MOTIONS AND FRAMES

2.1 GENERAL

In order to conduct the correlation study between deformation demands of frame type structures and selected ground motion parameters, eighty un-scaled ground motion records and sixteen reinforced concrete moment resisting frames were utilized in this study. Frames were selected to represent the typical low-to-mid rise reinforced concrete buildings in Turkey. The ground motion data set is intended to cover a wide range of earthquake intensity that would push the selected frames into various degrees of inelasticity.

Low-to-mid rise reinforced concrete buildings are very common in the Turkish construction practice. Sixteen reinforced concrete frames ranging from two to nine stories were employed in nonlinear response history analyses. Some of the frames used in this study were taken from the Duzce City, where the city is located in seismic zone 1 according to the recent seismic design code in Turkey, and the remaining frames were designed according to the Turkish seismic design code (1997). Fundamental period of the frames covers a broad range representing low-to-mid rise buildings (0.17 s-1.07 s).

The general principle of many design codes is to limit the damage to repairable level in medium-intensity earthquakes and to prevent collapse in high-intensity earthquakes, hence some degree of damage is permitted. It is believed that reinforced

concrete structures will exhibit inelastic behavior when subjected to a high intensity seismic excitations. Selected data set contains broad range of ground motion intensity that the elastic and inelastic responses of the analyzed frames are expected. The ground motion data set used in this study was extracted from the study of Erberik and Çulcu (2006).

2.2 GROUND MOTIONS

A total set of eighty individual un-scaled ground motion records (twenty eight different events) with moment magnitudes (M_w) ranging from 5.7 to 7.4, mostly recorded on alluvium sites, were employed in this study. Those ground motions were extracted from the study of Erberik and Çulcu (2006) where records were selected to form a set containing different PGV bins. Important features of these ground motions can be seen in Table 2.1. Selected ground motion data set is believed to cover a wide range of earthquake intensity that the analyzed frames would undergo elastic as well as inelastic deformations. PGA and PGV distributions for the selected ground motions are shown in Figure 2.1. The distribution of PGA falls mostly in the range 0.2g-0.6g and the distribution of PGV is nearly uniform covering a range of 10-100 cm/s.

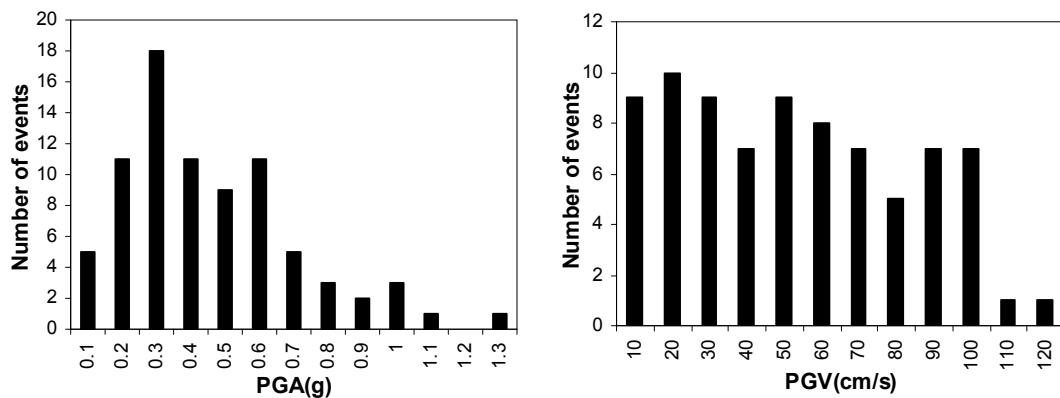


Figure 2.1 PGA and PGV distribution of the records

Table 2.1 Ground motions

#	Earthquake	Country	Date	Site Geology	Comp	M _s	M _w	CD (km)	Depth (km)	F. Type
1	Morgan Hill	USA	24.04.1984	Alluvium	0	6.1	6.1	11.8	8.4	Rt Lat Strike Slip
2	Vrancea	Romania	30.05.1990	Alluvium	EW	6.8	—	—	89	Thrust
3	Manjil	Iran	20.06.1990	Stiff Soil	NS	7.3	—	—	19	Oblique
4	Manjil	Iran	20.06.1990	Stiff Soil	EW	7.3	—	—	19	Oblique
5	Izmir	Turkey	06.11.1992	Stiff Soil	L	6.0	—	—	17	—
6	Livermore	USA	27.01.1980	Alluvium	270	5.8	—	—	14.5	Strike Slip
7	Morgan Hill	USA	24.04.1984	Alluvium / Sandstone	90	6.1	6.1	7.9	8.4	Rt Lat Strike Slip
8	Lazio Abruzzo	Italy	07.05.1984	Alluvium	EW	5.8	5.7	—	8	Normal
9	Vrancea	Romania	30.05.1990	Alluvium	NS	6.8	—	—	89	Thrust
10	Campano-Lucano	Italy	23.11.1980	Stiff Soil	NS	6.9	6.5	—	16	Normal
11	Coalinga	USA	02.05.1983	Alluvium / Sandstone	0	6.5	6.5	—	10	Thrust/Reverse
12	Loma Prieta	USA	18.10.1989	Alluvium	0	7.1	7.0	44.9	17.6	Oblique
13	Northridge	USA	17.01.1994	Alluvium	0	6.8	6.7	41.4	19	Thrust/Reverse
14	Northridge	USA	17.01.1994	Alluvium	360	6.8	6.7	46.2	19	Thrust/Reverse
15	Denizli	Turkey	19.08.1976	Stiff Soil	EW	5.1	—	—	5	Normal
16	Montenegro Aftershock	Form. Yugoslavia	24.05.1979	Alluvium	NS	6.3	—	—	5	Thrust
17	Imperial Valley	USA	15.10.1979	Alluvium	S40E	6.9	6.5	22.6	12	Rt Lat Strike Slip
18	Whittier Narrows	USA	01.10.1987	Alluvium / Siltstone	0	5.8	6.1	41.1	14.7	Thrust/Reverse
19	Landers	USA	28.06.1992	Stiff Soil	0	7.5	7.3	73.2	4.5	Rt. Lat. Strike Slip
20	Alkion	Greece	24.02.1981	Alluvium	L	6.7	—	—	10	Normal
21	Kalamata	Greece	13.09.1986	Stiff Soil	N10W	5.8	—	—	8	Normal
22	Whittier Narrows	USA	01.10.1987	Alluvium	180	5.8	6.1	13.9	14.7	Thrust/Reverse
23	Landers	USA	28.06.1992	Stiff Soil	90	7.5	7.3	73.2	4.5	Rt. Lat. Strike Slip
24	Northridge	USA	17.01.1994	Alluvium	360	6.8	6.7	27.4	19	Thrust/Reverse
25	San Fernando	USA	09.02.1971	Alluvium	N00W	6.5	6.6	16.5	8	Thrust / Reverse
26	Montenegro	Form. Yugoslavia	15.04.1979	Stiff Soil	EW	7.0	—	—	12	Thrust
27	Horasan	Turkey	30.10.1983	Stiff Soil	EW	6.7	—	—	14	Strike Slip
28	Northridge	USA	17.01.1994	Alluvium	90	6.8	6.7	12.9	19	Thrust/Reverse
29	Kalamata	Greece	13.09.1986	Stiff Soil	N265	5.8	—	—	8	Normal
30	Kalamata	Greece	13.09.1986	Stiff Soil	N80E	5.8	—	—	8	Normal
31	Northridge	USA	17.01.1994	Tertiary Sandstone	90	6.8	6.7	10.6	19	Thrust/Reverse
32	Loma Prieta	USA	18.10.1989	Rock	90	7.1	7.0	2.8	17.6	Oblique
33	Montenegro	Form. Yugoslavia	15.04.1979	Stiff Soil	NS	7.0	—	—	12	Thrust
34	Loma Prieta	USA	18.10.1989	Alluvium	0	7.1	7.0	15.9	17.6	Oblique
35	Kobe	Japan	16.01.1995	USGS (D)	90	—	6.9	11	—	—
36	Loma Prieta	USA	18.10.1989	Alluvium	0	7.1	7.0	4.1	17.6	Oblique
37	Loma Prieta	USA	18.10.1989	Alluvium	90	7.1	7.0	4.1	17.6	Oblique
38	Landers	USA	28.06.1992	Quaternary	90	7.5	7.3	10	4.5	Rt. Lat. Strike Slip
39	Northridge	USA	17.01.1994	Alluvium	N90E	6.8	6.7	14.3	19	Thrust/Reverse
40	Dinar	Turkey	01.10.1995	Soft Soil	EW	6.1	6.0	—	5	Normal
41	Montenegro	Form. Yugoslavia	15.04.1979	Stiff Soil	EW	7.0	—	—	12	Thrust
42	Imperial Valley	USA	15.10.1979	Alluvium	S40E	6.9	6.5	5.2	12	Rt Lat Strike Slip
43	Cape Mendocino	USA	25.04.1992	Alluvium	0	7.1	7.0	15.9	15	Thrust / Reverse
44	Marmara	Turkey	17.08.1999	Stiff Soil	NS	7.8	7.4	15	17	Strike Slip
45	Landers	USA	28.06.1992	Alluvium	270	7.5	7.3	31	4.5	Rt. Lat. Strike Slip
46	Northridge	USA	17.01.1994	Alluvium	N00E	6.8	6.7	14.3	19	Thrust/Reverse
47	Northridge	USA	17.01.1994	Sandstone	360	6.8	6.7	24.1	19	Thrust/Reverse
48	Marmara	Turkey	17.08.1999	Rock	EW	7.8	7.4	8	17	Strike Slip
49	Manjil	Iran	20.06.1990	Soft Soil	T	7.3	—	—	19	Oblique
50	Northridge	USA	17.01.1994	Nonmarine Deposit	N44W	6.8	6.7	9.4	19	Thrust/Reverse
51	Loma Prieta	USA	18.10.1989	Landslide Deposit	0	7.1	7.0	2.8	17.6	Oblique
52	Düzce	Turkey	12.11.1999	Soil	NS	7.3	7.1	5.5	10	Strike Slip
53	Marmara	Turkey	17.08.1999	Soft Soil	NS	7.8	7.4	11	17	Strike Slip
54	Northridge	USA	17.01.1994	Alluvium	180	6.8	6.7	12.9	19	Thrust/Reverse
55	Loma Prieta	USA	18.10.1989	Alluvium	0	7.1	7.0	17.2	17.6	Oblique
56	Imperial Valley	USA	15.10.1979	Alluvium	S40E	6.9	6.5	3.5	12	Rt Lat Strike Slip
57	Düzce	Turkey	12.11.1999	Soft Soil	NS	7.3	7.1	7	10	Strike Slip
58	Düzce	Turkey	12.11.1999	Soil	EW	7.3	7.1	5.5	10	Strike Slip
59	Kobe	Japan	16.01.1995	USGS (D)	0	—	6.9	1.2	—	—
60	Bucharest	Romania	04.03.1977	Alluvium	NS	7.1	—	—	86	Thrust
61	Northridge	USA	17.01.1994	Alluvium	90	6.8	6.7	10.9	19	Thrust/Reverse
62	Northridge	USA	17.01.1994	Alluvium	360	6.8	6.7	16.7	19	Thrust/Reverse
63	Northridge	USA	17.01.1994	Alluvium	360	6.8	6.7	9.5	19	Thrust/Reverse
64	Kobe	Japan	16.01.1995	USGS (B)	EW	—	6.9	1	—	—
65	Tabas	Iran	16.09.1978	Stiff Soil	N16W	7.3	—	—	5	Thrust

Table 2.1 Continued

#	Earthquake	Country	Date	Site Geology	Comp	M _s	M _w	CD (km)	Depth (km)	F. Type
66	Northridge	USA	17.01.1994	Alluvium	N41W	6.8	6.7	8.6	19	Thrust/Reverse
67	Northridge	USA	17.01.1994	Alluvium	270	6.8	6.7	9.5	19	Thrust/Reverse
68	Morgan Hill	USA	24.04.1984	Rock	285	6.1	6.1	1.5	8.4	Rt Lat Strike Slip
69	Cape Mendocino	USA	25.04.1992	Alluvium	90	7.1	7.0	15.9	15	Thrust / Reverse
70	Düzce	Turkey	12.11.1999	Soft Soil	EW	7.3	7.1	7	10	Strike Slip
71	Erzincan	Turkey	13.03.1992	Soil	EW	7.3	7.1	2	10	Strike Slip
72	Kobe	Japan	16.01.1995	USGS (D)	90	—	6.9	1.2	—	—
73	Tabas	Iran	16.09.1978	Stiff Soil	N74E	7.3	—	—	5	Thrust
74	Northridge	USA	17.01.1994	Alluvium	360	6.8	6.7	10.9	19	Thrust/Reverse
75	Kobe	Japan	16.01.1995	USGS (B)	NS	—	6.9	1	—	—
76	Imperial Valley	USA	15.10.1979	Alluvium	270	6.9	6.5	3.1	12	Rt Lat Strike Slip
77	Imperial Valley	USA	15.10.1979	Alluvium	S50W	6.9	6.5	5.2	12	Rt Lat Strike Slip
78	Imperial Valley	USA	15.10.1979	Alluvium	S50W	6.9	6.5	3.5	12	Rt Lat Strike Slip
79	Northridge	USA	17.01.1994	Alluvium	N38W	6.8	6.7	8.7	19	Thrust/Reverse
80	Northridge	USA	17.01.1994	Alluvium	292	6.8	6.7	8.6	19	Thrust/Reverse

CD, M_s and M_w given in Table 2.1 are closest distance to fault, surface wave magnitude and the moment magnitude respectively. Site classification according to US Geological Survey (USGS) represented in Table 2.1 is as follows:

- USGS (A), sites with shear wave velocities (V_s) > 750 m/s
- USGS (B), 360 m/s < V_s < 750 m/s
- USGS (C), 180 m/s < V_s < 360 m/s
- USGC (D), sites with V_s < 180 m/s

The magnitude versus closest distance plot of the ground motions employed is shown in Figure 2.2. The distance range covered suggests that the records represent both near and far field ground motions. Ground motion records with closest distance less than 20 km dominate the data set. Distribution of the moment magnitude and the closest distance to the fault are depicted in Figures 2.3 and 2.4 respectively.

Mean and 84-th percentile elastic pseudo acceleration and pseudo velocity spectra for 5% damping are plotted in Figures 2.5 and 2.6. It is apparent from these figures that a broad range of earthquake intensity was achieved in the compilation of the data set.

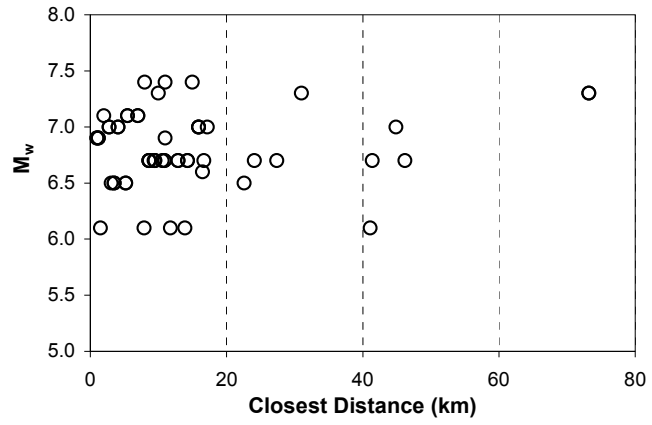


Figure 2.2 Moment magnitude vs. closest distance

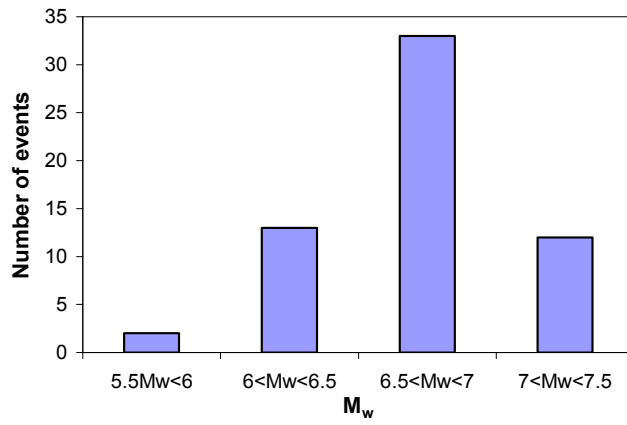


Figure 2.3 Moment magnitude distribution of data set

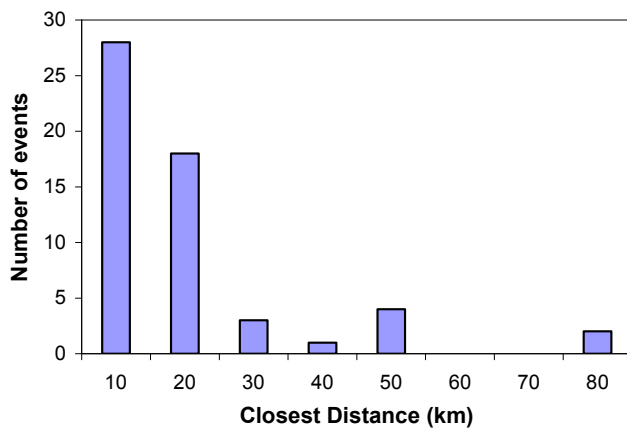


Figure 2.4 Closest distance distribution of data set

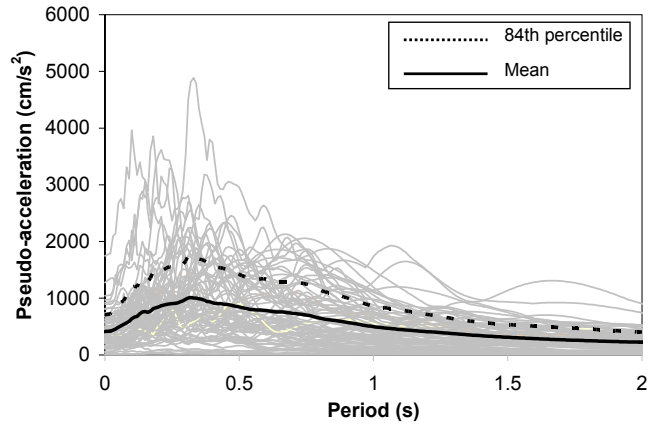


Figure 2.5 Mean and 84-th percentile 5% damped pseudo acceleration spectra

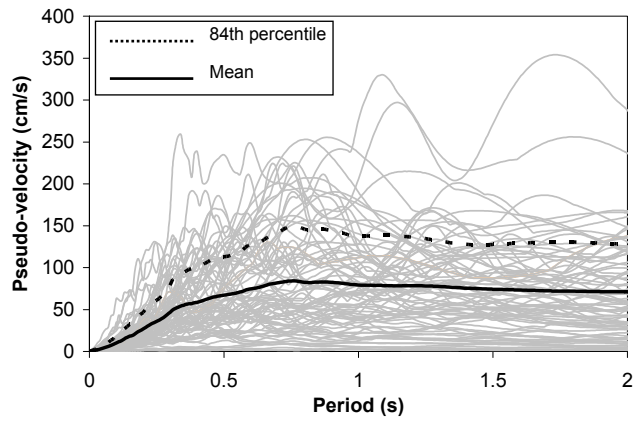


Figure 2.6 Mean and 84-th percentile 5% damped pseudo velocity spectra

The ground motion intensity parameters defined in the previous chapter were computed and depicted in Table 2.2. Distribution of these parameters are given in Figure 2.7. As shown in Figure 2.7, uniformity in the distribution is difficult to achieve since some parameters are computed directly using the time history of the record and some parameters are computed from the response spectrum. Large value of one parameter does not necessarily mean large values of other parameters. It is observed from Table 2.1 and Table 2.2 that the majority of the ground motion records used in this study conform some generality, and do not contain extreme records due to severe near field and soil site effects expect for records with high PGV ($PGV > 80\text{cm/s}$).

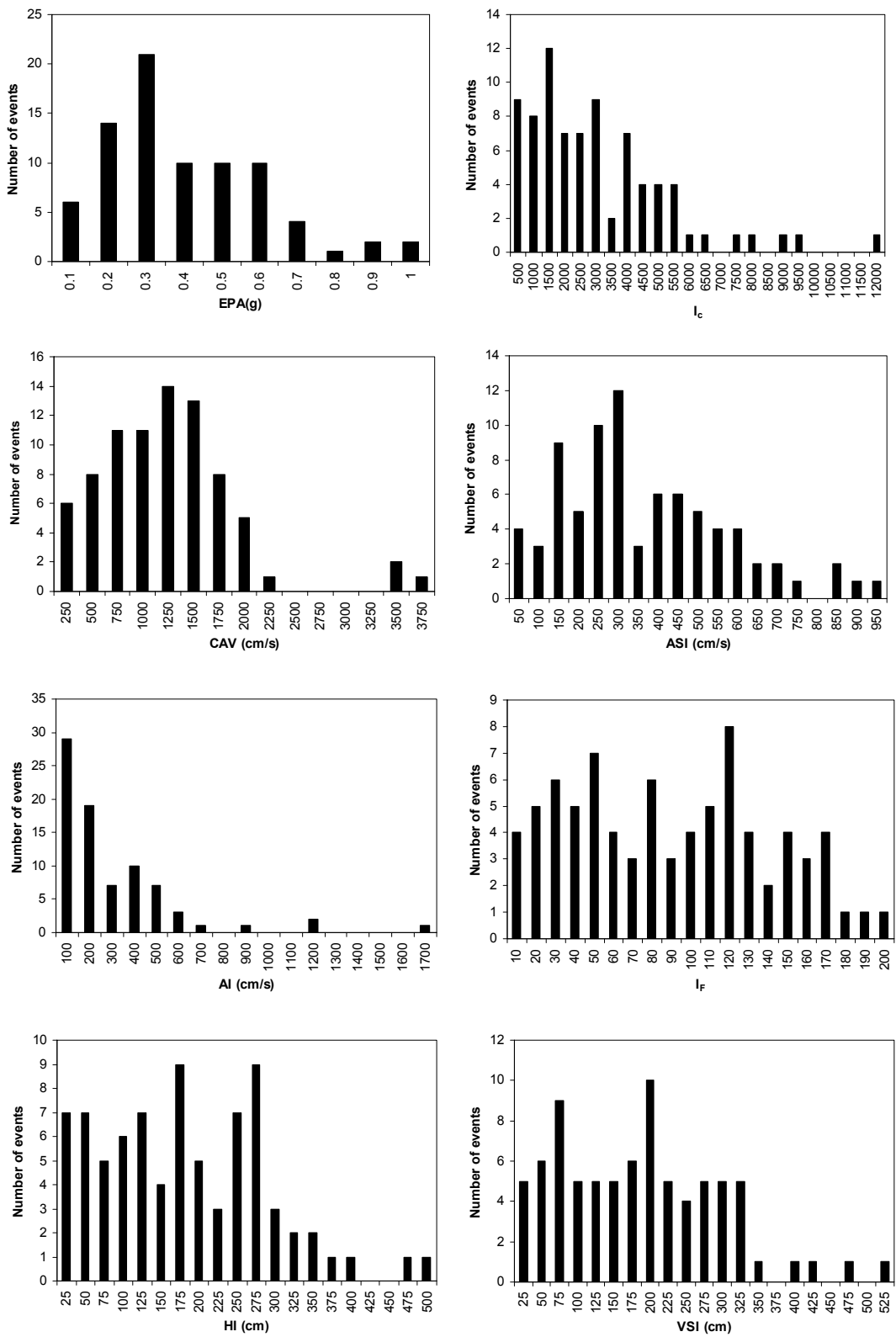


Figure 2.7 Distributions of ground motion parameters

Table 2.2 Computed ground motion parameters

#	Earthquake	PGA (g)	PGV (cm/s)	EPA (g)	AI (cm/s)	I _c	CAV (cm/s)	ASI (cm/s)	VSI (cm)	I _F	HI (cm)
1	Morgan Hill	0.16	5.0	0.10	16.3	365.0	392.0	96.2	29.1	10.4	26.9
2	Vrancea	0.05	2.1	0.04	1.7	85.0	96.9	35.1	8.4	3.6	7.1
3	Manjil	0.01	1.1	0.01	0.2	19.0	37.3	9.7	4.8	2.1	4.8
4	Manjil	0.01	1.2	0.01	0.3	22.8	40.8	12.5	4.2	2.4	4.3
5	Izmir	0.07	4.3	0.06	7.6	258.9	214.0	58.0	14.7	7.8	13.2
6	Livermore	0.25	9.7	0.21	20.1	472.0	214.0	207.0	32.0	13.0	19.8
7	Morgan Hill	0.11	5.8	0.13	20.6	433.0	409.9	130.0	25.6	10.7	19.9
8	Lazio Abruzzo	0.11	7.9	0.12	17.4	465.0	329.0	116.0	38.0	14.0	35.2
9	Vrancea	0.04	6.5	0.03	1.5	77.8	84.2	26.3	18.8	11.0	18.5
10	Campano-Lucano	0.23	11.3	0.21	51.5	1025.0	589.0	209.0	50.5	20.2	43.8
11	Coalinga	0.13	10.5	0.13	26.4	522.0	477.0	132.0	46.3	20.1	41.5
12	Loma Prieta	0.17	13.6	0.18	42.7	829.0	629.0	175.0	74.0	25.8	68.9
13	Northridge	0.15	14.9	0.11	29.6	569.0	533.0	110.0	67.0	29.0	60.1
14	Northridge	0.22	12.7	0.20	56.7	928.0	768.0	197.0	55.8	26.0	53.4
15	Denizli	0.26	15.5	0.26	47.4	1092.0	403.0	252.0	63.0	24.1	46.8
16	Montenegro	0.12	19.2	0.10	26.9	617.0	435.0	100.0	75.0	35.1	72.6
17	Imperial Valley	0.14	16.4	0.11	27.1	593.0	487.0	104.0	48.0	32.9	46.1
18	Whittier Narrows	0.41	19.2	0.41	193.5	2578.0	995.0	408.0	70.0	30.7	45.3
19	Landers	0.11	17.9	0.12	59.3	893.0	1112.0	114.0	64.3	43.4	70.5
20	Alkion	0.29	22.7	0.26	88.8	1468.0	879.0	260.0	126.0	45.0	118.1
21	Kalamata	0.27	23.6	0.30	74.1	1350.0	536.0	299.0	100.0	37.2	93.0
22	Whittier Narrows	0.29	21.7	0.30	80.7	1337.0	568.0	288.0	89.8	32.9	78.1
23	Landers	0.15	20.1	0.14	78.7	1104.0	1268.0	140.0	83.0	47.5	84.8
24	Northridge	0.37	24.9	0.27	118.1	1608.0	981.0	259.0	125.0	45.7	127.4
25	San Fernando	0.25	29.8	0.23	127.7	1709.0	1203.0	228.0	161.0	60.1	158.0
26	Montenegro	0.31	25.3	0.31	199.1	2513.0	1345.0	302.0	96.8	48.4	82.2
27	Horasan	0.16	26.0	0.13	39.5	856.0	624.0	123.0	88.9	53.9	96.6
28	Northridge	0.37	28.9	0.36	196.6	2804.0	1258.0	354.0	150.0	57.5	148.0
29	Kalamata	0.21	32.7	0.22	59.7	1190.0	526.0	213.0	129.0	50.1	122.9
30	Kalamata	0.24	31.5	0.25	55.3	1085.0	451.0	245.0	106.0	47.4	103.7
31	Northridge	0.30	30.9	0.26	160.8	2027.0	1126.0	262.0	140.9	55.6	132.9
32	Loma Prieta	0.44	33.8	0.55	167.5	2314.0	742.0	532.0	151.0	46.9	119.6
33	Montenegro	0.45	38.8	0.46	452.8	4655.0	1930.0	456.0	188.0	72.3	158.2
34	Loma Prieta	0.47	36.1	0.57	437.4	4753.0	1803.0	569.0	207.0	67.6	196.4
35	Kobe	0.50	36.6	0.43	226.8	2887.0	1196.0	423.0	158.0	67.0	143.0
36	Loma Prieta	0.50	41.3	0.30	145.6	2083.0	925.0	287.0	190.0	72.4	180.5
37	Loma Prieta	0.32	43.6	0.29	109.5	1682.0	822.0	277.0	116.0	73.9	115.4
38	Landers	0.28	42.7	0.21	240.4	2551.0	1976.0	210.0	173.0	98.4	168.7
39	Northridge	0.51	44.6	0.59	404.1	4521.0	1470.0	578.0	194.0	71.8	166.4
40	Dinar	0.32	40.6	0.33	194.3	2829.0	1310.0	327.0	212.0	80.6	212.8
41	Montenegro	0.24	47.1	0.19	129.4	1820.0	1200.0	190.0	199.0	106.3	191.4
42	Imperial Valley	0.55	49.7	0.41	166.0	2308.0	961.0	396.0	177.0	84.1	173.6
43	Cape Mendocino	0.59	48.3	0.36	343.2	3581.0	1633.0	352.0	197.0	99.4	168.2
44	Marmara	0.27	45.6	0.19	55.4	1084.0	533.0	182.0	74.6	75.5	81.9
45	Landers	0.24	50.8	0.18	94.3	1264.0	1133.0	175.0	150.0	106.6	154.6
46	Northridge	0.73	51.1	0.52	356.7	4117.0	1312.0	509.0	206.0	79.8	187.6
47	Northridge	0.51	52.6	0.42	316.2	3367.0	1551.0	414.0	254.0	90.3	240.8
48	Marmara	0.23	54.3	0.23	82.4	1460.0	793.0	227.0	115.0	105.0	108.9
49	Manjil	0.21	55.4	0.25	186.5	2708.0	1450.0	248.0	108.0	118.8	121.0
50	Northridge	0.35	59.9	0.25	100.2	1447.0	882.0	248.0	212.0	116.4	227.7
51	Loma Prieta	0.63	55.2	0.60	325.0	3804.0	1270.0	592.0	179.0	89.3	162.5
52	Düzce	0.75	58.2	0.65	386.6	3986.0	1519.0	643.0	241.0	99.6	227.5
53	Marmara	0.34	60.6	0.28	109.4	1851.0	869.0	275.0	160.9	112.7	160.3
54	Northridge	0.48	61.5	0.51	459.7	5302.0	1734.0	499.0	297.0	111.0	288.6
55	Loma Prieta	0.37	62.8	0.27	221.7	2580.0	1414.0	260.0	252.0	126.4	262.2
56	Imperial Valley	0.34	66.5	0.27	146.7	2108.0	974.0	252.0	199.0	122.3	213.2
57	Düzce	0.41	65.8	0.43	269.5	3686.0	1383.0	429.0	171.0	120.1	184.3
58	Düzce	0.82	66.9	0.49	252.4	2895.0	1197.0	480.0	263.0	116.0	254.1
59	Kobe	0.69	68.3	0.51	306.8	3622.0	1091.0	501.0	317.0	100.1	326.5
60	Bucharest	0.20	73.1	0.12	80.0	1667.0	575.0	120.0	229.0	118.3	253.2

Table 2.2 Continued

#	Earthquake	PGA (g)	PGV (cm/s)	EPA (g)	AI (cm/s)	I _c	CAV (cm/s)	ASI (cm/s)	VSI (cm)	I _F	HI (cm)
61	Northridge	0.58	74.8	0.63	435.7	4282.0	1521.0	624.0	239.0	116.8	244.5
62	Northridge	0.99	77.2	0.95	1667.8	11721.0	3623.0	933.0	305.0	145.5	268.3
63	Northridge	0.94	76.6	0.81	683.0	7514.0	1777.0	801.0	249.0	129.6	238.1
64	Kobe	0.63	75.0	0.53	543.3	5132.0	1809.0	523.0	293.0	131.9	273.5
65	Tabas	1.06	80.5	0.91	1148.0	8730.0	3424.0	900.0	300.0	166.0	293.0
66	Northridge	0.48	80.3	0.50	400.2	5693.0	1398.0	495.0	298.0	136.7	305.9
67	Northridge	0.75	84.8	0.49	444.1	5440.0	1450.0	478.0	303.0	142.0	272.9
68	Morgan Hill	1.30	80.8	0.67	384.5	4639.0	1047.0	658.0	295.0	108.0	253.3
69	Cape Mendocino	0.66	89.5	0.44	382.6	3885.0	1551.0	420.0	318.0	179.2	298.5
70	Düzce	0.51	86.1	0.40	290.8	3902.0	1342.0	393.0	259.0	156.4	273.7
71	Erzincan	0.47	92.1	0.39	212.5	3019.0	1036.0	387.0	258.0	165.3	254.6
72	Kobe	0.69	85.3	0.69	393.2	4363.0	1169.0	683.0	312.0	118.1	308.7
73	Tabas	0.91	90.2	0.83	1199.8	9023.0	3498.0	813.0	342.0	187.0	344.2
74	Northridge	0.59	94.7	0.58	566.6	5216.0	1689.0	572.0	398.0	145.2	362.8
75	Kobe	0.83	90.7	0.72	838.0	7446.0	2103.0	711.0	411.0	154.1	380.9
76	Imperial Valley	0.30	90.5	0.22	107.9	1784.0	726.0	219.0	220.0	145.8	247.5
77	Imperial Valley	0.37	95.9	0.39	167.6	2324.0	1002.0	390.0	187.0	168.8	224.4
78	Imperial Valley	0.44	113.1	0.31	177.5	2431.0	1045.0	300.0	179.0	191.6	227.2
79	Northridge	0.58	107.5	0.32	350.4	4383.0	1159.0	316.0	466.0	162.5	467.4
80	Northridge	0.59	99.3	0.45	559.7	6471.0	1600.0	441.0	503.0	155.1	477.7

2.2.1 Correlation Among Ground Motion Parameters

In order to investigate the correlation between ground motion parameters used in this study, Pearson's correlation coefficient were calculated as presented in Table 2.3. Correlation coefficient used to investigate the degree of interdependency among seismic parameters will be discussed in detail in Chapter 4.

Since AI, CAV and I_c are computed from the acceleration trace of the ground motion, strong correlation among them is observed (coefficient of correlation near 0.9). PGA is highly correlated with EPA, ASI and I_c. PGV on the other hand shows a high correlation with I_F, VSI and HI. As it can be inferred from Table 2.3, in general, acceleration-related indices show high correlation among them and same situation holds for velocity-related indices.

Table 2.3 Correlation among seismic parameters

GMI	PGA	PGV	EPA	AI	HI	I _c	CAV	ASI	VSI	I _F
PGA	1.000									
PGV	0.707	1.000								
EPA	0.922	0.651	1.000							
AI	0.796	0.591	0.868	1.000						
HI	0.731	0.915	0.681	0.651	1.000					
I _c	0.857	0.698	0.917	0.967	0.760	1.000				
CAV	0.735	0.593	0.811	0.918	0.657	0.908	1.000			
ASI	0.920	0.650	1.000	0.868	0.680	0.918	0.812	1.000		
VSI	0.775	0.884	0.725	0.692	0.990	0.797	0.683	0.724	1.000	
I _F	0.671	0.976	0.627	0.620	0.885	0.706	0.672	0.626	0.849	1.000

Among eleven ground motion parameters employed, PGA, AI, EPA, CAV, I_c and ASI can be regarded as acceleration-related indices and PGV, HI, VSI and I_F can be listed among velocity related parameters.

2.3 DESCRIPTION OF FRAMES

As stated before, low-to-mid rise reinforced concrete buildings constitute the majority of the building stock in Turkey. In order to achieve the goals of this study, sixteen reinforced concrete frames within the period of interest were employed. As shown in Figure 2.8, frames employed are 2-9 stories in height, majority of them having 3-6 stories.

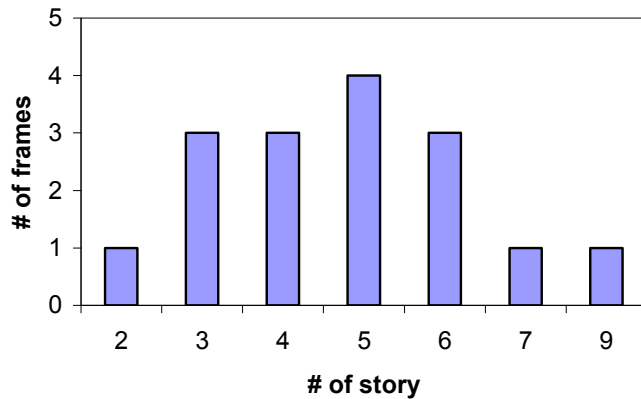


Figure 2.8 Story-wise distributions of frames

Selected frames for the analysis can be divided into two groups.

- Group 1, frames extracted from the Duzce database representing the general features of existing low-to-mid rise buildings in Turkish construction practice.
- Group 2, designed frames representing properly designed buildings that reflect the seismic provisions of the current code.

With the purpose of reflecting the peculiarities of existing buildings, frames F1-2S3B (two storey-two bay), F2-3S3B, F3-3S2B, F5-4S3B, F6-4S3B, F8-5S4B, F9-5S3B, F10-5S4B, F12-6S4B and F13-6S3B were extracted from the Düzce damage database. Düzce damage database was compiled after the 17 August 1999 Kocaeli and 12 November 1999 Düzce earthquakes and this database is comprised of 484 low-rise to medium-rise monolithic reinforced concrete buildings ranging from two to six stories, where all the buildings forming the database are located in the highest seismic zone of Turkey (Ozcebe et al., 2003).

Remaining frames are designed frames obtained from two different sources. F4-3S3B, F11-5S3B, F15-7S3B and F16-9S3B were taken from Ay (2006) where these frames were designed in order to have adequate structural capacity in terms of strength and ductility in a severe earthquake and satisfy the seismic provisions of Turkish seismic design code (1997). Design consideration and details about frames can be found in Ay (2006). The frames F7-4S3B and F14-6S3B were designed according to the highest seismic zone (zone 1, where effective peak ground acceleration of the design spectrum is considered to be 0.4g) requirements of Turkish seismic design code (1997).

Important features of these frames are presented in Table 2.4. Frames extracted from Duzce database have longitudinal reinforcement with yield strength (f_{yk}) of 220 MPa (typical value for older constructions in Turkey) whereas reinforcing steel with 420 MPa yield strength was used in designed frames. Average concrete compressive

strength (f_{ck}) of the analyzed frames is 18.6 MPa. It is important to note that the concrete strength values of the existing frames are in general much higher than the average concrete strength of the Duzce damage database (near 8 MPa) except for frame F3-3S2B.

Since the information on detailing of members was not available for Düzce frames, %1 reinforcement ratio was used for columns and beam reinforcements were provided under the action of gravity loads. The dynamic properties of the frames were obtained using the structural analysis software IDARC-2D (Valles et al., 1996). Details about the modeling of the frames will be discussed in Chapter 3. Appendix A presents additional information about the frames.

Table 2.4 Properties of the frames

FRAME	# of story	fck (Mpa)	fyk (Mpa)	Height (m)	Fundamental Period T_1 (s)	Total Weight (kN)	Modal participation factor (PF ₁)	Modal mass coefficient (α_1)
F1-2S3B	2	22	220	6.1	0.19	827	1.198	0.906
F2-3S3B	3	20	220	8.1	0.17	327	1.244	0.878
F3-3S2B	3	10	220	8.1	0.36	405	1.240	0.810
F4-3S3B	3	20	420	9.0	0.49	1507	1.265	0.862
F5-4S3B	4	20	220	10.8	0.42	753	1.257	0.877
F6-4S3B	4	20	220	10.8	0.32	637	1.239	0.930
F7-4S3B	4	20	420	12.0	0.53	2081	1.283	0.832
F8-5S4B	5	20	220	14.3	0.53	1628	1.218	0.935
F9-5S3B	5	22	220	14.5	0.46	886	1.289	0.824
F10-5S4B	5	14	220	15.9	0.55	2290	1.252	0.873
F11-5S3B	5	20	420	15.0	0.76	2546	1.302	0.820
F12-6S4B	6	15	220	16.9	0.49	1730	1.268	0.834
F13-6S3B	6	14	220	16.1	0.52	1443	1.295	0.814
F14-6S3B	6	20	420	18.0	0.72	3131	1.288	0.824
F15-7S3B	7	20	420	21.0	0.94	3585	1.338	0.783
F16-9S3B	9	20	420	27.0	1.07	4625	1.352	0.771

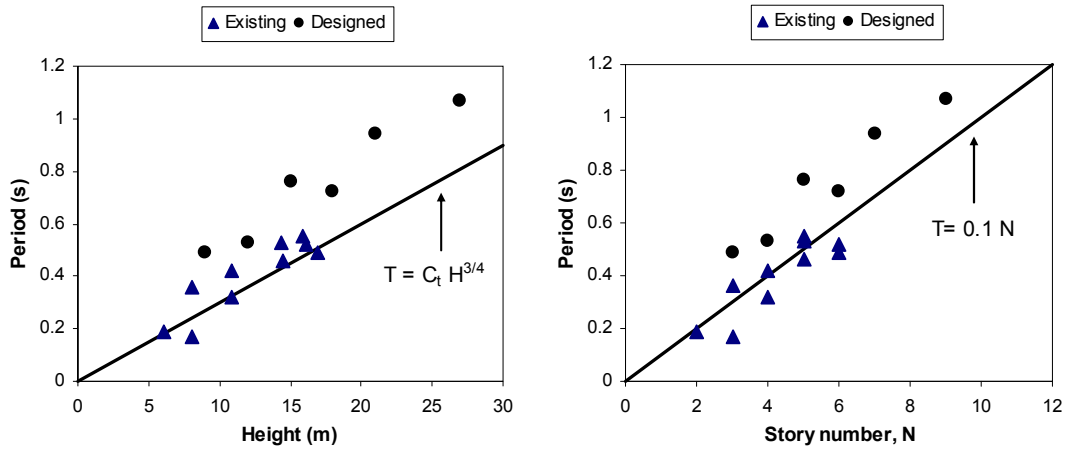


Figure 2.9 Computed and approximated periods

The fundamental periods of the frames computed from eigen-value analysis with respect to building height and story number (N) are shown in Figure 2.9 together with the approximate expressions used to calculate the fundamental period. Constant C_t depends on the type of the structural system and is equal to 0.07 for reinforced concrete frames as defined in Turkish seismic code (1997). In general, existing frames are in agreement with the approximate expressions whereas designed frames are softer than the approximated period values.

CHAPTER 3

ANALYSIS OF FRAMES

3.1 GENERAL

Evaluation of expected seismic deformation demands of structures under a prescribed or selected ground motion is the central theme of performance based earthquake engineering. It is experienced from the previous earthquakes that many buildings exhibit inelastic deformations when subjected to severe intensities, in other words they exceed their elastic limits. Structures have often been designed using the results of elastic analysis in many codes for decades. Considering the behavior of many structures beyond their elastic limits under high intensity excitations, nonlinearity in design and seismic evaluation becomes an important aspect of earthquake engineering. Traditional elastic procedures, also known as force-based procedures, could not identify the post-elastic behavior of structures, whereas displacement-based procedures are mainly based on deformations beyond elastic limit rather than forces and could handle the nonlinear behavior of the structure to some extent. Nonlinear static analysis (pushover analysis) and nonlinear response history analysis are the major components of the inelastic analysis used to compute displacement demands under a seismic event in performance based engineering.

Nonlinear response history analysis is the rigorous way of determining the displacement demand of a structure under a seismic excitation. Since preparing input, modeling and interpreting outputs is intricate and demanding, various approximate methods have been proposed in literature. Discussion and evaluation of those

methods can be found in Miranda and Garcia (2001) and Akkar and Miranda (2005). The estimation of inelastic deformation demand of MDOF structure from the maximum deformation demand of corresponding equivalent SDOF system forms the base of most of the approximate procedures. MDOF system is reduced to an equivalent SDOF system using the nonlinear static analyses results. Among two inelastic analysis procedures mentioned above, nonlinear response history analysis is a more rational approach to the nonlinear behavior of structures under seismic excitation. However due to its difficulty and computational effort required, nonlinear static analysis has been preferred for its simplicity in many applications.

This chapter presents the inelastic dynamic analysis results of selected sixteen reinforced concrete frames using both SDOF and MDOF models subjected to eighty un-scaled ground motion records. Firstly, nonlinear static analyses of the frames were carried out and results later were used in the derivation of corresponding equivalent SDOF system parameters. Then, nonlinear response history analyses of SDOF and MDOF systems were conducted and response parameters were computed. Finally, comparison of the nonlinear dynamic analyses results of equivalent SDOF and MDOF systems are presented.

3.2 MODELING

Inelastic analysis takes the post-yielding behavior of the structure into account contrary to traditional elastic analysis procedures where nonlinear behavior is considered confined to the elastic analysis assumptions. The accuracy of inelastic analyses of structural systems depends on the capabilities of the selected software and the interaction between the analyst and the program. In this study, frames were modeled using the well-known structural analysis software IDARC-2D (Valles et al., 1996). Both nonlinear static analyses (pushover analysis) and nonlinear response history analyses of MDOF models were carried out using the same software.

Following the traditional approach, selected reinforced concrete frames were modeled using beam and column elements using bilinear hysteretic model with no stiffness and strength degradation as shown in Figure 3.1. Column elements were modeled considering flexural, shear and axial deformations. Bilinear hysteretic model were used in order to model the flexural and shear components of the deformation. The axial deformation component was modeled using linear-elastic spring. Beam elements were modeled as flexural elements with shear deformations. The flexural component of the beam element was modeled using bilinear hysteretic model.

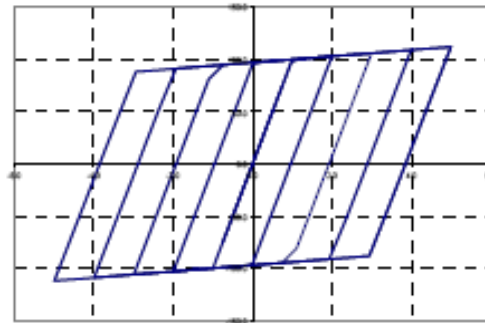


Figure 3.1 Bilinear hysteretic model (Valles et al., 1996)

Floor masses were lumped at the beam column joints. Rigid diaphragms were assigned to each floor level thus only one horizontal degree of freedom is required per floor, eventually this action reduces the computational effort. Rigid length zones were defined at the beam and column element ends to simulate the increase in stiffness at joints and the length of the rigid zone was taken as the half of the cross-section dimension of the connecting element. Effect of the infill walls was not taken into account and pure frame behavior was considered ignoring P- Δ effect. Mass proportional default 5% damping was used in the analyses.

It is well known that in reinforced concrete members, an effective confinement both increases the ductility and the strength of a member. Minimal, nominal and well confinement was defined in IDARC-2D (Valles et al., 1996) in order to reflect the

effectiveness of the confinement. Effectiveness of the confinement is defined by parameter CEFF (Figure 3.2). Minimal confinement was used for frames extracted from Duzce and well confinement was used for designed frames. Detailed information about IDARC-2D can be found in Valles et al. (1996).

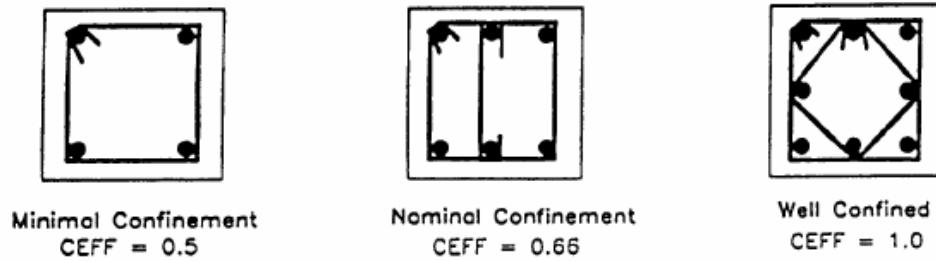


Figure 3.2 Confinement effectiveness (Valles et al., 1996)

3.3 NONLINEAR STATIC (PUSHOVER) ANALYSIS

Nonlinear static analysis, namely pushover analysis, is a simple and efficient technique to predict the seismic response prior to full dynamic analysis and has been widely used in predicting the seismic demand as a substitute to complex nonlinear response history analysis. The structure is being pushed laterally with a prescribed loading pattern until the structure reaches a limit state. Capacity of the structure is represented by a pushover curve plotted as base shear versus roof displacement and gives an insight into the structure's performance. Pushover curve gives an idea about how the structure behaves in elastic range as well as beyond its elastic limit.

As mentioned before, predicting the seismic demand of structures using approximate procedures mainly depends on the pushover results. Nonlinear dynamic analyses of the equivalent SDOF system, Capacity spectrum method (ATC-40, 1996) and Displacement Coefficients Method in FEMA 356 (ASCE, 2000) can be listed among the approximate procedures which make use of the pushover result of the structure.

The pushover analysis may be conducted using force control or displacement control. Force-controlled pushover analyses were conducted in this study using inverse triangular lateral load distribution (used in many building codes). Frames were subjected to an incremental distribution of lateral forces computed proportional to the mass and height of each story and the incremental displacements were computed accordingly. In the inverse triangular load distribution approach, the structure is considered to be subjected to a linear distribution of acceleration throughout the building height which is consistent with the first-mode dominant behavior. The high values of modal mass participation ratios of the first mode of the analyzed frames support the selection of lateral load distribution used in the analysis. Pushover curves attained for each frame using IDARC-2D (Valles et al., 1996) are depicted in Figure 3.3-3.5. Total weight and height of the employed frames are given in Table 3.1.

Table 3.1 Total weight and height of the selected frames

FRAME	H(m)	W(kN)	FRAME	H(m)	W(kN)
F1-2S3B	6.1	827	F9-5S3B	14.5	886
F2-3S3B	8.1	327	F10-5S4B	15.9	2290
F3-3S2B	8.1	405	F11-5S3B	15.0	2546
F4-3S3B	9.0	1507	F12-6S4B	16.9	1730
F5-4S3B	10.8	753	F13-6S3B	16.1	1443
F6-4S3B	10.8	637	F14-6S3B	18.0	3131
F7-4S3B	12.0	2081	F15-7S3B	21.0	3585
F8-5S4B	14.3	1628	F16-9S3B	27.0	4625

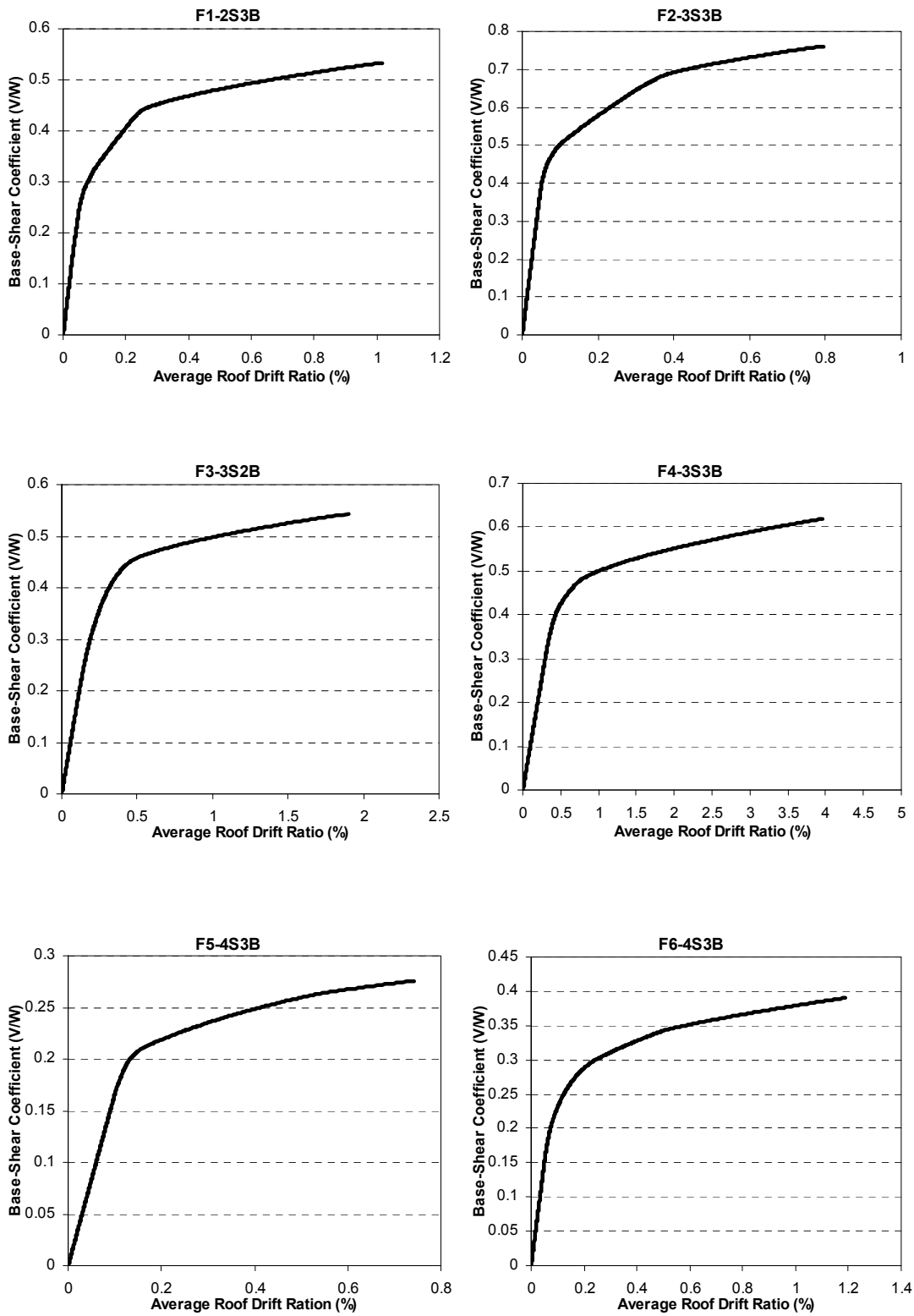


Figure 3.3 Pushover curves for frames F1-F6

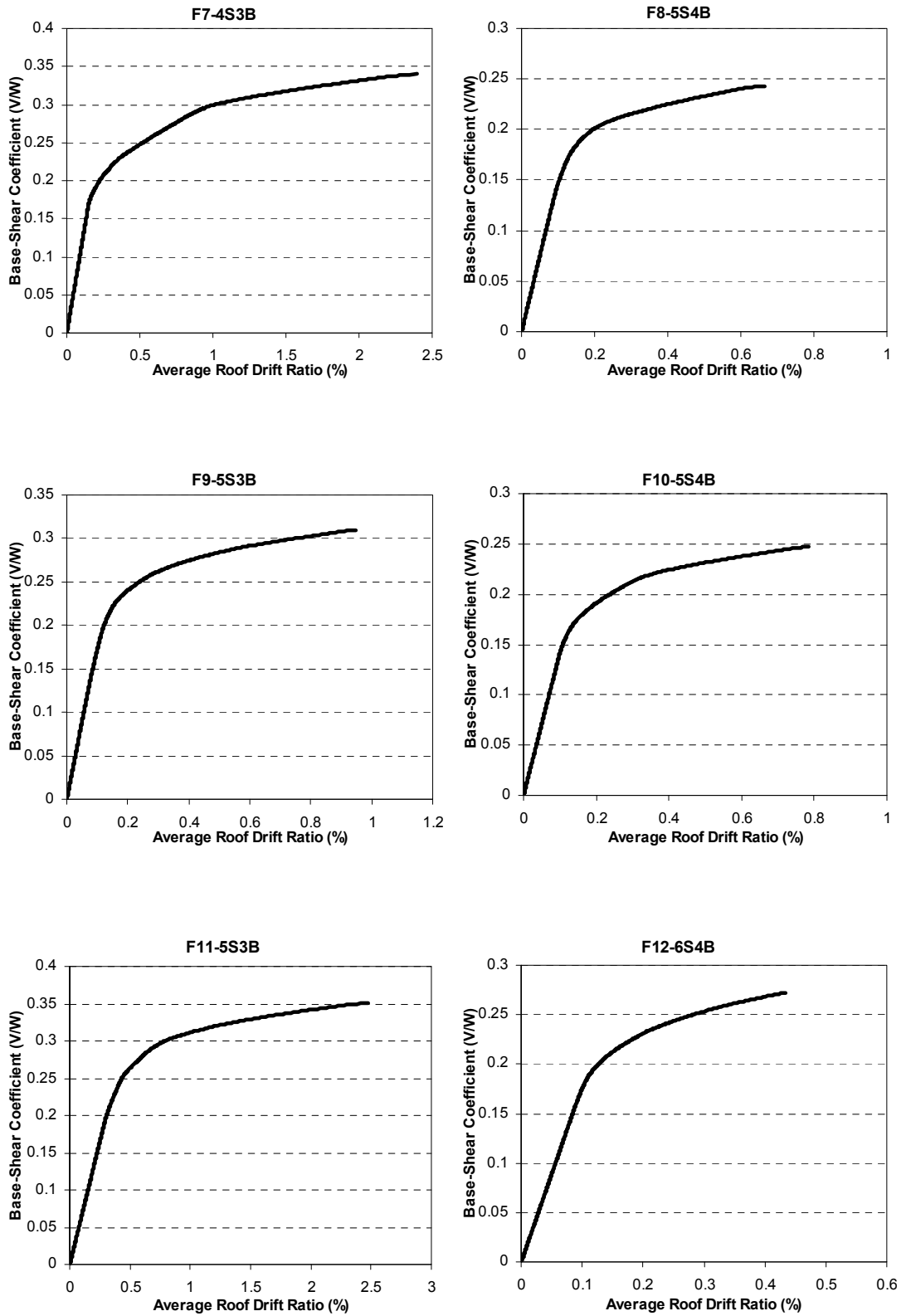


Figure 3.4 Pushover curves for frames F7-F12

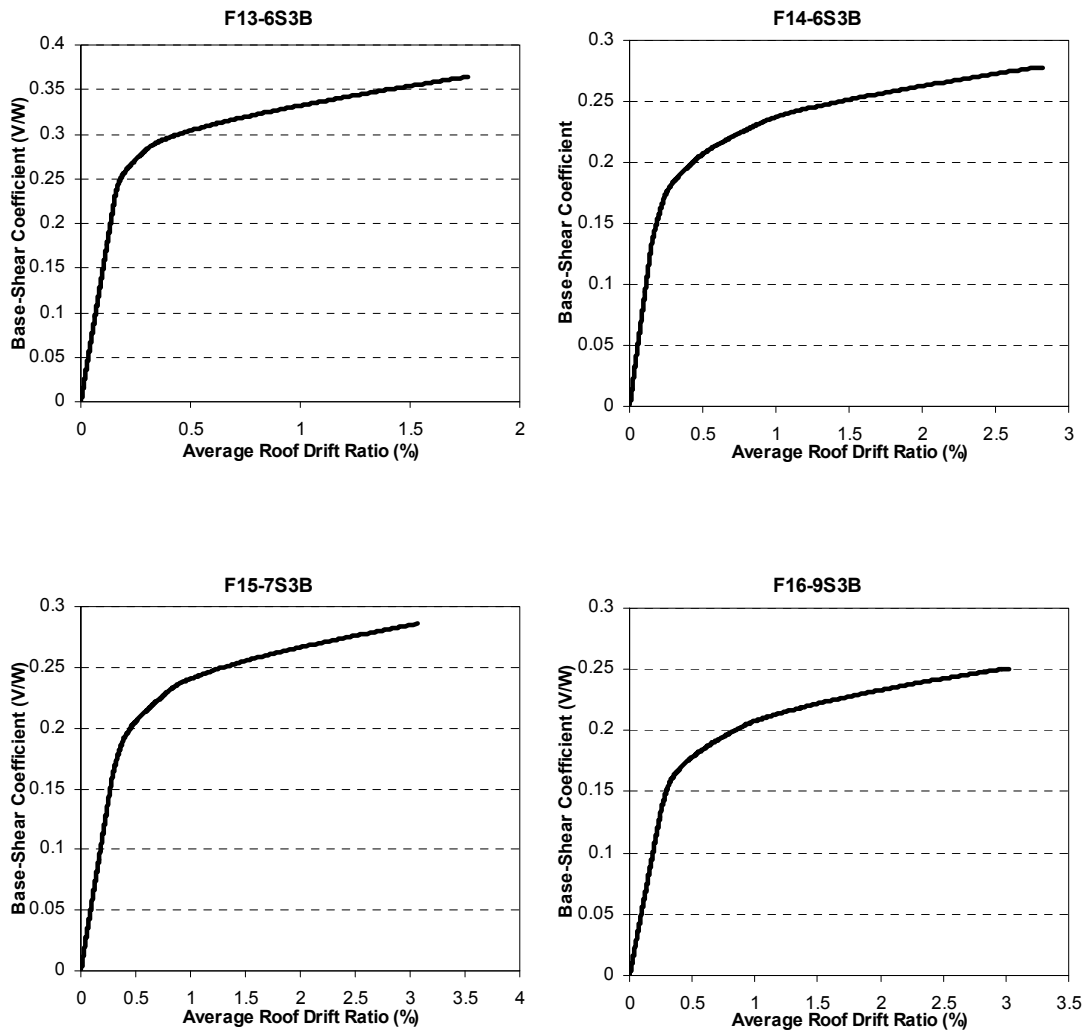


Figure 3.5 Pushover curves for frames F11-F16

3.3.1 Idealization of Pushover Curves

For common approximate procedures, bilinear representation of pushover curve is essential in order to obtain the inelastic displacement demand. Methods defined in ATC-40 (1996) and FEMA 356 (ASCE, 2000) are the two idealization procedures commonly used in literature. Pushover curves obtained from the nonlinear static analyses were bilinearized using the approach given in FEMA 356 (ASCE, 2000) for bilinearizing the capacity curve. In this approach, areas under the original and the idealized curve are set equal and the bilinear curve intersects the original curve at the 60% of the yield strength value. In other words, the effective stiffness K_e is taken as the secant stiffness calculated at 60% of yield strength of the structure. The post yield slope, α , is computed using the second line segment of the bilinearized curve passing through ultimate displacement. As inferred from the previous statement, iteration is required for bilinearization. This bilinearization approach can be seen graphically in Figure 3.6.

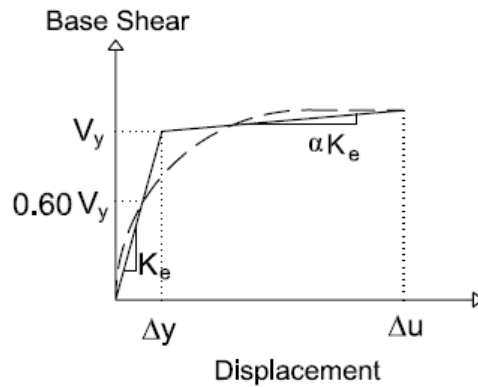


Figure 3.6 Original and idealized force-displacement curves

Idealized capacity curves will further be used in the determination of equivalent SDOF systems. Main features of idealized pushover curves derived are displayed in Table 3.2.

Table 3.2 Idealized pushover curve parameters

FRAME	Yield Base Shear coefficient (V/W)	Yield Roof Drift Ratio (%)	Ultimate Base Shear coefficient (V/W)	Maximum Roof Drift Ratio (%)
F1-2S3B	0.42	0.10	0.53	1.02
F2-3S3B	0.59	0.08	0.76	0.79
F3-3S2B	0.45	0.28	0.54	1.90
F4-3S3B	0.48	0.48	0.62	3.95
F5-4S3B	0.22	0.13	0.28	0.74
F6-4S3B	0.30	0.11	0.39	1.19
F7-4S3B	0.26	0.24	0.34	2.39
F8-5S4B	0.20	0.13	0.24	0.67
F9-5S3B	0.25	0.14	0.31	0.95
F10-5S4B	0.20	0.14	0.25	0.78
F11-5S3B	0.29	0.44	0.35	2.47
F12-6S4B	0.22	0.12	0.27	0.43
F13-6S3B	0.29	0.20	0.36	1.76
F14-6S3B	0.22	0.26	0.28	2.82
F15-7S3B	0.23	0.40	0.29	3.07
F16-9S3B	0.19	0.34	0.25	3.03

3.4 NONLINEAR RESPONSE HISTORY ANALYSIS

The nonlinear response history analysis is the most accurate way of determining the response of a structure subjected to an earthquake since the dynamic characteristics of a structure changes with time during a seismic excitation. The major advantage of the nonlinear response history analysis is that it captures the response of structure deforming into inelastic range during intense ground shaking in time domain.

Sixteen reinforced concrete frames utilized for this study were subjected to eighty un-scaled ground motions having a broad range of amplitude, frequency and duration characteristics. Since the structural damage sustained in reinforced concrete structures is highly related with lateral deformations, roof displacement for SDOF models, the roof displacement and the interstory drift ratio for MDOF models are the response parameters that are computed and used in the scope of this study.

3.4.1 SDOF Response History Analysis

Maximum roof displacement demand of a structure under a seismic excitation can be predicted using the nonlinear dynamic analysis result of equivalent SDOF system. The accuracy of the results depends on the ground motions and the properties of the MDOF system. Nonlinear response history analyses of the equivalent SDOF systems derived from the corresponding MDOF models of the selected frames were carried out using nonlinear SDOF models with bilinear force-deformation relationship with post-elastic stiffness.

The basic properties of the equivalent SDOF system were obtained using the guidelines in ATC-40 (1996). In this approach MDOF system is represented by a SDOF system having an effective modal mass (M^*) and an effective stiffness (K^*) as represented in Figure 3.7. Effective mass and stiffness values were attained using the bilinearized pushover curve of the MDOF system. The reader is referred to ATC-40 (1996) for detailed information about the derivation of equivalent SDOF systems. Equivalent SDOF system parameters computed for sixteen frames are shown in Table 3.3.

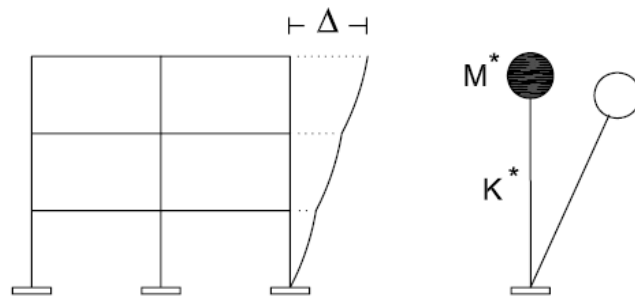


Figure 3.7 Equivalent SDOF system with mass M^* and stiffness K^*

Table 3.3 Properties of the equivalent SDOF systems

ID	T _{eff} (s)	S _{a_y} (g)	S _{d_y} (m)	F _y (kN)	K*(kN/m)	αK*	α(%)
F1-2S3B	0.210	0.463	0.0051	347.5	68236.8	1995.5	2.92
F2-3S3B	0.171	0.672	0.0049	192.7	39464.1	1185.0	3.00
F3-3S2B	0.364	0.555	0.0183	182.1	9957.5	352.5	3.54
F4-3S3B	0.497	0.557	0.0341	723.2	21185.0	842.4	3.98
F5-4S3B	0.423	0.251	0.0112	165.6	14818.9	792.2	5.35
F6-4S3B	0.346	0.323	0.0096	191.2	19937.6	610.7	3.06
F7-4S3B	0.538	0.313	0.0224	541.1	24108.2	826.9	3.43
F8-5S4B	0.536	0.214	0.0153	325.6	21338.8	1111.3	5.21
F9-5S3B	0.457	0.303	0.0158	221.5	14064.6	581.2	4.13
F10-5S4B	0.555	0.226	0.0173	451.2	26092.1	1403.8	5.38
F11-5S3B	0.760	0.354	0.0507	738.4	14566.6	661.8	4.54
F12-6S4B	0.503	0.261	0.0164	377.2	22999.0	2262.8	9.84
F13-6S3B	0.523	0.356	0.0242	418.6	17270.8	548.6	3.18
F14-6S3B	0.749	0.261	0.0363	673.1	18527.3	551.6	2.98
F15-7S3B	0.938	0.287	0.0628	806.7	12854.7	518.9	4.04
F16-9S3B	1.053	0.247	0.0679	878.7	12945.7	520.9	4.02

S_{a_y} and S_{d_y} in Table 3.3 are the yield spectral acceleration and displacement respectively computed from the idealized curve represented in acceleration-displacement response spectrum (ADRS) format. Force-displacement relationship and required modeling parameters of a simple SDOF system can be seen in Figure 3.8.

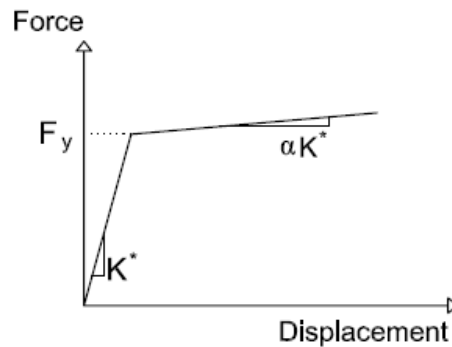


Figure 3.8 Force-displacement relationship of equivalent SDOF model

Roof displacement values and the corresponding ductility demands of the bilinear models were recorded for each analysis. Displacement ductility (μ) is simply the ratio of displacement demand under seismic excitation to the yield displacement of the corresponding system, where ductility demand equal or less than 1 implies elastic response. Distribution of the displacement ductility (μ) demands computed from the nonlinear response history analyses of SDOF systems are displayed in Figures 3.9 and 3.10 for elastic and inelastic range respectively.

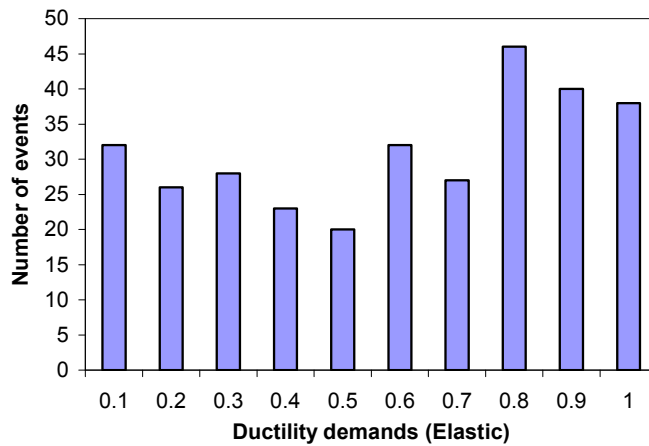


Figure 3.9 Elastic ductility demands

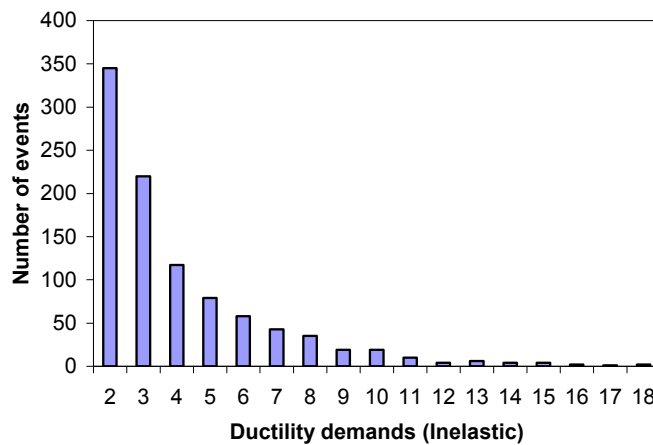


Figure 3.10 Inelastic ductility demands

Examining the Figure 3.9 and 3.10, it is obvious that both elastic and inelastic responses of SDOF models were obtained under the action of selected ground motion data set. Among the 1280 nonlinear analysis, 312 cases resulted in displacement ductility less than 1.

3.4.2 MDOF Response History Analysis

A total number of 1280 nonlinear response history analyses of reinforced concrete frames modeled as beam and column elements were conducted. The deformation measures of interest here are the roof displacements and the interstory drift ratios to quantify the response of MDOF models. Maximum interstory drift ratio was employed for correlation study.

Interstory drift ratio is simply calculated by dividing the difference between lateral deformations of two consecutive stories by the height of the corresponding story; similarly global drift ratio is computed by dividing the roof displacement by building height. Global drift ratio is also called average interstory drift ratio (AIDR). Maximum interstory drift refers to the maximum drift over the height of the structure, which may occur in different stories under different ground motions.

It is obvious that elastic and inelastic responses will be different due to the inherent nonlinear properties of structures. In order to approximately determine the elastic limits for the MIDR of each frame pushover curve results were used. In this approximate method, yield points were identified on the idealized curves employing the approach proposed in FEMA 356 (ASCE, 2000) for bilinearizing the capacity curve and later maximum MIDR values corresponding to the yield point were computed for each frame (Figure 3.11).

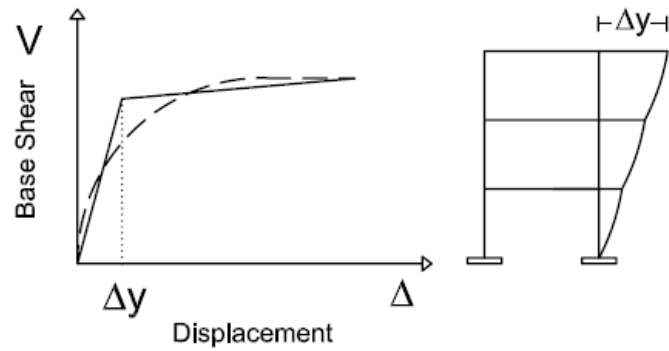


Figure 3.11 Computation of yield MIDR

As shown in Figure 3.11, structure was pushed to the yield displacement of the idealized capacity curve and the corresponding lateral deformations of each story were computed. Yield MIDR values were determined by taking the maximum value of the interstory demands calculated. Table 3.4 shows yield MIDR values computed for the frames.

Table 3.4 Yield MIDR values of the selected frames

FRAME	Yield MIDR (%)	FRAME	Yield MIDR (%)
F1-2S3B	0.11	F9-5S3B	0.30
F2-3S3B	0.09	F10-5S4B	0.20
F3-3S2B	0.44	F11-5S3B	0.60
F4-3S3B	0.60	F12-6S4B	0.18
F5-4S3B	0.16	F13-6S3B	0.26
F6-4S3B	0.16	F14-6S3B	0.36
F7-4S3B	0.32	F15-7S3B	0.52
F8-5S4B	0.23	F16-9S3B	0.46

Figure 3.12 presents the distribution of MIDR obtained from response history analyses for the frames employed under the ground motion set considered. Yield MIDR values for the frames presented in Table 3.4 and distribution of computed MIDR's in Figure 3.12 provide sufficient evidence that the analyzed frames were subjected to significant nonlinearity for most cases.

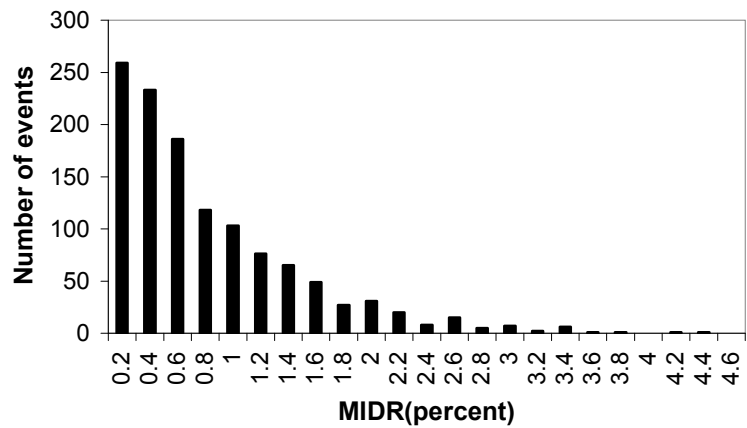


Figure 3.12 MIDR distribution of results

Association between average and the maximum interstory drift demands computed may be used to assess the response of the frames. Examining the Figure 3.13, where relationship between average interstory drift ratio and the maximum interstory drift ratio is depicted, it can be concluded that the frames employed did not show significant irregular response as evidenced by the strong correlation between the maximum and average interstory drift ratios. Displacement profiles of the frames subjected to Morgan Hill (#1), Companso Lucano (#10) and Northridge (#24) earthquakes are displayed in Figures 3.14, 3.15 and 3.16.

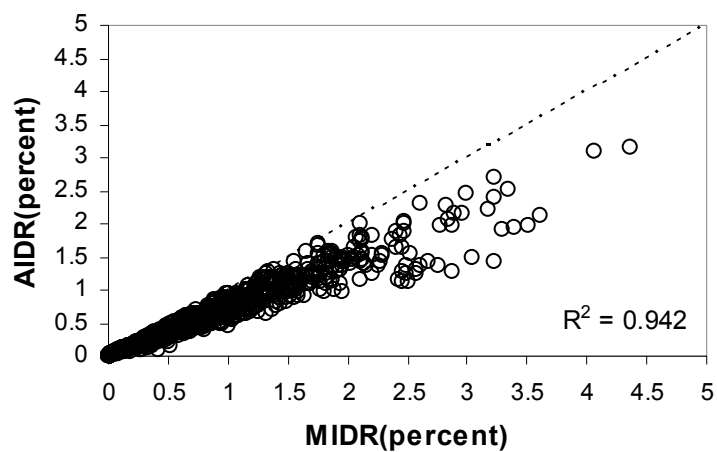


Figure 3.13 Relationship between average and maximum interstory drift ratio

◆ 1-Morgan Hill ■ 10-Campano-Luc. ▲ 24-Northridge

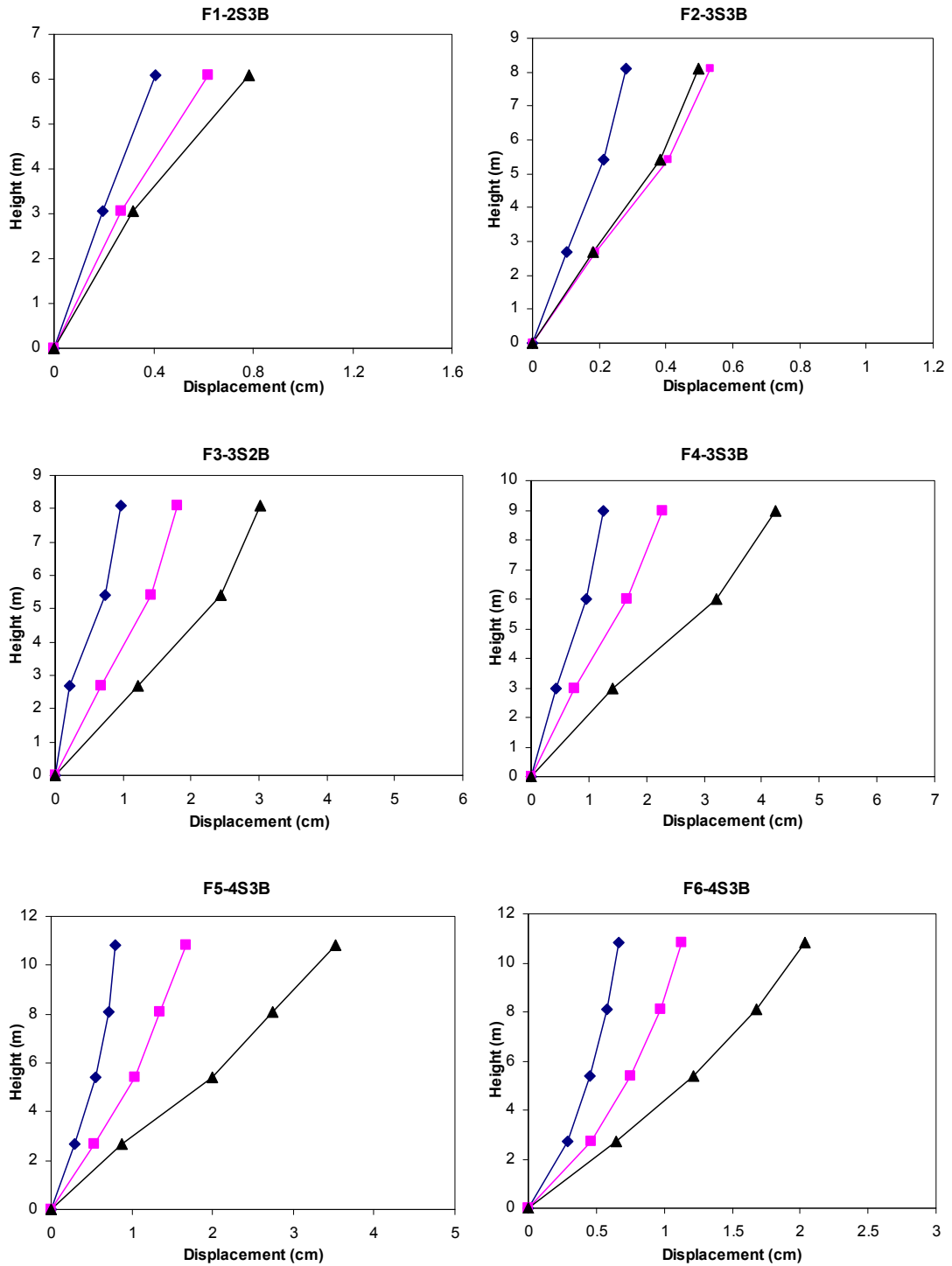


Figure 3.14 Displacement profiles of frames F1-F6

◆ 1-Morgan Hill ■ 10-Campano-Luc. ▲ 24-Northridge

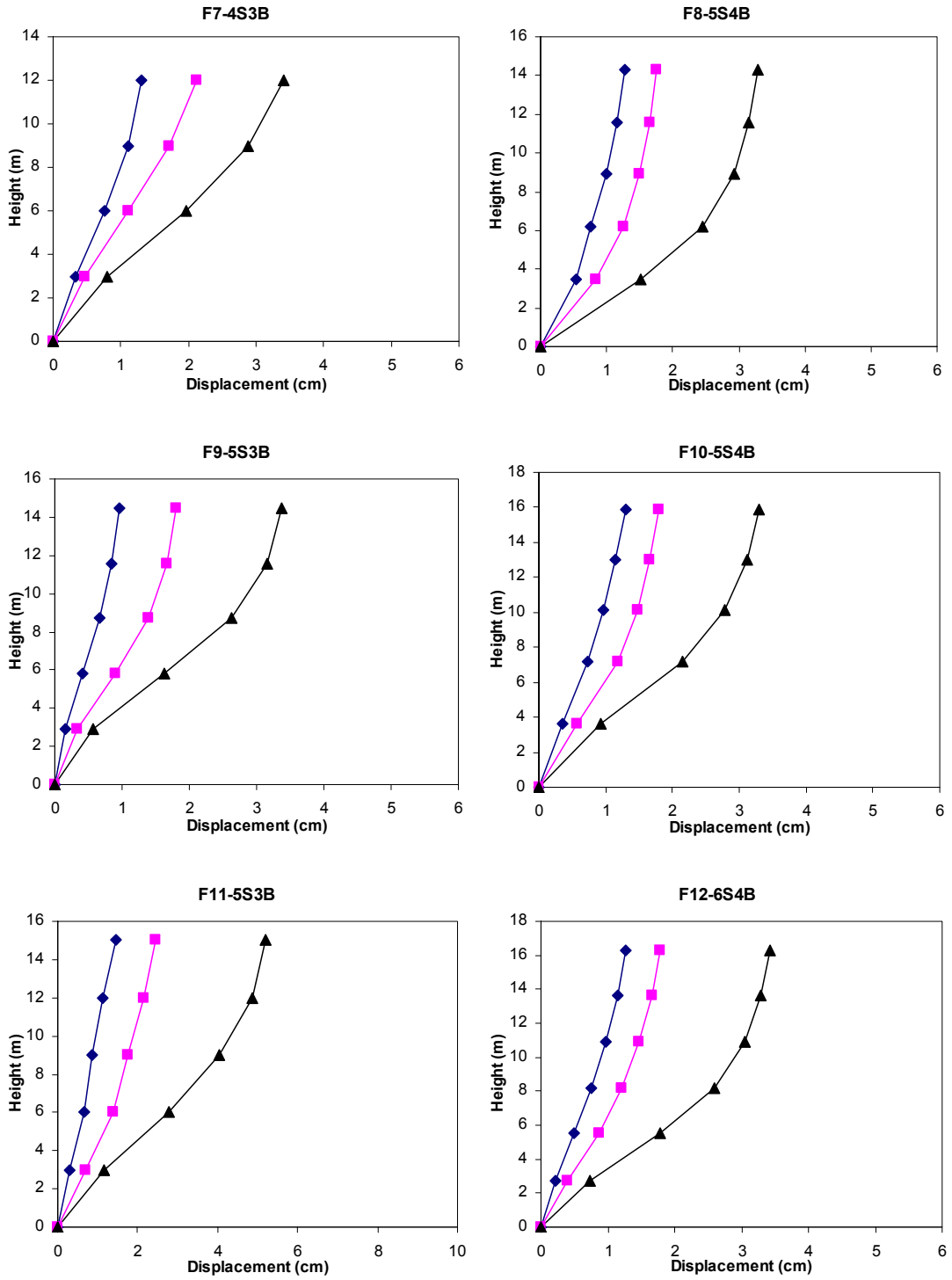


Figure 3.15 Displacement profiles of frames F7-F12

◆ 1-Morgan Hill ■ 10-Campano-Luc. ▲ 24-Northridge

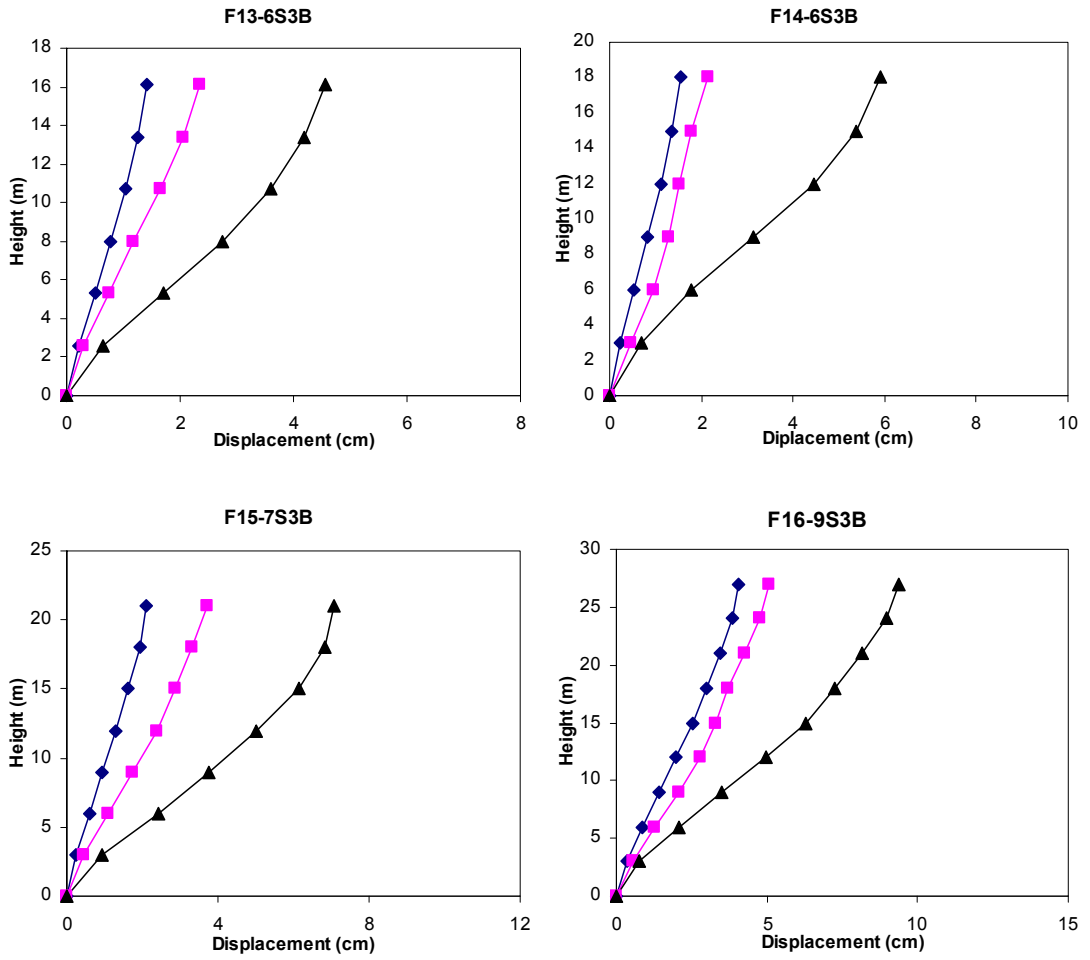


Figure 3.16 Displacement profiles of frames F13-F16

3.4.3 Comparison of SDOF and MDOF Results

Reduction of MDOF system to equivalent SDOF representation is an approximate method to compute the displacement demands of MDOF system. Roof displacements obtained using the equivalent SDOF system is plotted against the roof displacements attained from the nonlinear response history analyses of MDOF system as presented in Figure 3.17. Graphical comparison of the roof displacement results in Figure 3.17 reveals that the equivalent SDOF system yields adequate results for small displacement demands, however difference between MDOF and SDOF results increases as the level of inelasticity increases. In general, equivalent SDOF system underestimates the results for large deformations.

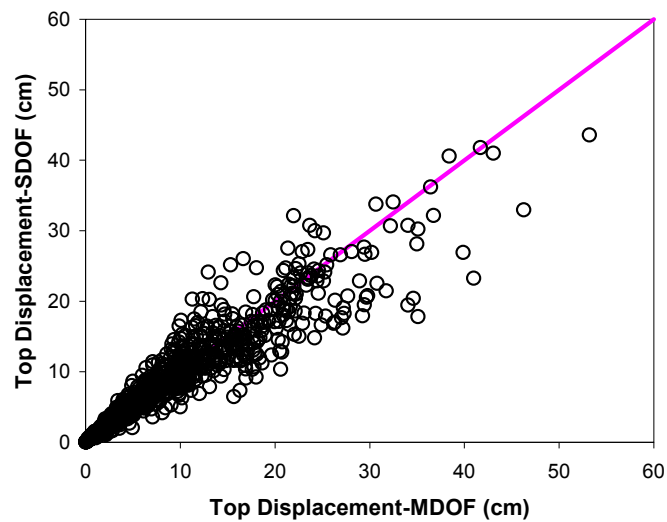


Figure 3.17 Comparison of SDOF and MDOF results

It is well known that the degree of higher mode effects and the irregularities existing in the system that can not be reflected in equivalent SDOF model may alter the results of approximate methods. General agreement of SDOF and MDOF results implies first mode dominant regular response of the employed frames.

3.5 DISCUSSION OF RESULTS

Validity of the outcomes of a particular study aiming to investigate the interdependency between ground motion parameters and the structural demand measures depends on the ground motions used and the properties of the employed frames. General features of the ground motion records and the selected ground motion parameters were discussed in the previous section. The motivation behind the compilation of the dataset with broad range of intensities was to observe both elastic and inelastic response of the frames. Distribution of response parameters for SDOF (ductility demand) and MDOF (maximum interstory drift) models are the evidences for the response beyond elastic limits.

General agreement of the SDOF and MDOF model's inelastic analyses results suggest that the employed frames do not show irregular response. Moreover, employed frames were not subjected to significant higher mode effects since the reduction of MDOF system to equivalent SDOF system in order to compute displacement demand relies on the first mode dominant behavior of the MDOF model. Also high interdependency between average and maximum interstory drift ratios implies the proper response of the selected frames.

CHAPTER 4

CORRELATION STUDY

4.1 GENERAL

Defining the destructiveness of an earthquake to building structures is a very important task in design and performance evaluation. An appropriate assessment of the intensity of an earthquake is essential for seismic hazard analysis. Many ground motion parameters have been defined as a measure of earthquake damage potential in the literature. Adequacy of ground motion parameters to reflect the severity of ground shaking has been studied by researcher through analytical studies as well as investigating the observed damage after earthquakes. Correlation coefficients are widely employed in these studies to investigate the efficiency of the parameters.

Peak ground acceleration (PGA), peak ground velocity (PGV), effective peak acceleration (EPA), Arias intensity (AI), cumulative absolute velocity (CAV), characteristic intensity (I_c), acceleration spectrum intensity (ASI), Housner intensity (HI), velocity spectrum intensity (VSI), Fajfar intensity (I_F) and spectral acceleration at the fundamental period (S_a) are selected and employed in the correlation study. Previous studies point out the relationship between the above mentioned parameters and the structural response (Riddell, 2007; Akkar and Ozen, 2005; Elenas and Meskouris, 2001; Cabanas et. al, 1999).

This chapter is devoted to the correlation study. First part of this chapter includes the correlation study for analytical models. Correlation of response parameters with

ground motion indices were investigated using the results presented for the sixteen reinforced concrete frames described in Chapter 2. Damage inducing response parameters of interest are maximum displacement demand for SDOF models and maximum interstory drift demand for MDOF models. In the second part, relationship between the observed damage after Northridge earthquake and the recorded ground motion parameters were examined using the database in ATC-38 (2000) that includes the performance of buildings in the vicinity of the recording stations.

4.2 CORRELATION WITH ANALYTICAL RESULTS

Interrelationship between the selected ground motion intensity indices and the structural response parameters has been quantified. First, nonlinear dynamic analyses were carried out to provide the structural response for a given seismic event and a given model (results are presented and discussed in Chapter 3). Then, the degree of interdependency between the computed response parameters and the seismic indices were investigated through correlation coefficients. The presented methodology is applied to both SDOF and MDOF models derived from sixteen reinforced concrete frames.

4.2.1 Correlation Measures

In order to get a measure of how strongly ground motion parameters and the selected demand measures are related, coefficient of correlation measures were used. In order to evaluate the relative adequacy of each ground motion parameter, coefficients of determination (R^2) were computed for each curve fit in addition to Pearson's correlation coefficient (ρ).

Pearson correlation coefficient (ρ) measures the strength and the direction of a linear relationship between two variables and ranges from -1 to +1, where + and - signs

indicate the positive and negative correlation respectively. Needless to say ρ value of 1 indicates a perfect fit. A correlation greater than 0.8 is generally described as strong, whereas a correlation less than 0.5 is generally described as weak. Values in between can be interpreted as moderate correlation. The R^2 value is an indicator that takes values between 0-1.0 and reveals how closely the values predicted (Y_{pi}) through a trend line correspond to the actual data (Y_i). These coefficients are determined using Equations 4.1 and 4.2, where Y_m is the mean value and n is the total number of points.

$$R^2 = \frac{\sum (Y_{pi} - Y_m)^2}{\sum (Y_i - Y_m)^2} \quad (4.1)$$

$$\rho = \frac{n(\sum XY) - (\sum X)(\sum Y)}{\sqrt{[n\sum X^2 - (\sum X)^2][n\sum Y^2 - (\sum Y)^2]}} \quad (4.2)$$

As it is well known, Pearson correlation coefficient is equal to the square root of uncorrected R^2 value computed for the linear fit. The R^2 values that will be presented in this study are the corrected ones.

4.2.2 Demand Measures

A proper response parameter as an indicator of damage in reinforced concrete frames must be set in order to conduct a valid study. Roof displacement, interstory drift, concrete and steel strain, curvature ductility, plastic rotation, hysteretic energy dissipated are widely employed engineering demand measures. Among the several engineer demand measures, attention has been paid to the maximum displacement for SDOF models and maximum interstory drift for MDOF models considering the dependence between lateral deformation and the damage sustained in reinforced concrete frames.

Researchers (Algan, 1982; Moehle, 1994; Moehle, 1992; Miranda, 1999; Gulkan and Sozen, 1999) employed maximum interstory drift and global drift as a damage inducing parameter in their studies. FEMA 356 (ASCE, 2000), ATC-40 (1996) and Eurocode 8 (2003) employed the expected performance expressed in terms of these response parameters for seismic performance assessment of individual buildings.

4.2.3 Correlation Study for SDOF Response

After performing the nonlinear response history analyses for the SDOF system, maximum displacement demands were computed for each analysis and compared with the ground motion intensity measures through coefficients of correlation and determination. Coefficient of correlation (Pearson's linear correlation coefficient) was computed for the overall response whereas coefficients of determination (R^2) values were computed in three ranges as follows:

- Linear and nonlinear range, for all displacement ductility (μ) values.
- Linear range, where μ is equal or less than 1.
- Nonlinear range, where μ is greater than 1.

As it is well known, the general trend of structural response with the seismic intensity follows a nonlinear relation especially in the nonlinear response range. This is the motivation behind the computation of coefficients of determination values for three discrete ranges. The coefficients of determination values were computed first based on linear lines fitted through the data, overall response. In addition, in the linear and nonlinear response ranges, linear and exponential relationships were assumed (Figure 4.1). Table 4.1 presents the results for Pearson's correlation coefficient for overall response. Results attained for coefficient of determination for sixteen frames in three ranges are given in Table 4.2.

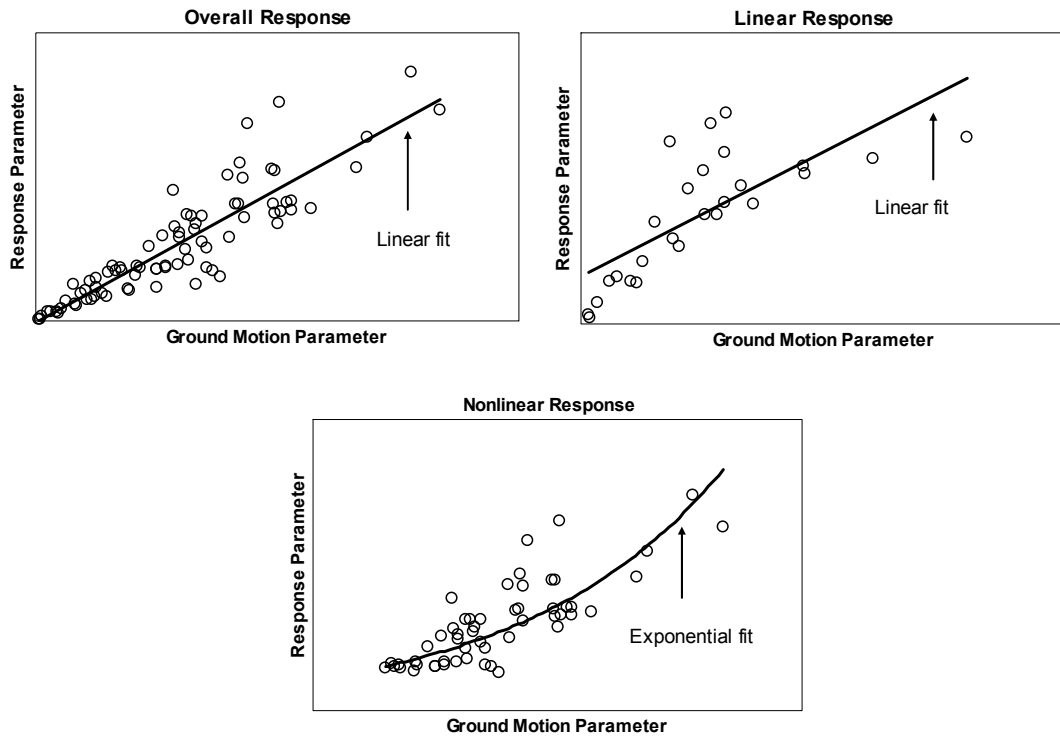


Figure 4.1 Fitted lines for overall, linear and nonlinear response

Table 4.1 Pearson's coefficient results for overall response (SDOF)

ID	PGA	PGV	S _a	ASI	VSI	I _c	I _F	CAV	AI	HI	EPA	OVERALL RESPONSE
F1-2S3B	0.900	0.623	0.784	0.862	0.720	0.817	0.562	0.642	0.760	0.666	0.862	
F2-3S3B	0.917	0.557	0.927	0.889	0.615	0.803	0.524	0.682	0.781	0.571	0.890	
F3-3S2B	0.850	0.693	0.845	0.850	0.775	0.812	0.639	0.675	0.770	0.729	0.851	
F4-3S3B	0.856	0.688	0.876	0.805	0.791	0.765	0.638	0.634	0.699	0.745	0.807	
F5-4S3B	0.802	0.794	0.703	0.730	0.891	0.765	0.736	0.613	0.669	0.860	0.731	
F6-4S3B	0.852	0.737	0.742	0.780	0.843	0.803	0.681	0.644	0.732	0.802	0.782	
F7-4S3B	0.809	0.785	0.815	0.749	0.877	0.782	0.741	0.645	0.686	0.849	0.751	
F8-5S4B	0.733	0.822	0.730	0.643	0.907	0.707	0.767	0.565	0.599	0.890	0.646	
F9-5S3B	0.801	0.775	0.766	0.738	0.863	0.752	0.724	0.615	0.662	0.832	0.739	
F10-5S4B	0.733	0.818	0.737	0.649	0.902	0.708	0.762	0.567	0.598	0.885	0.651	
F11-5S3B	0.717	0.784	0.831	0.648	0.893	0.710	0.737	0.587	0.590	0.874	0.649	
F12-6S4B	0.827	0.799	0.800	0.741	0.902	0.777	0.746	0.626	0.677	0.871	0.743	
F13-6S3B	0.806	0.739	0.838	0.753	0.829	0.743	0.695	0.617	0.655	0.794	0.754	
F14-6S3B	0.716	0.817	0.809	0.629	0.896	0.693	0.771	0.580	0.585	0.883	0.630	
F15-7S3B	0.690	0.834	0.888	0.599	0.913	0.676	0.795	0.569	0.558	0.909	0.600	
F16-9S3B	0.635	0.809	0.905	0.547	0.917	0.650	0.771	0.546	0.535	0.915	0.548	

Table 4.2 Coefficient of determination values for the three ranges (SDOF)

ID	PGA	PGV	S _a	ASI	VSI	I _c	I _F	CAV	AI	HI	EPA	OVERALL RESPONSE
F1-2S3B	0.809	0.388	0.615	0.742	0.518	0.667	0.315	0.413	0.578	0.444	0.744	
F2-3S3B	0.841	0.311	0.860	0.790	0.379	0.645	0.274	0.465	0.610	0.326	0.792	
F3-3S2B	0.723	0.480	0.715	0.723	0.601	0.660	0.408	0.455	0.593	0.532	0.724	
F4-3S3B	0.732	0.473	0.767	0.649	0.626	0.586	0.407	0.402	0.488	0.555	0.652	
F5-4S3B	0.643	0.631	0.494	0.533	0.794	0.585	0.541	0.376	0.447	0.740	0.534	
F6-4S3B	0.726	0.543	0.551	0.609	0.711	0.645	0.464	0.415	0.536	0.644	0.611	
F7-4S3B	0.655	0.617	0.664	0.561	0.769	0.611	0.550	0.416	0.471	0.720	0.564	
F8-5S4B	0.538	0.675	0.532	0.414	0.822	0.499	0.588	0.320	0.359	0.792	0.417	
F9-5S3B	0.642	0.601	0.587	0.544	0.745	0.565	0.525	0.378	0.438	0.693	0.546	
F10-5S4B	0.538	0.669	0.543	0.421	0.814	0.502	0.581	0.321	0.358	0.783	0.423	
F11-5S3B	0.514	0.615	0.691	0.420	0.797	0.504	0.543	0.345	0.349	0.764	0.421	
F12-6S4B	0.684	0.638	0.641	0.550	0.814	0.603	0.556	0.393	0.458	0.758	0.553	
F13-6S3B	0.650	0.547	0.702	0.567	0.687	0.552	0.483	0.380	0.430	0.631	0.569	
F14-6S3B	0.513	0.667	0.654	0.396	0.803	0.480	0.594	0.336	0.342	0.780	0.397	
F15-7S3B	0.476	0.695	0.788	0.358	0.834	0.457	0.632	0.324	0.311	0.827	0.360	
F16-9S3B	0.403	0.654	0.818	0.299	0.841	0.422	0.594	0.298	0.286	0.838	0.301	

ID	PGA	PGV	S _a	ASI	VSI	I _c	I _F	CAV	AI	HI	EPA	LINEAR RESPONSE
F1-2S3B	0.613	0.152	1.000	0.668	0.168	0.352	0.202	0.467	0.316	0.152	0.671	
F2-3S3B	0.655	0.172	0.998	0.746	0.254	0.505	0.173	0.380	0.396	0.201	0.748	
F3-3S2B	0.757	0.307	0.997	0.897	0.352	0.500	0.320	0.341	0.345	0.292	0.895	
F4-3S3B	0.711	0.547	0.995	0.669	0.675	0.660	0.510	0.374	0.475	0.644	0.671	
F5-4S3B	0.722	0.854	0.999	0.932	0.939	0.963	0.874	0.864	0.867	0.909	0.938	
F6-4S3B	0.843	0.333	0.999	0.928	0.442	0.622	0.405	0.520	0.571	0.394	0.922	
F7-4S3B	0.497	0.721	0.993	0.518	0.811	0.644	0.621	0.431	0.477	0.717	0.521	
F8-5S4B	0.706	0.670	0.999	0.774	0.896	0.900	0.573	0.666	0.878	0.728	0.785	
F9-5S3B	0.767	0.658	1.000	0.842	0.662	0.894	0.562	0.658	0.889	0.519	0.850	
F10-5S4B	0.635	0.728	0.997	0.712	0.827	0.805	0.614	0.601	0.685	0.711	0.719	
F11-5S3B	0.274	0.457	1.000	0.221	0.547	0.323	0.437	0.359	0.243	0.540	0.219	
F12-6S4B	0.786	0.688	0.999	0.847	0.708	0.797	0.596	0.580	0.628	0.592	0.851	
F13-6S3B	0.623	0.466	0.999	0.673	0.746	0.733	0.482	0.589	0.627	0.694	0.676	
F14-6S3B	0.458	0.691	1.000	0.459	0.872	0.556	0.730	0.704	0.460	0.810	0.463	
F15-7S3B	0.422	0.699	1.000	0.274	0.801	0.351	0.695	0.477	0.275	0.818	0.274	
F16-9S3B	0.164	0.633	1.000	0.170	0.776	0.287	0.643	0.435	0.202	0.849	0.169	

ID	PGA	PGV	S _a	ASI	VSI	I _c	I _F	CAV	AI	HI	EPA	NONLINEAR RESPONSE
F1-2S3B	0.776	0.304	0.573	0.750	0.498	0.620	0.230	0.353	0.506	0.411	0.754	
F2-3S3B	0.692	0.099	0.738	0.693	0.083	0.407	0.099	0.324	0.407	0.063	0.700	
F3-3S2B	0.674	0.395	0.609	0.657	0.506	0.574	0.308	0.358	0.504	0.424	0.659	
F4-3S3B	0.587	0.233	0.645	0.449	0.429	0.380	0.173	0.218	0.334	0.335	0.455	
F5-4S3B	0.649	0.632	0.538	0.571	0.738	0.579	0.554	0.380	0.430	0.696	0.573	
F6-4S3B	0.707	0.546	0.503	0.608	0.710	0.635	0.451	0.399	0.499	0.648	0.611	
F7-4S3B	0.591	0.476	0.516	0.470	0.676	0.517	0.400	0.314	0.393	0.621	0.473	
F8-5S4B	0.575	0.700	0.601	0.458	0.791	0.496	0.613	0.282	0.353	0.767	0.462	
F9-5S3B	0.653	0.597	0.599	0.561	0.719	0.555	0.515	0.330	0.417	0.670	0.564	
F10-5S4B	0.553	0.659	0.574	0.432	0.774	0.484	0.573	0.303	0.344	0.747	0.436	
F11-5S3B	0.362	0.393	0.579	0.283	0.640	0.354	0.314	0.173	0.236	0.571	0.284	
F12-6S4B	0.666	0.600	0.638	0.543	0.765	0.562	0.596	0.580	0.628	0.592	0.851	
F13-6S3B	0.615	0.451	0.678	0.506	0.624	0.485	0.381	0.296	0.370	0.557	0.508	
F14-6S3B	0.466	0.575	0.638	0.344	0.720	0.431	0.509	0.295	0.307	0.702	0.345	
F15-7S3B	0.324	0.517	0.741	0.196	0.745	0.298	0.428	0.155	0.193	0.734	0.197	
F16-9S3B	0.252	0.562	0.705	0.142	0.795	0.296	0.502	0.159	0.189	0.795	0.142	

In order to have an idea about the degree of correlation in general, correlation results were averaged for each ground motion parameter and presented in Table 4.3. Examining the average results in Table 4.3, ground motion intensity parameters VSI and HI have the highest correlation with SDOF displacement demand followed by S_a , PGA and PGV. It is apparent from the average results that the spectrum based parameters have stronger correlation with the structural demand. I_c , EPA, ASI and I_F provided poor results on average for the analyzed frames covering a period range of 0.17-1.07 s. AI and CAV have the lowest correlation with response.

Due to dominant first mode response, correlation coefficient obtained for S_a is nearly 1 for all models in the linear range (Table 4.2). It is important to note that bilinear models with post elastic stiffness were used in the computation of response parameters.

Table 4.3 Average correlation of ground motion parameters with roof displacement

GMI	Coefficient of determination (R^2)			Pearson's correlation
	Linear response	Nonlinear response	All	
VSI	0.655	0.638	0.722	0.846
HI	0.598	0.583	0.677	0.817
S_a	0.998	0.617	0.664	0.812
PGA	0.602	0.571	0.630	0.790
PGV	0.548	0.484	0.575	0.755
I_c	0.618	0.480	0.561	0.748
EPA	0.648	0.501	0.538	0.727
ASI	0.646	0.479	0.536	0.726
I_F	0.527	0.415	0.503	0.705
AI	0.521	0.382	0.441	0.660
CAV	0.528	0.307	0.377	0.613

Among the eleven ground motions employed, PGA, EPA, CAV, AI, I_c and ASI are acceleration related parameters whereas PGV, I_F , VSI and HI are velocity related parameters (Riddell, 2007). Indices in each group are well correlated among themselves, as discussed in Chapter 2.

Examining the correlation results of overall response of the frames presented in Table 4.2, in general there is tendency in acceleration related parameters to have a higher degree of correlation with displacement demand as the number of stories, or periods, decreases. Similarly, this trend can be observed in velocity related parameters, where the correlation increases as the number of stories increases. To observe this trend for each frame graphically, coefficient of determination values presented in Table 4.2 are plotted against period in Figures 4.2 and 4.3 for acceleration and velocity related parameters respectively.

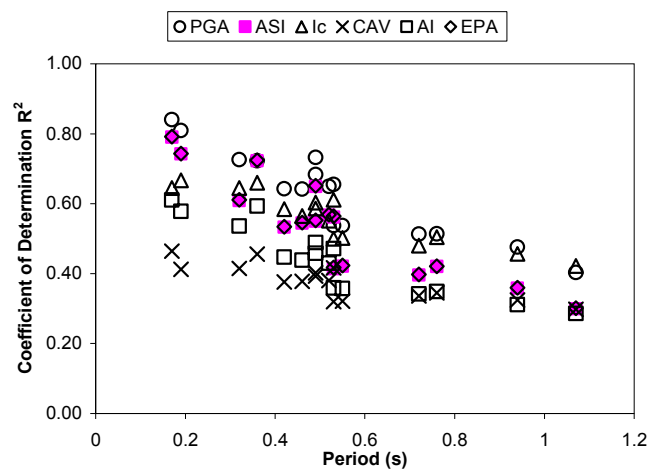


Figure 4.2 Correlation of acceleration related parameters (SDOF)

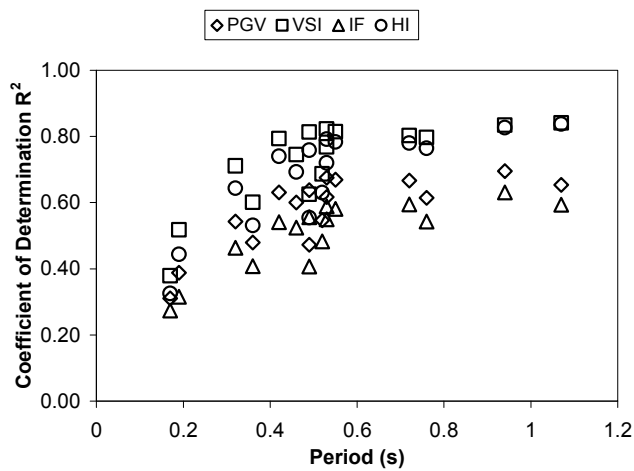


Figure 4.3 Correlation of velocity related parameters (SDOF)

As it is evidenced in these figures; acceleration related indices have stronger correlation for short-to-medium period structures. In this period range PGA, EPA and ASI have the strongest correlation, CAV being the worse. Velocity related parameters have higher degree of correlation for medium-high period structures. VSI and HI have the highest correlation with demand for this period range.

The overall results indicate that spectrum based intensity parameters that account for the structural characteristics (fundamental period) reflecting its likely response intervals are the most reliable ground motion intensity parameters representing the destructiveness of the ground motion for the structures having periods between 0.2-1.1 seconds.

The main conclusion drawn from the results presented here is that selection of a suitable ground motion parameter as an intensity measure mainly depends on the period of interest. Promising parameters considering the total number of 1280 response history analyses results of SDOF system are spectral parameters VSI and HI in general. But for a particular period interest PGA, EPA and ASI are proper for stiffer structures and similarly VSI and HI can be used for softer structures as an intensity measure.

4.2.4 Comparison with Other Studies (SDOF)

As a part of their study on the effect of PGV on SDOF deformation demands, Akkar and Ozen (2005) studied period dependence of the correlation of PGV, PGA, PGV/PGA and S_a with SDOF deformation demands using elastoplastic hysteretic models within the period range of 0.1-4 s. General tendency of the decline in the degree of correlation of PGA with the increase in period and the low correlation of PGV for short period systems observed in Akkar and Ozen (2005) are consistent with the arguments of this study. However, considering the average correlation results of this study, PGA and S_a showed better correlation than PGV with the SDOF

deformation demand contrary to the priority given to PGV in Akkar and Ozen (2005). Difference in the outcomes may be attributed to the difference in the ground motion data set used and the period range covered. Distribution of the PGV and PGA used in Akkar and Ozen (2005) is displayed in Figure 4.4. The range of PGV covered is smaller than the one used in this study.

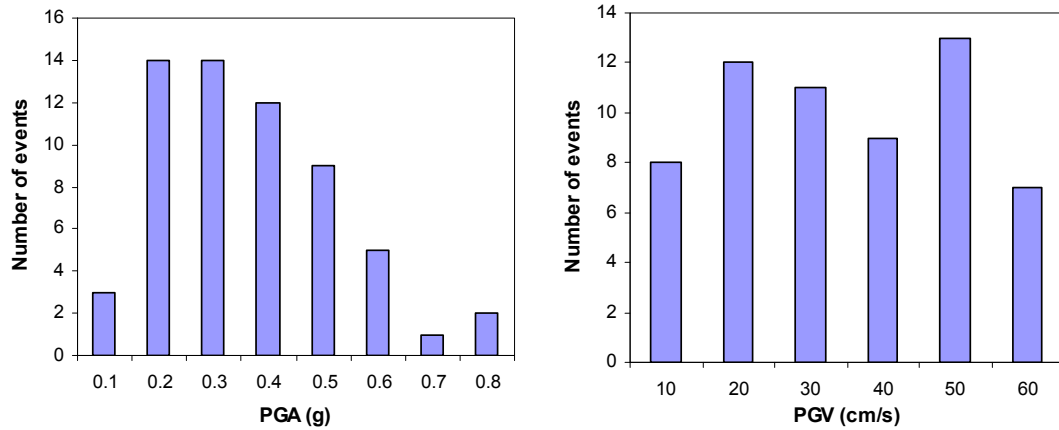


Figure 4.4 Distribution of PGA and PGV used in Akkar and Ozen (2005)

In a similar study, Riddell (2007) investigated the correlation between 23 ground motion intensity parameters and SDOF response variables: elastic and inelastic deformation demands, input energy and hysteretic energy. He employed ninety records using SDOF models with fundamental periods of 0.2, 1.0, and 5.0 seconds to represent the acceleration-sensitive, velocity-sensitive and the displacement-sensitive spectral regions respectively and concluded that no index is satisfactory over the entire period range. According to the outcomes of Riddell's (2007) study, acceleration-related parameters are best for stiff structures and velocity-related parameters are proper measures of earthquake intensity for intermediate period systems. As evidenced from Figure 4.2 and 4.3, superiority of acceleration related parameters for short periods and the velocity related parameters for intermediate periods are in agreement with the Riddell's conclusions. PGA and PGV distribution of the ground motions used in Riddell (2007) is shown in Figure 4.5. Amplitude

range and the distribution of the PGA and PGV values of the records fairly agree with the ground motion data set used in this study.

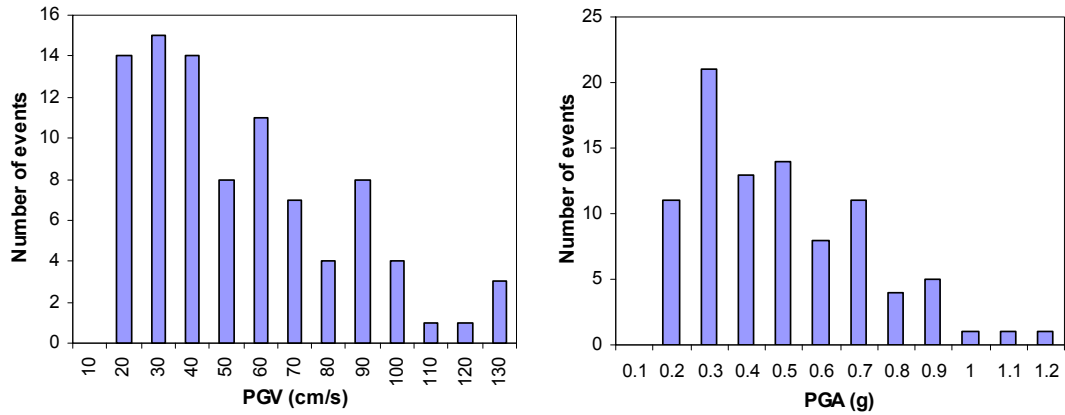


Figure 4.5 Distribution of PGA and PGV used in Riddell (2007)

4.2.5 Correlation Study for MDOF Response

Maximum interstory drift ratios were computed from 1280 nonlinear time history analyses. Pearson's correlation coefficient was computed for overall response whereas R^2 values were computed in three ranges, as stated before to consider the nonlinear behavior of the frames. These three ranges are as follows:

- Linear-nonlinear range, for all MIDR values
- Linear range, where MIDR values are equal or less than yield MIDR
- Nonlinear range, where MIDR values are greater than yield MIDR.

Procedure followed for the determination of yield MIDR is presented in Chapter 3. Table 4.4 displays the coefficient of determination results computed for each frame in three response ranges, respectively. It is worthwhile to remind that linear fit were assumed for overall and linear response whereas exponential fit was used for nonlinear response. Pearson's correlation results were displayed in Table 4.5 as well.

Table 4.4 Coefficient of determination values for the three ranges (MDOF)

ID	PGA	PGV	S _a	ASI	VSI	I _c	I _F	CAV	AI	HI	EPA	OVERALL RESPONSE
F1-2S3B	0.837	0.449	0.712	0.762	0.595	0.737	0.371	0.445	0.739	0.515	0.765	
F2-3S3B	0.827	0.336	0.825	0.792	0.428	0.622	0.266	0.406	0.586	0.361	0.795	
F3-3S2B	0.753	0.435	0.710	0.771	0.540	0.640	0.357	0.388	0.496	0.476	0.772	
F4-3S3B	0.790	0.463	0.693	0.641	0.669	0.648	0.393	0.424	0.560	0.594	0.644	
F5-4S3B	0.606	0.491	0.365	0.397	0.734	0.591	0.384	0.283	0.578	0.660	0.399	
F6-4S3B	0.713	0.520	0.457	0.586	0.722	0.587	0.419	0.332	0.458	0.653	0.588	
F7-4S3B	0.669	0.624	0.683	0.561	0.829	0.699	0.556	0.439	0.626	0.767	0.565	
F8-5S4B	0.611	0.661	0.595	0.492	0.770	0.567	0.621	0.432	0.437	0.745	0.496	
F9-5S3B	0.705	0.573	0.639	0.578	0.762	0.635	0.513	0.419	0.548	0.693	0.582	
F10-5S4B	0.530	0.546	0.626	0.452	0.729	0.558	0.480	0.363	0.498	0.661	0.455	
F11-5S3B	0.582	0.659	0.771	0.464	0.856	0.647	0.594	0.429	0.610	0.828	0.466	
F12-6S4B	0.560	0.551	0.551	0.412	0.746	0.526	0.471	0.307	0.444	0.687	0.417	
F13-6S3B	0.661	0.617	0.674	0.564	0.837	0.689	0.537	0.446	0.625	0.782	0.566	
F14-6S3B	0.589	0.716	0.785	0.504	0.835	0.517	0.679	0.444	0.381	0.811	0.506	
F15-7S3B	0.564	0.743	0.805	0.502	0.888	0.570	0.659	0.359	0.467	0.878	0.505	
F16-9S3B	0.416	0.738	0.760	0.334	0.856	0.431	0.663	0.288	0.287	0.862	0.337	

ID	PGA	PGV	S _a	ASI	VSI	I _c	I _F	CAV	AI	HI	EPA	LINEAR RESPONSE
F1-2S3B	0.804	0.274	0.940	0.818	0.311	0.546	0.284	0.362	0.461	0.278	0.820	
F2-3S3B	0.582	0.196	0.958	0.673	0.221	0.360	0.202	0.253	0.268	0.192	0.676	
F3-3S2B	0.693	0.230	0.942	0.871	0.281	0.479	0.216	0.263	0.349	0.222	0.866	
F4-3S3B	0.696	0.491	0.938	0.660	0.580	0.654	0.420	0.325	0.458	0.510	0.660	
F5-4S3B	0.797	0.631	0.978	0.959	0.760	0.861	0.619	0.715	0.721	0.658	0.969	
F6-4S3B	0.822	0.287	0.901	0.908	0.393	0.628	0.353	0.558	0.583	0.342	0.914	
F7-4S3B	0.574	0.528	0.951	0.671	0.791	0.727	0.521	0.528	0.617	0.706	0.672	
F8-5S4B	0.719	0.643	0.996	0.776	0.892	0.898	0.551	0.681	0.877	0.726	0.786	
F9-5S3B	0.688	0.466	0.960	0.770	0.713	0.737	0.390	0.388	0.629	0.632	0.770	
F10-5S4B	0.647	0.776	0.993	0.715	0.835	0.811	0.652	0.604	0.686	0.717	0.726	
F11-5S3B	0.570	0.522	0.855	0.516	0.775	0.598	0.464	0.442	0.498	0.701	0.516	
F12-6S4B	0.860	0.592	0.987	0.900	0.687	0.809	0.493	0.723	0.794	0.549	0.903	
F13-6S3B	0.554	0.411	0.977	0.609	0.755	0.664	0.411	0.499	0.534	0.705	0.614	
F14-6S3B	0.456	0.656	0.946	0.417	0.908	0.545	0.700	0.635	0.429	0.867	0.418	
F15-7S3B	0.590	0.466	0.749	0.606	0.731	0.559	0.452	0.569	0.467	0.651	0.605	
F16-9S3B	0.566	0.444	0.645	0.559	0.773	0.595	0.439	0.607	0.464	0.655	0.561	

ID	PGA	PGV	S _a	ASI	VSI	I _c	I _F	CAV	AI	HI	EPA	NONLINEAR RESPONSE
F1-2S3B	0.724	0.348	0.484	0.706	0.527	0.649	0.247	0.303	0.594	0.435	0.712	
F2-3S3B	0.717	0.267	0.659	0.656	0.235	0.341	0.191	0.173	0.334	0.195	0.666	
F3-3S2B	0.620	0.249	0.565	0.645	0.400	0.475	0.172	0.210	0.353	0.319	0.646	
F4-3S3B	0.584	0.207	0.502	0.438	0.497	0.469	0.143	0.239	0.407	0.384	0.440	
F5-4S3B	0.700	0.563	0.517	0.568	0.754	0.711	0.459	0.397	0.692	0.684	0.570	
F6-4S3B	0.709	0.519	0.430	0.608	0.734	0.595	0.397	0.312	0.449	0.664	0.611	
F7-4S3B	0.564	0.516	0.610	0.441	0.750	0.589	0.439	0.301	0.513	0.677	0.445	
F8-5S4B	0.598	0.691	0.633	0.486	0.786	0.526	0.636	0.358	0.392	0.772	0.490	
F9-5S3B	0.624	0.432	0.528	0.464	0.682	0.520	0.359	0.272	0.446	0.592	0.468	
F10-5S4B	0.570	0.591	0.681	0.473	0.813	0.583	0.519	0.377	0.498	0.753	0.478	
F11-5S3B	0.429	0.503	0.642	0.294	0.754	0.438	0.391	0.142	0.419	0.724	0.299	
F12-6S4B	0.610	0.602	0.615	0.493	0.774	0.577	0.515	0.301	0.478	0.726	0.498	
F13-6S3B	0.561	0.473	0.580	0.439	0.725	0.582	0.386	0.312	0.520	0.660	0.441	
F14-6S3B	0.441	0.643	0.653	0.333	0.757	0.378	0.595	0.297	0.287	0.750	0.333	
F15-7S3B	0.361	0.614	0.659	0.252	0.818	0.344	0.500	0.132	0.283	0.825	0.255	
F16-9S3B	0.231	0.630	0.542	0.136	0.749	0.237	0.532	0.091	0.155	0.779	0.136	

Table 4.5 Pearson's coefficient results for overall response (MDOF)

ID	PGA	PGV	S _a	ASI	VSI	I _c	I _F	CAV	AI	HI	EPA	OVERALL RESPONSE
F1-2S3B	0.915	0.670	0.844	0.873	0.771	0.859	0.609	0.667	0.859	0.718	0.875	
F2-3S3B	0.910	0.579	0.908	0.890	0.654	0.789	0.516	0.637	0.766	0.601	0.892	
F3-3S2B	0.868	0.659	0.842	0.878	0.735	0.800	0.597	0.622	0.704	0.690	0.879	
F4-3S3B	0.889	0.680	0.833	0.801	0.818	0.805	0.627	0.651	0.748	0.771	0.803	
F5-4S3B	0.778	0.700	0.604	0.630	0.856	0.769	0.619	0.532	0.760	0.812	0.632	
F6-4S3B	0.845	0.721	0.676	0.766	0.850	0.766	0.647	0.576	0.676	0.808	0.767	
F7-4S3B	0.818	0.790	0.826	0.749	0.910	0.836	0.746	0.662	0.791	0.876	0.751	
F8-5S4B	0.782	0.813	0.771	0.702	0.877	0.753	0.788	0.657	0.661	0.863	0.704	
F9-5S3B	0.840	0.757	0.800	0.760	0.873	0.797	0.716	0.647	0.740	0.833	0.763	
F10-5S4B	0.728	0.739	0.791	0.672	0.854	0.747	0.693	0.602	0.706	0.813	0.675	
F11-5S3B	0.763	0.812	0.878	0.681	0.925	0.804	0.771	0.655	0.781	0.910	0.683	
F12-6S4B	0.748	0.742	0.742	0.642	0.864	0.725	0.686	0.554	0.666	0.829	0.646	
F13-6S3B	0.813	0.785	0.821	0.751	0.915	0.830	0.733	0.668	0.791	0.884	0.752	
F14-6S3B	0.768	0.846	0.886	0.710	0.914	0.719	0.824	0.666	0.617	0.900	0.711	
F15-7S3B	0.751	0.862	0.897	0.709	0.942	0.755	0.812	0.599	0.683	0.937	0.711	
F16-9S3B	0.645	0.859	0.872	0.578	0.925	0.656	0.814	0.537	0.536	0.928	0.580	

Averaged results computed for coefficient of determination and Pearson's correlation coefficients are presented in Table 4.6. As evidenced in Table 4.6, VSI and HI turned out to be the two parameters that have the strongest correlation with MIDR based on 1280 nonlinear response history analyses for sixteen frames. S_a and PGA follow the former two parameters. It is apparent from the average results that the parameters showing higher degree of correlation are the ones that are computed from response spectrum. It is important to remind that, analyzed frames were selected with an intention to represent typical low-to-mid rise buildings and the period range of the selected frames is in between 0.2-1.1 s.

The largest coefficient of determination value was determined for S_a, in the linear range as depicted in Table 4.6. Individual correlations can be observed for the frames in Table 4.4 as well. This indicates that the behavior of the frames selected is dominated by the response in the first mode. Furthermore, correlation of determination value of 0.920 for S_a proves the validity of approximation used in the computation of yield MIDR.

Table 4.6 Average correlation of ground motion parameters with MIDR

GMI	Coefficient of determination (R^2)			Pearson's correlation
	Linear response	Nonlinear response	All	
VSI	0.650	0.672	0.737	0.855
HI	0.569	0.621	0.686	0.823
S_a	0.920	0.581	0.666	0.812
PGA	0.663	0.565	0.651	0.804
I_c	0.654	0.501	0.604	0.776
PGV	0.476	0.490	0.570	0.751
EPA	0.717	0.468	0.554	0.739
ASI	0.714	0.464	0.551	0.737
AI	0.552	0.426	0.521	0.718
I_F	0.448	0.405	0.498	0.700
CAV	0.509	0.264	0.388	0.621

Examining Figures 4.6 and 4.7, general tendencies of acceleration related and velocity related parameters observed in SDOF analyses are also valid for MDOF models. Degree of correlation of acceleration related parameters decreases as the period increases within the period range covered for the frames. Similarly, velocity related parameters are superior for increasing periods.

AI, I_F and CAV provided poorest results both in SDOF and MDOF nonlinear response history analyses. As stated in Chapter 3, selected reinforced concrete frames were modeled using beam and column elements using bilinear hysteretic model with no stiffness and strength degradation. This statement should be taken into account in the evaluation of the correlation results of the parameters that reflect the duration characteristics of strong ground motion.

Based on the observations related to Figures 4.6 and 4.7, PGA, EPA and ASI have strongest correlation with response for short periods whereas VSI and HI provide sufficient correlation for intermediate periods.

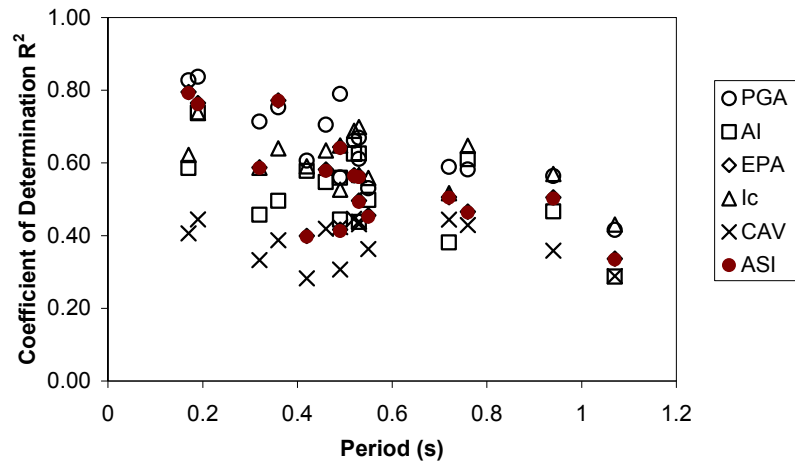


Figure 4.6 Correlation of acceleration related parameters (MDOF)

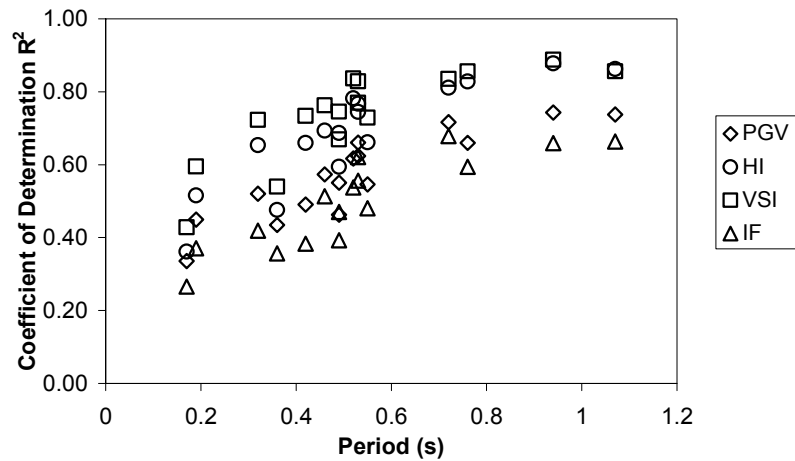


Figure 4.7 Correlation of velocity related parameters (MDOF)

Among the ground motion intensity parameters considered in this study, AI, CAV, and I_c include terms that reflect the effects of the duration, amplitude and the frequency content of the ground motion but do not consider the properties of the structure. Similarly PGA, PGV and I_F do not take into account structural characteristics that are known to significantly influence the structural response. On the other hand S_a is directly based on the fundamental period of the structure and also ASI, HI and VSI are spectrum based parameters that are indirectly related to the fundamental period of a structure reflecting its likely response intervals.

Despite the priority given to PGV (Akkar and Ozen, 2006), it turned out to have a moderate degree of correlation with structural demand. Frequently criticized parameter PGA showed better correlation than PGV on the average.

As mentioned before, coefficient of determination values for response of the MDOF models were evaluated in the nonlinear range based on exponential fit. These coefficients were recalculated based on linear fit. Averaged results presented in Table 4.7 reveals that assumed exponential relationship provides better results than linear relationship assumption.

Table 4.7 Average correlation results for exponential and linear fit

	Exponential Fit	Linear Fit
VSI	0.672	0.634
HI	0.621	0.568
S_a	0.581	0.520
PGA	0.565	0.520
I_c	0.501	0.446
PGV	0.490	0.445
EPA	0.468	0.390
ASI	0.464	0.381
AI	0.426	0.387
I_F	0.405	0.331
CAV	0.264	0.212

Two different groups of frames were utilized in this study. First group is composed of existing frames extracted from Düzce database to represent the peculiarities of existing buildings. Second group includes designed frames that reflect seismic provisions of the current seismic code. Coefficient of determination values computed for the frames are plotted against period for each ground motion parameter in Figures 4.8 and 4.9. In general, existing and designed frames follow the same trend however difference in response is mostly pronounced for spectral acceleration at the fundamental period. However, since period of these frames do not overlap, a valid evaluation can not be made.

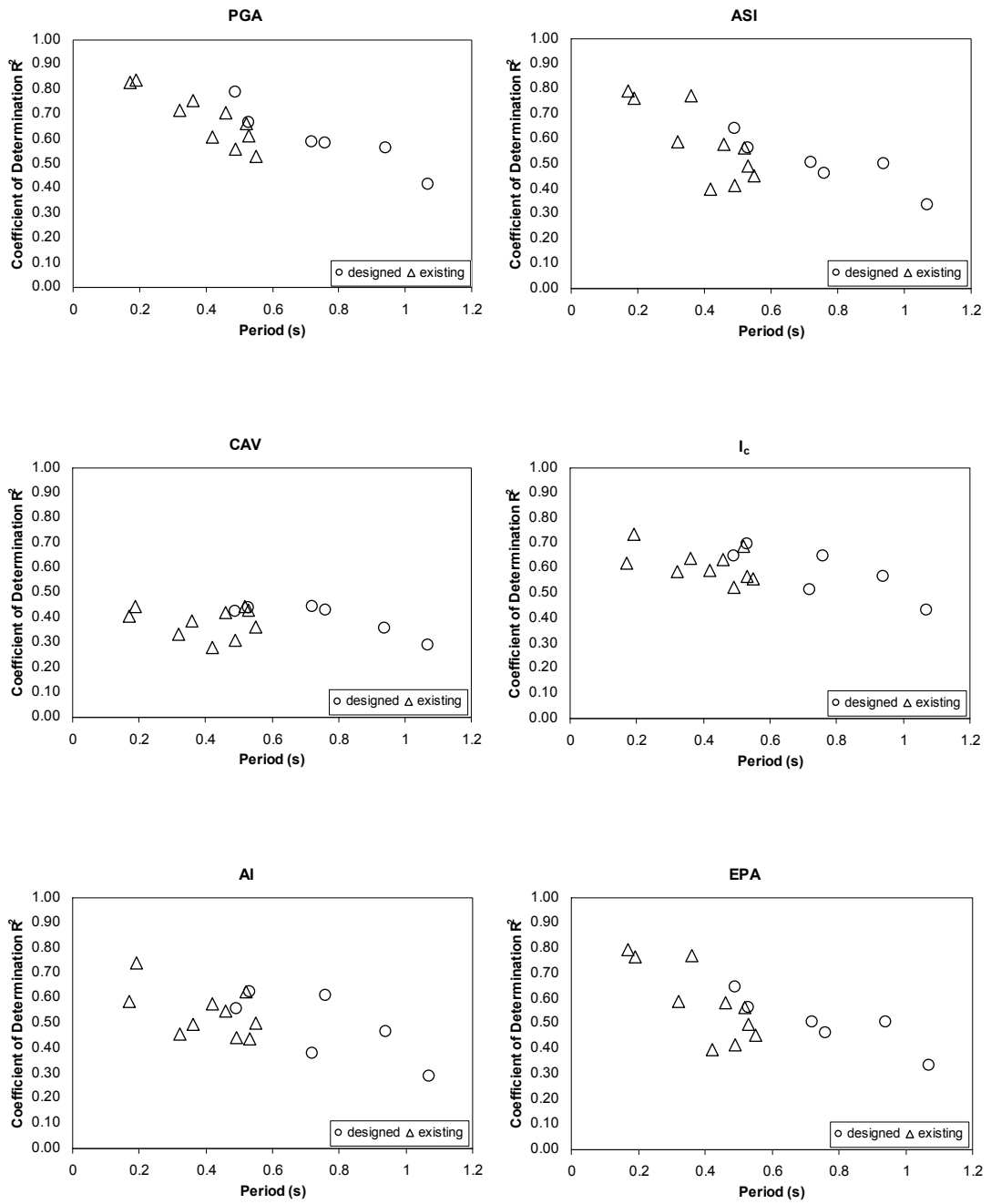


Figure 4.8 Correlation of existing and designed frames
(PGA, ASI, CAV, I_c , AI, EPA)

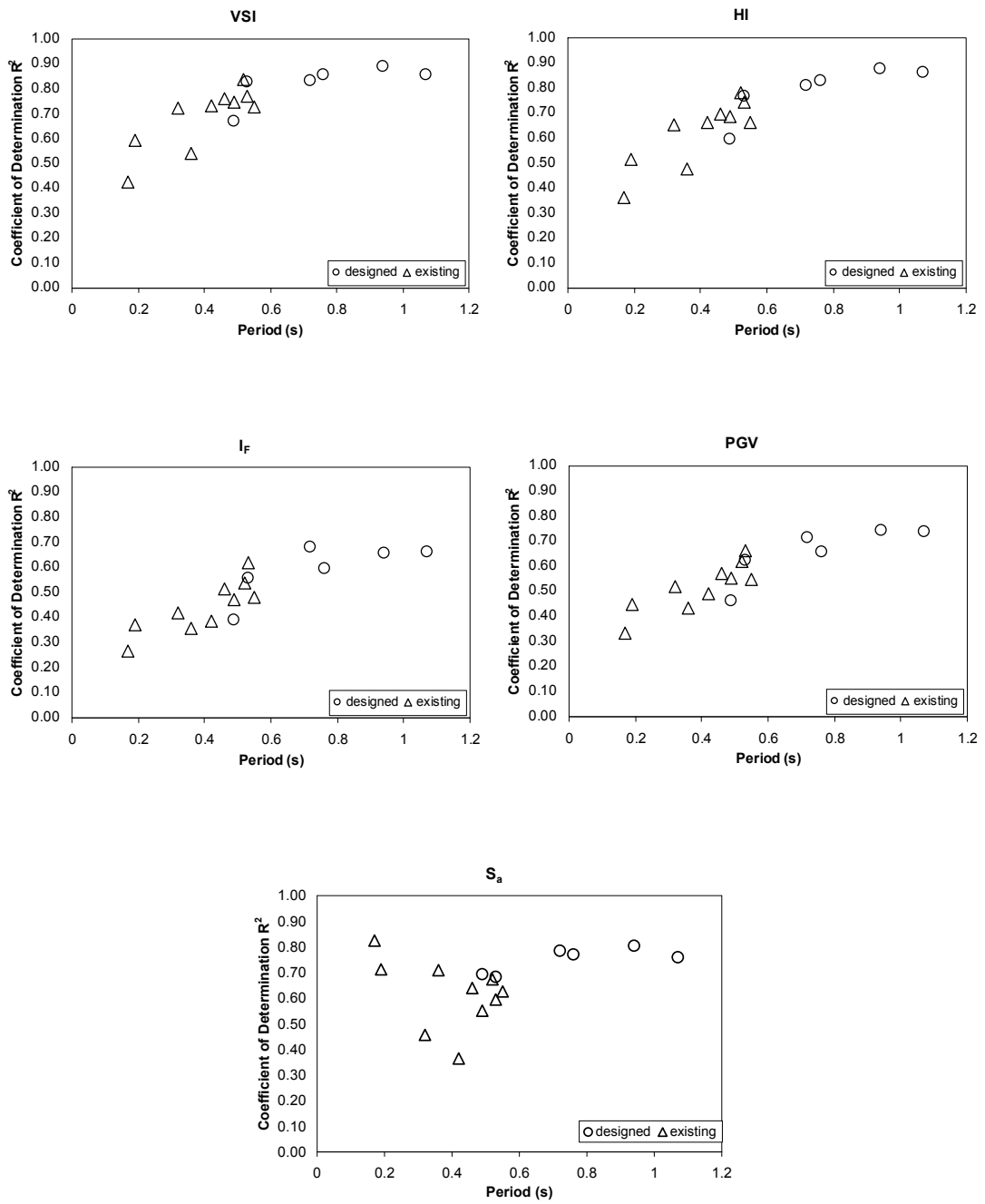


Figure 4.9 Correlation of existing and designed frames
(VSI, HI, I_F , PGV, S_a)

Depending on the conclusion drawn that the spectrum based parameters have higher degree of correlation and the results of interrelation is mainly influenced by the period of interest, period range (0.1-0.5 s) used in the computation of ASI has been shifted to 0.1-2.5 s. The corresponding Pearson's correlation coefficient was calculated as 0.871 which is close to the ones computed for HI and VSI. This clearly reveals the influence of the period range covered in the computation of ASI.

Previous results showed that the adequacy of the ground motion parameters in describing the destructiveness of an earthquake is dependent on the period of interest. Acceleration related parameters are superior for short period systems whereas velocity related parameters show higher degrees of correlation in intermediate period range. Another conclusion of the study is that the spectrum based ground motion parameters that account for the structural characteristics (predominant period) reflecting its likely response intervals are promising parameters.

ASI is simply defined as the area under the elastic acceleration spectrum between the periods 0.1-0.5 sec. It is previously stated that, shifting the period range used in the computation of ASI to 0.1-2.5 s. increases the degree of correlation considerably (Pearson correlation coefficient of 0.871), and VSI turned out to be the best parameter on average. Accordingly, revised ASI and VSI measures were formed setting the lower bound of period range to T and upper bound to (cT) where T is the fundamental period of the system (Equations 4.3 and 4.4). The constant c in the formulation will be determined next.

$$ASI = \int_T^{cT} S_a(T) dT \quad (4.3)$$

$$VSI = \int_T^{cT} S_v(T) dT \quad (4.4)$$

Revised ASI and VSI parameters were calculated setting c to 1.2, 1.4, 1.6, 1.8, 2.0, 2.2, 2.4, 2.6, 2.8 and 3. Interdependency of maximum interstory drift ratios computed with the proposed ground motion intensity parameters were investigated through Pearson's correlation coefficient. Correlation coefficients for revised ASI and VSI calculated for varying values of c ranging from 1.2 to 3 are depicted in Tables 4.8 and 4.9 for ASI and VSI respectively for each frame.

Table 4.8 Pearson's correlation coefficient for ASI for different c values

ID	ASI (T-1.2T)	ASI (T-1.4T)	ASI (T-1.6T)	ASI (T-1.8T)	ASI (T-2T)	ASI (T-2.2T)	ASI (T-2.4T)	ASI (T-2.6T)	ASI (T-2.8T)	ASI (T-3T)
F1-2S3B	0.820	0.836	0.847	0.849	0.853	0.851	0.852	0.855	0.860	0.867
F2-3S3B	0.897	0.882	0.888	0.892	0.889	0.885	0.877	0.874	0.875	0.876
F3-3S2B	0.868	0.905	0.908	0.905	0.903	0.903	0.906	0.906	0.903	0.897
F4-3S3B	0.865	0.882	0.899	0.918	0.926	0.923	0.917	0.909	0.900	0.892
F5-4S3B	0.647	0.696	0.730	0.769	0.799	0.823	0.842	0.861	0.877	0.883
F6-4S3B	0.735	0.755	0.791	0.806	0.814	0.828	0.842	0.857	0.873	0.884
F7-4S3B	0.864	0.891	0.914	0.927	0.937	0.946	0.948	0.946	0.944	0.941
F8-5S4B	0.810	0.844	0.875	0.893	0.901	0.905	0.908	0.907	0.904	0.901
F9-5S3B	0.848	0.884	0.910	0.923	0.930	0.934	0.935	0.935	0.933	0.930
F10-5S4B	0.840	0.870	0.883	0.889	0.896	0.900	0.900	0.897	0.892	0.887
F11-5S3B	0.918	0.948	0.958	0.954	0.945	0.937	0.932	0.927	0.923	0.919
F12-6S4B	0.789	0.832	0.855	0.873	0.887	0.898	0.907	0.909	0.907	0.903
F13-6S3B	0.845	0.881	0.905	0.926	0.939	0.950	0.954	0.953	0.951	0.948
F14-6S3B	0.822	0.856	0.891	0.907	0.907	0.910	0.914	0.916	0.917	0.916
F15-7S3B	0.921	0.925	0.921	0.919	0.920	0.919	0.916	0.910	0.903	0.894
F16-9S3B	0.892	0.898	0.902	0.905	0.908	0.907	0.902	0.895	0.885	0.875

Table 4.9 Pearson's correlation coefficient for VSI for different c values

ID	VSI (T-1.2T)	VSI (T-1.4T)	VSI (T-1.6T)	VSI (T-1.8T)	VSI (T-2T)	VSI (T-2.2T)	VSI (T-2.4T)	VSI (T-2.6T)	VSI (T-2.8T)	VSI (T-3T)
F1-2S3B	0.771	0.801	0.807	0.810	0.815	0.815	0.813	0.815	0.821	0.831
F2-3S3B	0.835	0.852	0.864	0.871	0.870	0.866	0.856	0.851	0.852	0.854
F3-3S2B	0.847	0.883	0.890	0.887	0.887	0.890	0.896	0.901	0.900	0.893
F4-3S3B	0.827	0.852	0.880	0.908	0.924	0.926	0.921	0.913	0.903	0.894
F5-4S3B	0.556	0.621	0.675	0.730	0.773	0.804	0.831	0.860	0.884	0.893
F6-4S3B	0.694	0.707	0.743	0.764	0.778	0.798	0.818	0.839	0.862	0.876
F7-4S3B	0.836	0.864	0.893	0.912	0.927	0.940	0.945	0.943	0.940	0.938
F8-5S4B	0.766	0.809	0.848	0.871	0.884	0.890	0.896	0.897	0.895	0.891
F9-5S3B	0.790	0.851	0.890	0.909	0.921	0.926	0.930	0.933	0.932	0.929
F10-5S4B	0.821	0.854	0.867	0.875	0.886	0.894	0.898	0.897	0.893	0.890
F11-5S3B	0.893	0.929	0.946	0.944	0.937	0.930	0.924	0.921	0.919	0.918
F12-6S4B	0.724	0.793	0.828	0.852	0.870	0.890	0.903	0.908	0.908	0.903
F13-6S3B	0.813	0.854	0.885	0.912	0.931	0.947	0.954	0.953	0.949	0.947
F14-6S3B	0.785	0.827	0.869	0.890	0.893	0.898	0.906	0.912	0.915	0.916
F15-7S3B	0.897	0.913	0.915	0.919	0.922	0.927	0.932	0.932	0.929	0.925
F16-9S3B	0.877	0.894	0.905	0.912	0.922	0.929	0.932	0.931	0.927	0.920

Averaged coefficient results computed are displayed numerically in Table 4.10 and graphically in Figure 4.10 for different c values. Constant c was determined as 2 according to the results presented in Table 4.10 and Figure 4.10. Figure 4.10 supports the idea behind the selection of c as 2 where the saturation starts.

Table 4.10 Averaged Pearson's results for ASI and VSI

	T-1.2T	T-1.4T	T-1.6T	T-1.8T	T-2T	T-2.2T	T-2.4T	T-2.6T	T-2.8T	T-3.T
ASI	0.836	0.862	0.880	0.891	0.897	0.901	0.903	0.904	0.903	0.901
VSI	0.796	0.831	0.857	0.873	0.884	0.892	0.897	0.900	0.902	0.901

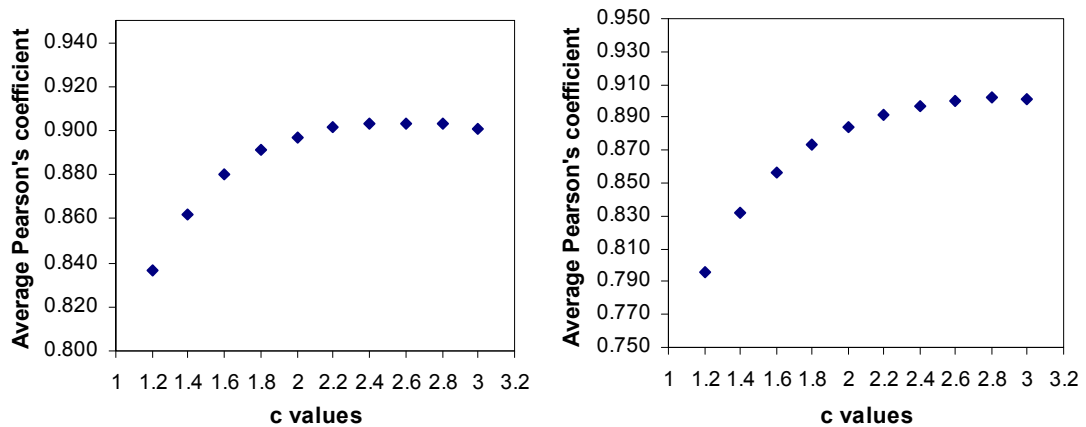


Figure 4.10 Average Pearson's results for revised ASI and VSI

Averaged values of revised ASI and VSI computed for c equals to 2, setting lower bound to T and upper bound to $2T$, resulted in a correlation measure of 0.897 and 0.884 respectively. These results are superior to computed correlations for VSI and HI on average. Revised ASI and VSI, where lower and upper bounds depend on the period of the structure employed are believed to take the elongated periods and the shape of the spectrum into account. These revised parameters can be employed for a particular frame whereas ASI and VSI computed between 0.1-2.5 s. can be employed for group of frames in seismic hazard analyses. It is also important to note that, outcomes of the SDOF and MDOF response history analyses are in agreement as observed in Figure 4.11.

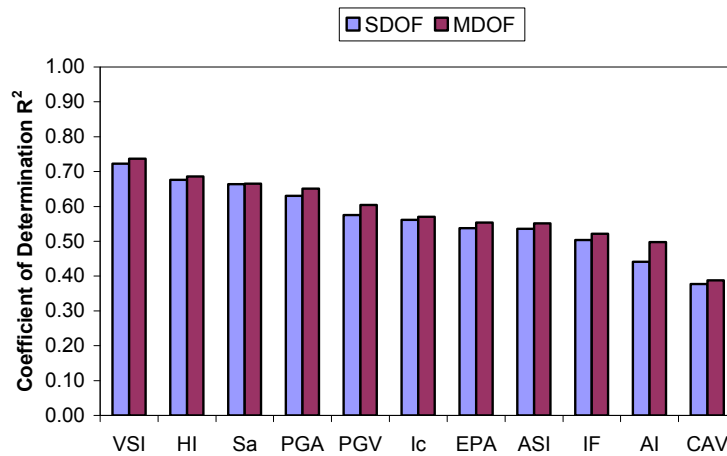


Figure 4.11 Comparison of SDOF and MDOF results

4.2.6 Comparison with Other Studies (MDOF)

Elenas (2000) investigated the interdependency between seismic parameters and structural response defined in terms of overall structural damage indices employing a single frame subjected to twenty ground motion records. S_a was found to be the parameter that has the highest correlation with the overall structural damage.

Elenas and Meskouris (2001) studied the correlation between seismic acceleration parameters and the damage indices of structures. Nonlinear dynamic analyses are conducted using an eight storey reinforced concrete plane frame (having a fundamental period of 1.18 s.) under a set of twenty ground motion records. Pearson correlation coefficients obtained for response parameter MIDR are presented in Table 4.11 together with average results obtained for the sixteen frames in this study. In addition, results for F16-9S3B (with fundamental period of 1.07 s.) are presented in Table 4.11 in addition. Strong correlation of AI with MIDR computed in Elenas and Meskouris (2001) for a flexible system is surprising. Results do not agree with the outcomes of this study which can be attributed to the limited number of records used as well as a single frame having a fundamental period of 1.18 seconds employed.

Table 4.11 Comparison of Pearson' correlation coefficient results

	Elenas and Meskouris	This study (average)	F16-9S3B
PGA	0.419	0.804	0.645
PGV	0.651	0.751	0.859
S_a	0.854	0.812	0.872
AI	0.802	0.718	0.536

4.3 CORRELATION WITH OBSERVED DAMAGE

Despite its destructive effects, earthquake provides invaluable data for earthquake engineering field. Relationship between the earthquake damage surveyed and the strong motion parameters have been investigated using the earthquake damage and ground motion data presented in ATC-38 (2000).

ATC-38 (2000) report documents the performance of structures near strong motion recording stations after magnitude 6.8 Northridge, California earthquake occurred on January 17, 1994. Approximately 500 buildings in the vicinity of strong motion recording sites (within approximately 300 m.) are surveyed and the characteristics and performance of buildings are documented in ATC-38 (2000) database.

The survey data are specifically collected to correlate the relationship between recorded ground shaking and the observed performance of buildings. ATC-38 (2000) building database is composed of concrete, steel, wood and masonry structures. Concrete moment frame (C1) and concrete frame with infill masonry shear walls (C3) type buildings were extracted from the database and examined in this study. Basic correlation studies conducted for wood frames that constitute the majority of the surveyed buildings can be found in ATC-38 (2000).

4.3.1 Damage States

Damage sustained after the Northridge earthquake is defined in qualitative terms relating to reparability and quantitative terms. General damage state and the structural damage state are the two performance parameters considered for the concrete buildings selected in this study. These damage states are defined in ATC-38 (2000) as follows:

General damage state is defined by the earthquake performance of the primary structural and nonstructural elements, described in terms of qualitative damage states relating to extent of needed repairs. Description of each general damage state is given below. Numerical values assigned to damage states are presented at the end of each description.

- None (N), No damage is visible, either structural or nonstructural.(1)
- Insignificant (I), Damage requires no more than cosmetic repair. No structural repairs are necessary.(2)
- Moderate (M), Repairable structural damage has occurred. The existing elements can be repaired in place, without substantial demolition or replacement of elements.(3)
- Heavy (H), Damage is so extensive that repair of elements is either not feasible or requires major demolition or replacement.(4)

Besides general damage state, structural and non-structural damage sustained in the surveyed buildings are also reported in the documentation. *Structural damage* state is defined as the ratio of estimated repair cost by estimated replacement cost as represented in Table 4.12.

Table 4.12 Structural damage states

Damage State	Percent Damage (damage value/replacement value)
None (1)	0%
Slight (2)	0%-1%
Light (3)	1%-10%
Moderate (4)	10%-30%
Heavy (5)	30%-60%
Major (6)	60%-100%
Destroyed (7)	100%

4.3.2 Strong Motion Data

Strong ground motion data of the Northridge, California earthquake recorded at 31 strong motion recording stations are presented in ATC-38 (2000) database. Acceleration, velocity and displacement time series of three orthogonal components at each recording station are available. It is important to note that, surveyed buildings are selected on purpose in the vicinity of the recording stations, maximum building-to-station distance being 300 m. The ground motion record at a particular building site was taken as the motion recorded at the nearest recording station.

Ground motion intensity parameters were computed for each horizontal component of a single recording station and the average value of the two horizontal components were assigned to that station. In addition, approximate value of $0.1N$ (where N is the number of storey) has been taken as the fundamental period in the computation of spectral acceleration.

4.3.3 Building Survey Data

Included in ATC-38 (2000), database of the surveyed buildings is comprised of 530 buildings with different structural characteristics, dominated by wood light frames. 33 concrete buildings (concrete moment frame and concrete frame with infill

masonry walls) were utilized in the correlation study. Story-wise distribution of the selected reinforced concrete buildings is displayed in Figure 4.12. General and structural damage states of the surveyed buildings together with the information about the design dates are presented in Table 4.13. It is important to note that these buildings were chosen in order to perform a preliminary analysis of the relationship between damage sustained and the ground motion parameters. Buildings were not discriminated by number of stories, design date, hazard level etc.

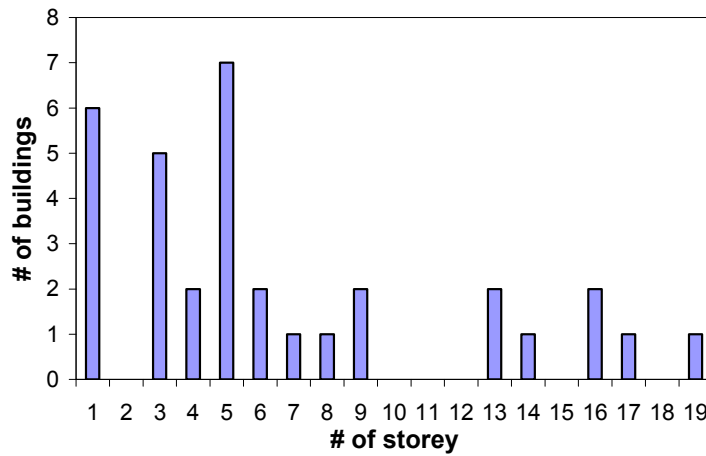


Figure 4.12 Story-wise distribution of surveyed buildings

Table 4.13 Surveyed damage states of the selected buildings

#	Model Building Type	Number of Stories	Design Date	General Damage State	Structural Damage State
1	C1	1	1965	I	2
2	C1	1	1960	H	4
3	C1	1	1970	M	4
4	C1	1	1971	N	1
5	C3	1	1952	M	4
6	C3	1	1970	I	2
7	C3	3	1931	N	1
8	C3	3	1931	M	-
9	C3	3	1928	-	1
10	C3	3	1931	-	-
11	C3	3	1950	I	2
12	C3	4	1959	I	1
13	C3	4	1960	M	3
14	C1	5	1971	I	2
15	C1	5	1980	M	3
16	C1	5	1965	I	1
17	C3	5	1932	I	2
18	C3	5	1920	I	2
19	C3	5	1950	I	1
20	C3	5	1960	I	1
21	C1	6	1966	M	3
22	C1	6	1963	M	3
23	C1	7	1965	H	5
24	C1	8	1967	I	3
25	C1	9	1993	I	1
26	C1	9	1924	I	1
27	C1	13	1963	I	1
28	C1	13	1963	M	2
29	C1	14	1988	I	1
30	C1	16	1990	M	2
31	C1	16	1960	I	1
32	C1	17	1994	I	1
33	C1	19	1965	I	2

4.3.4 Correlation Study

The degree of interdependency between the recorded ground motion parameters were examined numerically and graphically. Ground motion intensity parameters were plotted against general damage and structural damage states for each building in Figures 4.13-4.15. Line passing from the mean values for each damage state is also presented in these figures. Coefficient of determination values were computed for general damage state and structural damage state for each strong motion indices through linear fitted line to the data. In addition, mean values of the ground motion parameters for each damage states were computed and correlations were computed for the linear line fitted to mean values. Results are presented in Table 4.14.

Table 4.14 Coefficient of determination values for observed damage

	General Damage State	General Damage State (mean)	Structural Damage State	Structural Damage State (mean)
PGA	0.0541	0.6308	0.0556	0.6125
PGV	0.0853	0.4475	0.1271	0.6717
S_a	0.0444	0.2543	0.1303	0.673
ASI	0.1453	0.6084	0.214	0.6837
VSI	0.0888	0.4174	0.1231	0.6202
I_c	0.1134	0.5426	0.1499	0.6183
I_F	0.0854	0.4509	0.1223	0.6629
CAV	0.1099	0.543	0.1283	0.6175
AI	0.1291	0.5648	0.1626	0.6091
HI	0.0734	0.3918	0.0982	0.6011
EPA	0.1456	0.6099	0.2133	0.6839

Based on the preliminary analysis of this data set, no clear trend has been observed between the observed damage and the seismic parameters as evidenced by the Figures 4.13-4.15 and the results presented in Table 4.14. None of the ground motion parameters have showed satisfactory correlation with the observed damage. It is difficult to distinguish any correlations between damage states and the utilized seismic parameters. This evaluation requires details of the buildings included in the database to have reliable conclusions.

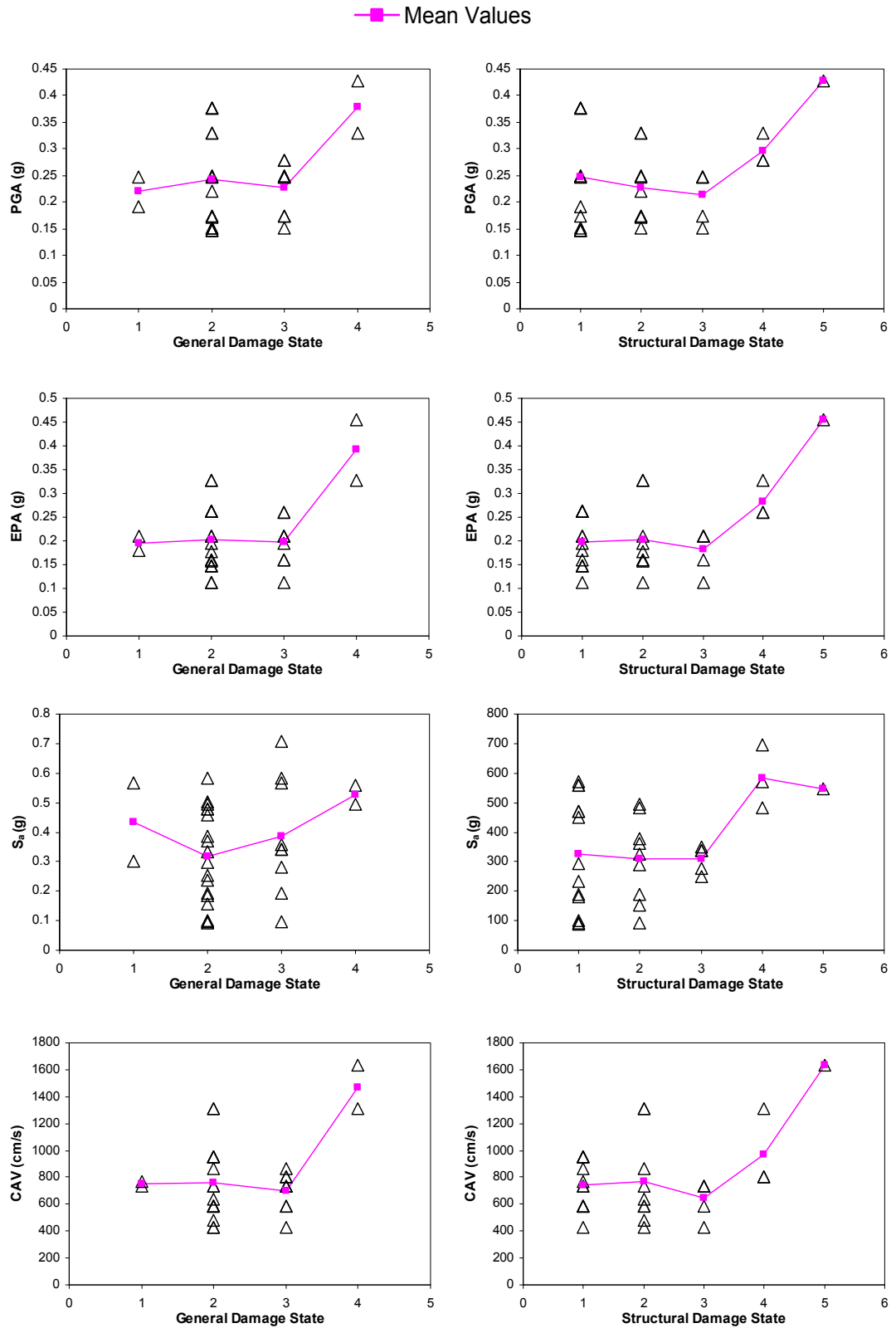


Figure 4.13 Damage state versus CAV, ASI, AI and I_c

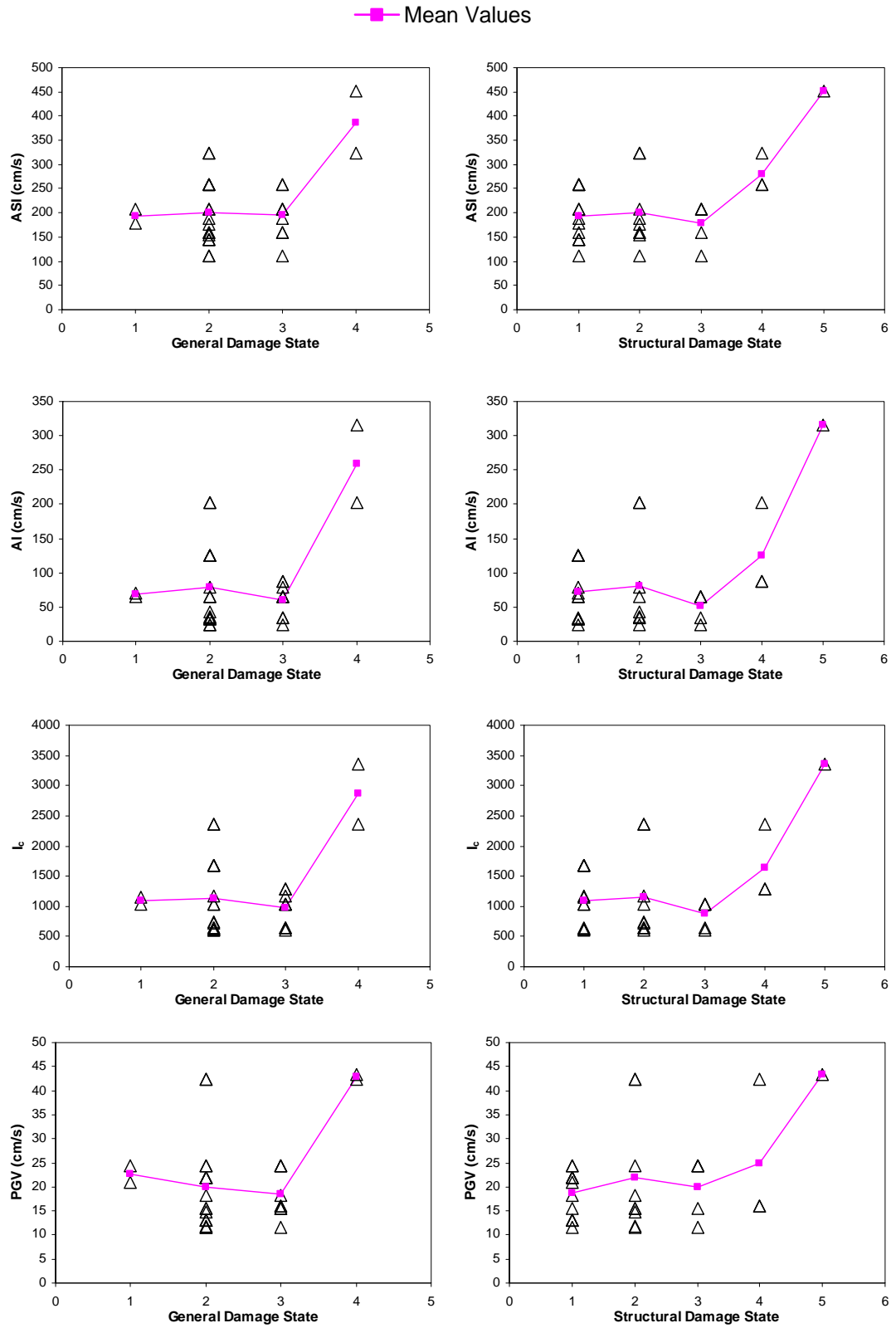


Figure 4.14 Damage state versus PGV, I_F , VSI and HI

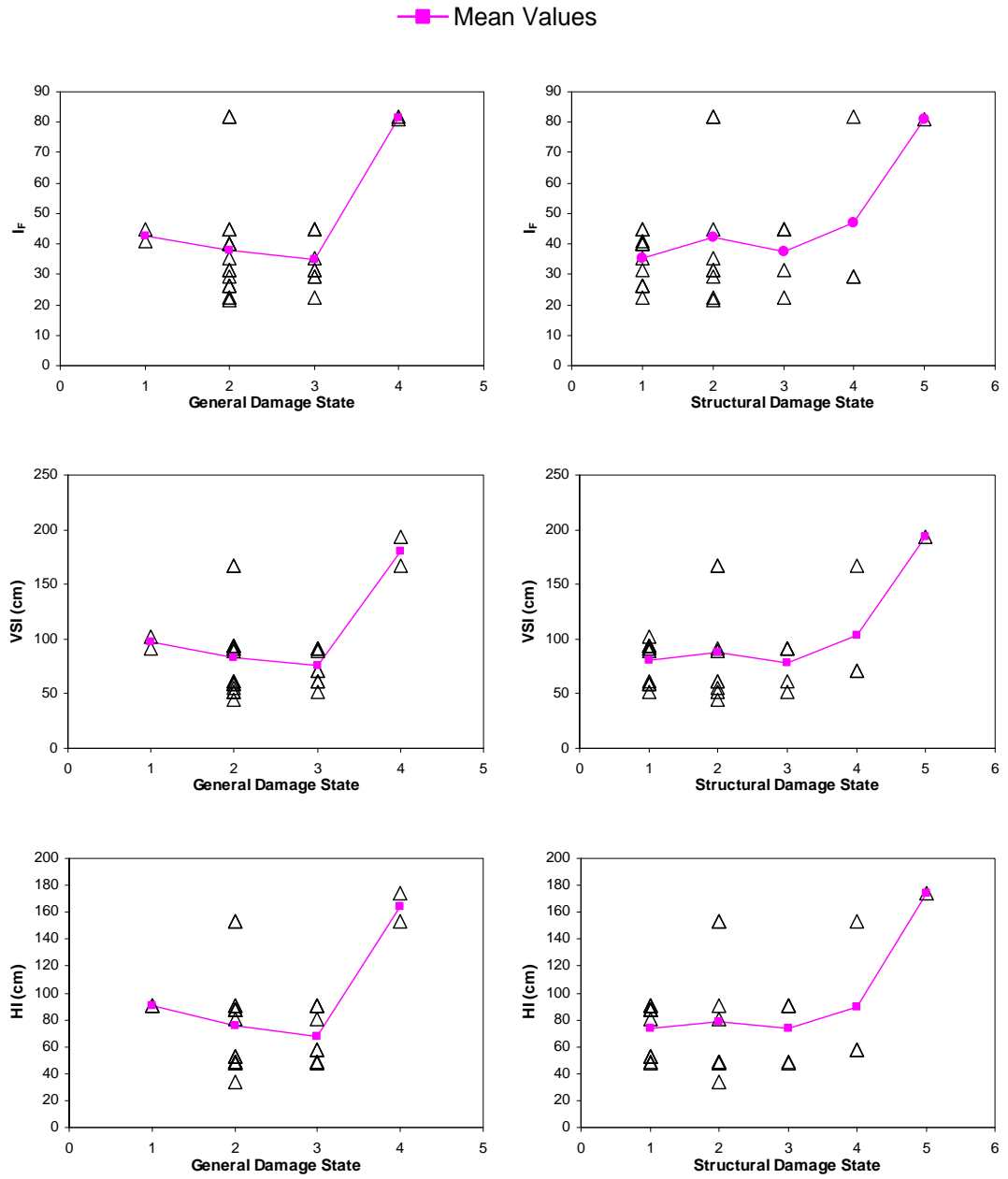


Figure 4.15 Damage state versus PGV, I_F , VSI and HI

CHAPTER 5

SUMMARY AND CONCLUSIONS

5.1 SUMMARY

A comprehensive study has been conducted to investigate the correlation of deformation demands with ground motion intensity parameters. Salient ground motion parameters deemed to represent the damage potential of earthquake were chosen. Sixteen reinforced concrete frames were selected and analyzed under a set of eighty ground motion records with varying amplitude, frequency content and duration characteristics.

Selected ground motion intensity parameters were computed for each ground motion record. Distributions of these parameters were examined and correlations among seismic parameters were evaluated using Pearson's correlation coefficient.

Reinforced concrete frames were modeled and analyzed using the structural analysis software IDARC-2D (Valles et, al, 1996). At first step, nonlinear static analyses were carried out for the frames. Pushover curves were obtained and idealized according to the FEMA-356 (2000). MDOF models later were reduced to equivalent SDOF models following the guidelines in ATC-40 (1996). Then, nonlinear response history analyses of the equivalent SDOF and MDOF models were performed and the response parameters were computed. Attention has been paid to maximum displacement demand and maximum interstory drift ratio for SDOF and MDOF response respectively. Roof displacement results obtained from the nonlinear

dynamic analyses of the equivalent SDOF system and the MDOF system were compared and discussed.

Next, correlation of seismic parameters with computed response of SDOF and MDOF models were investigated using coefficient of determination and Pearson's correlation coefficient. Finally, association between the seismic indices and the observed damage surveyed after Northridge, California earthquake were investigated.

5.2 CONCLUSIONS

Based on the discussions of this thesis following conclusions can be drawn for the following areas;

Ground Motion and Frames;

- Acceleration related and velocity related ground motion parameters are highly correlated among themselves.
- While compiling a ground motion data set, it is very difficult to achieve a uniform distribution of ground motion parameters since some parameters are computed directly using time history of the record and some parameters are computed from the response spectrum.
- Code based approximate period formulas underestimated the periods for the designed frames used in this study.
- Approximate methods are widely employed in the computation of inelastic displacement demand of structures. Nonlinear dynamic analysis of equivalent SDOF system provides satisfactory results for small displacements. Accuracy of SDOF results decreases as the level of nonlinearity increases. In general SDOF system underestimates the displacement demand for large deformations.

- The frames employed do not show strength degradation and predominantly respond in the first mode of vibration.

Correlation Study:

- In general, spectrum based parameters that account for the structural characteristics (fundamental period) reflecting its likely response intervals are found to be the most reliable ground motion intensity parameters representing the destructiveness of the ground motion for the structures having periods between 0.2-1.1 seconds.
- VSI and HI turned out to be two parameters that have strongest correlation with response followed by S_a and PGA.
- I_F , AI and CAV provided poorest correlations for SDOF and MDOF systems.
- I_c , PGV, EPA and ASI have moderate correlation with deformation demands.
- Selection of a proper ground motion intensity parameter is mainly influenced by the period of interest.
- Shifting the period range used in the formulation of ASI to 0.1-2.5 s. increased the correlation considerably. This clearly indicates that the period range covered influences the correlation.
- Revised ASI and VSI computed in T-2T range provided strong correlation and can be used in the assessment of a particular frame.
- Acceleration related ground motion intensity parameters are better for short period systems whereas velocity related indices provide sufficient correlation for intermediate period systems.
- Prediction equations for VSI and HI can be derived for seismic hazard analysis.
- No clear trend has been observed between the seismic indices and the damage surveyed after Northridge, California earthquake.

5.3 FUTURE RECOMMENDATIONS

Establishing a relationship between instrumental intensity and structural response is a very important task in earthquake engineering field. For future related studies addressing the interdependency between structural demand and ground motion intensity parameters can consider following issues;

- Following the same procedure, this study can be performed for narrower period ranges (for short, intermediate and long periods) with increased number of frames and ground motions.
- Effect of ground motion records with special attributes (near field, far field) on correlation can be studied.
- Different hysteretic models can be used. Dependency of the results on the selection of hysteretic models can be investigated.
- Ground motion intensity parameters can be combined.
- Each ground motion parameter can be scaled to a fixed value and effect of scaling on response can be examined.
- Maximum displacement and maximum interstory drift ratio were selected as the response parameters for SDOF and MDOF models. Different response parameters can be selected and compared.

REFERENCES

Akkar, S., Ozen, Ö. (2005), Effect of peak ground velocity on deformation demands for SDOF systems, *Earthquake Engineering and Structural Dynamics*, 34, 1551-1571.

Akkar, S., and Miranda, E. (2005), Statistical evaluation of approximate methods for estimating maximum deformation demands on existing structures, *Journal of Structural Engineering, ASCE*, 131(1), 160-172.

Akkar, S., Bommer J.J., (2007), Empirical prediction equations for peak ground velocity derived from strong-motion records from Europe and the Middle East, *Bulletin of the Seismological Society of America*, 97(2), 511-530.

Algan, B. B. (1982), Drift and damage considerations in earthquake resistant design of reinforced concrete buildings, *PhD Thesis*, University of Illinois, Urbana.

Applied Technology Council (ATC) (1978), Tentative provisions for the development of seismic regulations for buildings, *ATC-3*, California.

Applied Technology Council (ATC) (1996), Seismic evaluation and retrofit of concrete buildings, *ATC-40*, California.

Arias, A. (1970), A measure of earthquake intensity, *In Seismic Design for Nuclear Power Plants*, Hansen RJ (ed.). MIT Press: Cambridge, MA, 438–483.

ASCE (American Society of Civil Engineers) (2000), Prestandard and commentary for the seismic rehabilitation of buildings, *FEMA-356*, Washington, DC.

Ay, B.Ö., (2006), Fragility based assessment of low-rise and mid-rise reinforced concrete frame buildings in Turkey, *Msc Thesis*, Middle East Technical University, Ankara.

Cabanas, L., Benito, B., Herraiz, M. (1997), An approach to the measurement of the potential structural damage of earthquake ground motions, *Earthquake Engineering and Structural Dynamics*, 26, 79-92.

Chopra, A.K. (2000), Dynamics of Structures: theory and applications to earthquake engineering, Prentice Hall, New Jersey.

Cordova, P.P., Deierleing, G.G., Mehanny, S.S., and Cornell C.A. (2000), Development of a two-parameter seismic intensity measure and probabilistic assessment procedure, *Proceedings of the 2nd U.S.-Japan Workshop on Performance-Based Earthquake Engineering for Reinforced Concrete Building Structures*, Sapparo, Japan.

Douglas, J., (2001), A comprehensive worldwide summary of strong-motion attenuation relationships for peak ground acceleration and spectral ordinates (1969 to 2000), *ESEE Report* No. 01.1, Imperial College of Science, Technology and Medicine.

Elenas, A. (2000), Correlation between seismic acceleration parameters and overall structural damage indices of buildings, *Soil Dynamics and Earthquake Engineering*, 20, 93-100.

Elenas, A., Meskouris, K. (2001), Correlation study between seismic acceleration parameters and damage indices of structure, *Engineering Structures*, 23, 698-704.

EPRI (Electrical Power Research Institute) (1998), A criterion for determining exceedence of the operating basis earthquake, *EPRI NP-5930*, Palo Alto, CA.

Erberik, M.A., and Çulcu S. (2006), Assessment of seismic fragility curves for low and mid-rise reinforced concrete frame buildings using Düzce field database, *Proceedings of the NATO Science of Peace Workshop on Advances in Earthquake Engineering for Urban Risk Reduction*, NATO Science Series, IV. Earth and Environmental Sciences, 66, 151-166.

European Committee for Standardization (2003), Eurocode 8: Design of structures for earthquake resistance Part 3: Strengthening and repair of buildings – Draft No:4 *Eurocode 8*, Brussels.

Fajfar, P., Vidic, T., and Fischinger., M. (1990), A measure of earthquake motion capacity to damage medium-period structures, *Soil Dynamics and Earthquake Engineering*, 9(5), 236–242.

Gülkan, P., and Sozen, M.A. (1999), Procedure for determining seismic vulnerability of building structures, *ACI Structural Journal*, 96, 336–342.

Housner, G.W. (1952), Spectrum intensities of strong motion earthquakes, *Proceedings of the Symposium on Earthquake and Blast Effects on Structures*, Earthquake Engineering Research Institute.

Kramer, S.L. (1996), *Geotechnical Earthquake Engineering*, Prentice Hall, New Jersey.

Liao, W., Loh, C., Wan, S. (2001), Earthquake responses of RC moment frames subjected to near-fault ground motions, *Structural Design of Tall Buildings*, 10, 219-229.

Miranda E. (1999), Approximate lateral deformation demands in multistory buildings subjected to earthquakes, *Journal of Structural Engineering ASCE*, 125, 417-425.

Miranda, E. and Ruiz-Garcia, J. (2001), Evaluation of approximate methods to estimate maximum inelastic displacement demands, *Earthquake Engineering and Structural Dynamics*, 31(3), 539-560.

Moehle, J. P. (1992), Displacement-based design of RC structures subjected to earthquakes, *Earthquake Spectra*, 8, 403–428

Moehle, J. P. (1994), Seismic drift and its role in design, *Proceedings of the 5th U.S.–Japan Workshop on the Improvement of Building Structural Design and Construction Practices*, San Diego, 65–78.

Özcebe, G., Yüçemen, M.S., Yakut, A., and Aydoğan V. (2003), Seismic vulnerability assessment procedure for low-to-medium-rise RC buildings, *Middle East Technical University Civil Engineering Department Structural Engineering Research Unit*, Technical Report No. 2003/2, Ankara.

Park, Y.-J., Ang, A. H.-S., and Wen, Y.K. (1985), Seismic damage analysis of reinforced concrete buildings, *Journal of Structural Engineering*, ASCE, 111(4), 740-757.

Riddell R. (2007), On Ground Motion Intensity Indices, *Earthquake Spectra*, 23 (1), 147-173.

Sucuoğlu, H., and Nurtuğ, A. (1995), Earthquake ground motion characteristic and seismic energy dissipation, *Earthquake Engineering and Structural Dynamics*, 24, 1195-1213.

Sucuoğlu, H. (1997), Discussion of “An approach to the measurement of the potential structural damage of earthquake ground motions”, *Earthquake Engineering and Structural Dynamics*, 26, 1283-1285.

Sucuoğlu, H., Gülkan, P., Erberik, A., and Akkar, S. (1999), Measures of ground motion intensity in seismic design, *Proceedings of the Uğur Ersoy Symposium on Structural Engineering*, Ankara, 105-119.

Travasarou, T., Bray, J.D., and Abrahamson, N.A. (2003), Empirical attenuation relationship for Arias Intensity, *Earthquake Engineering and Structural Dynamics*, 32, 1133-1155.

Turkish Ministry of Public Works and Settlement (1997), Specification for Structures to be Built in Disaster Areas, Ankara.

Uang, C.H., and Bertero V.V. (1988), Implications of recorded earthquake ground motions on seismic design of buildings structures, *UCB/EERC-88/13*, California.

Valles, R.E., Reinhorn, A.M., Kunn ath, S.K., Li, C., and Madan, A. (1996), IDARC-2D: A program for the inelastic damage analysis of buildings, *National Center for Earthquake Engineering Research*, State University of New York at Buffalo.

Von Thun J.L., Roehim L.H., Scott G.A., and Wilson J.A. (1988). Earthquake ground motions for design and analysis of dams, *Earthquake Engineering and Soil Dynamics II-Recent Advances in Ground Motion Evaluation*, Geotechnical Special Publication, 20, 463-481.

Wu, Y.M., Hsiao, N.C., and Teng, T.L., (2004), Relationship between strong motion peak values and seismic loss during the 1999 Chi-Chi, Taiwan earthquake, *Natural Hazards*, 32, 357-373.

APPENDIX A

FRAME DETAILS

A.1 F1-2S3B

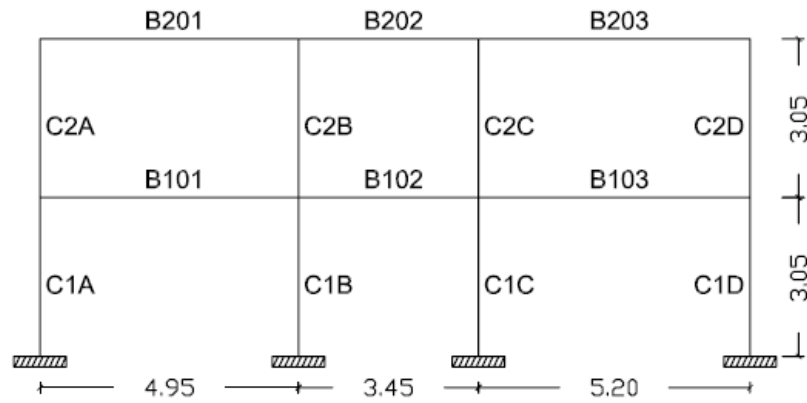


Figure A.1 Frame F1-2S3B

Table A.1 Column properties (F1-2S3B)

Column	Depth (cm)	Width (cm)	Reinf. Area (mm ²)
C1A	60	30	1800
C2A	60	30	1800
C1B	60	30	1800
C2B	60	30	1800
C1C	60	30	1800
C2C	60	30	1800
C1D	60	30	1800
C2D	60	30	1800

Table A.2 Beam properties (F1-2S3B)

Beam		Depth (cm)	Width (cm)	Bottom Reinf. (mm ²)	Top Reinf. (mm ²)
B101	LEFT	60	30	387	781
	RIGHT	60	30	368	742
B102	LEFT	60	30	329	665
	RIGHT	60	30	329	671
B103	LEFT	60	30	374	755
	RIGHT	60	30	381	774
B201	LEFT	60	30	265	535
	RIGHT	60	30	277	568
B202	LEFT	60	30	232	465
	RIGHT	60	30	239	477
B203	LEFT	60	30	290	587
	RIGHT	60	30	271	542

A.2 F2-3S3B

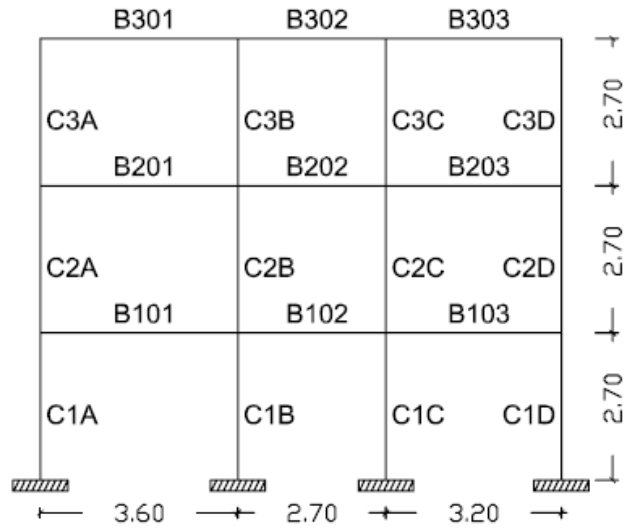


Figure A.2 Frame F2-3S3B

Table A.3 Column properties (F2-3S3B)

Column	Depth (cm)	Width (cm)	Reinf. Area (mm ²)
C1A	50	25	1250
C2A	50	25	1250
C3A	50	25	1250
C1B	50	25	1250
C2B	50	25	1250
C3B	50	25	1250
C1C	50	25	1250
C2C	50	25	1250
C3C	50	25	1250
C1D	50	25	1250
C2D	50	25	1250
C3D	50	25	1250

Table A.4 Beam properties (F2-3S3B)

Beam		Depth (cm)	Width (cm)	Bottom Reinf. (mm ²)	Top Reinf. (mm ²)
B101	LEFT	50	25	335	619
	RIGHT	50	25	277	561
B102	LEFT	50	25	335	542
	RIGHT	50	25	335	529
B103	LEFT	50	25	310	548
	RIGHT	50	25	387	613
B201	LEFT	50	25	265	542
	RIGHT	50	25	239	477
B202	LEFT	50	25	277	465
	RIGHT	50	25	277	465
B203	LEFT	50	25	239	458
	RIGHT	50	25	271	523
B301	LEFT	50	25	155	310
	RIGHT	50	25	148	303
B302	LEFT	50	25	135	265
	RIGHT	50	25	129	258
B303	LEFT	50	25	135	271
	RIGHT	50	25	142	290

A.3 F3-3S2B

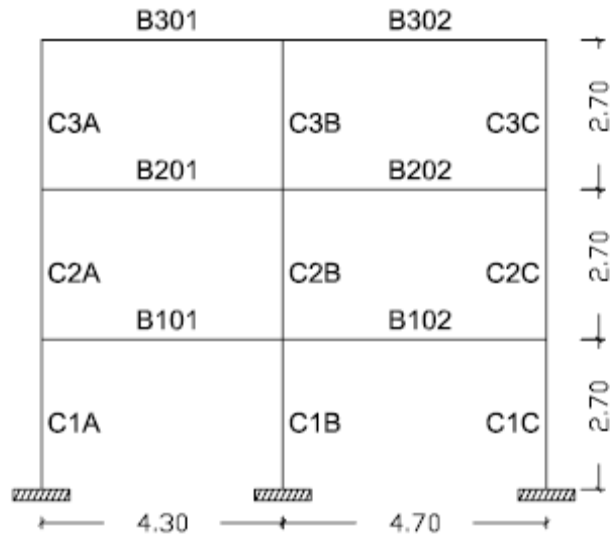


Figure A.3 Frame F3-3S2B

Table A.5 Column properties (F3-3S2B)

Column	Depth (cm)	Width (cm)	Reinf. Area (mm ²)
C1A	50	25	1250
C2A	50	25	1250
C3A	50	25	1250
C1B	25	50	1250
C2B	25	50	1250
C3B	25	50	1250
C1C	50	25	1250
C2C	50	25	1250
C3C	50	25	1250

Table A.6 Beam properties (F3-3S2B)

Beam		Depth (cm)	Width (cm)	Bottom Reinf. (mm ²)	Top Reinf. (mm ²)
B101	LEFT	50	20	510	819
	RIGHT	50	20	400	632
B102	LEFT	50	20	348	561
	RIGHT	50	20	458	697
B201	LEFT	50	20	484	774
	RIGHT	50	20	400	632
B202	LEFT	50	20	348	561
	RIGHT	50	20	426	671
B301	LEFT	50	20	310	561
	RIGHT	50	20	284	561
B302	LEFT	50	20	252	516
	RIGHT	50	20	271	555

A.4 F4-3S3B

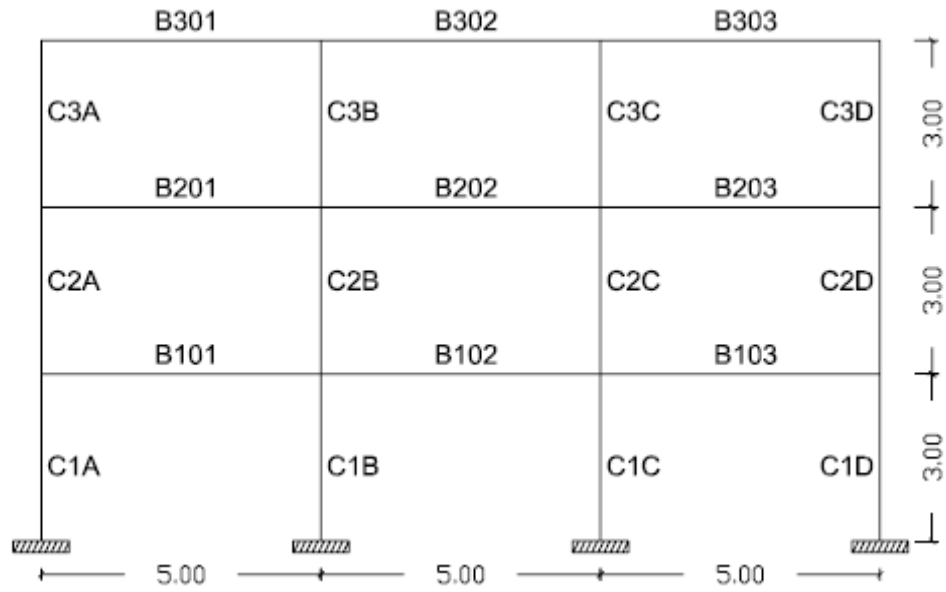


Figure A.4 Frame F4-3S3B

Table A.7 Column properties (F4-3S3B)

Column	Depth (cm)	Width (cm)	Reinf. Area (mm ²)
C1A	40	40	2948
C2A	40	40	1916
C3A	40	40	1600
C1B	40	40	2303
C2B	40	40	1600
C3B	40	40	1600
C1C	40	40	2303
C2C	40	40	1600
C3C	40	40	1600
C1D	40	40	2948
C2D	40	40	1916
C3D	40	40	1600

Table A.8 Beam properties (F4-3S3B)

Beam		Depth (cm)	Width (cm)	Bottom Reinf. (mm ²)	Top Reinf. (mm ²)
B101	LEFT	50	30	845	1406
	RIGHT	50	30	845	1510
B102	LEFT	50	30	845	1368
	RIGHT	50	30	845	1368
B103	LEFT	50	30	845	1510
	RIGHT	50	30	845	1406
B201	LEFT	50	30	813	1258
	RIGHT	50	30	832	1290
B202	LEFT	50	30	787	1219
	RIGHT	50	30	787	1219
B203	LEFT	50	30	832	1290
	RIGHT	50	30	813	1258
B301	LEFT	50	30	432	845
	RIGHT	50	30	587	897
B302	LEFT	50	30	548	845
	RIGHT	50	30	548	845
B303	LEFT	50	30	587	897
	RIGHT	50	30	432	845

A.5 F5-4S3B

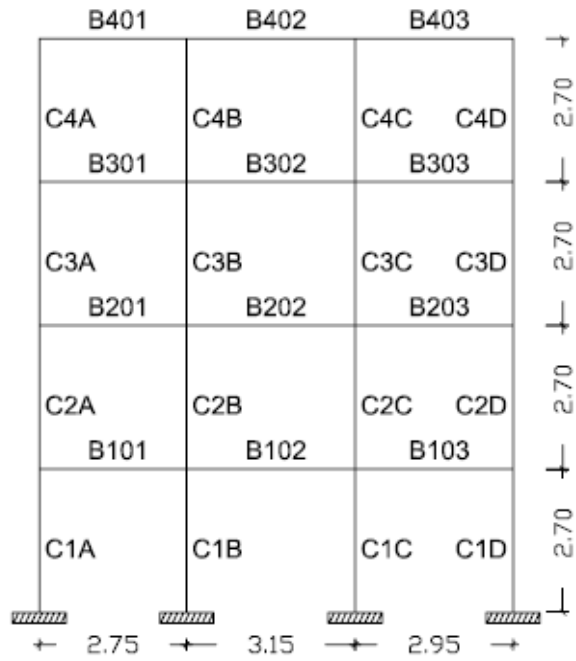


Figure A.5 Frame F5-4S3B

Table A.9 Column properties (F5-4S3B)

Column	Depth (cm)	Width (cm)	Reinf. Area (mm ²)
C1A	25	80	2000
C2A	25	80	2000
C3A	25	80	2000
C4A	25	80	2000
C1B	25	80	2000
C2B	25	80	2000
C3B	25	80	2000
C4B	25	80	2000
C1C	25	80	2000
C2C	25	80	2000
C3C	25	80	2000
C4C	25	80	2000
C1D	25	80	2000
C2D	25	80	2000
C3D	25	80	2000
C4D	25	80	2000

Table A.10 Beam properties (F5-4S3B)

Beam		Depth (cm)	Width (cm)	Bottom Reinf. (mm ²)	Top Reinf. (mm ²)
B101	LEFT	50	20	703	703
	RIGHT	50	20	523	703
B102	LEFT	50	20	374	574
	RIGHT	50	20	368	587
B103	LEFT	50	20	497	703
	RIGHT	50	20	703	703
B201	LEFT	50	20	606	703
	RIGHT	50	20	452	606
B202	LEFT	50	20	355	555
	RIGHT	50	20	355	561
B203	LEFT	50	20	426	613
	RIGHT	50	20	581	703
B301	LEFT	50	20	381	516
	RIGHT	50	20	277	419
B302	LEFT	50	20	239	432
	RIGHT	50	20	232	432
B303	LEFT	50	20	258	426
	RIGHT	50	20	361	516
B401	LEFT	50	20	135	219
	RIGHT	50	20	97	194
B402	LEFT	50	20	123	194
	RIGHT	50	20	123	252
B403	LEFT	50	20	103	206
	RIGHT	50	20	129	226

A.6 F6-4S3B

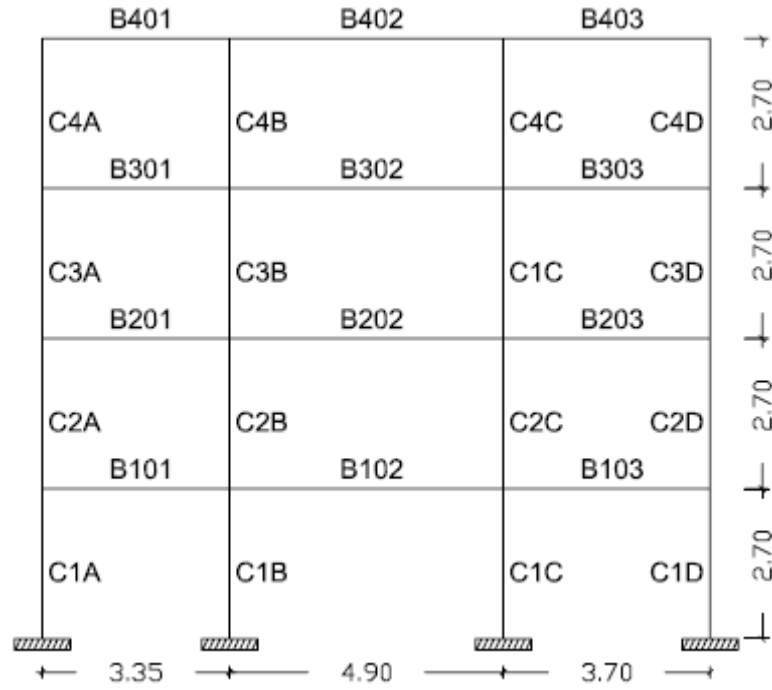


Figure A.6 Frame F6-4S3B

Table A.11 Column properties (F6-4S3B)

Column	Depth (cm)	Width (cm)	Reinf. Area (mm ²)
C1A	80	25	2000
C2A	80	25	2000
C3A	80	25	2000
C4A	80	25	2000
C1B	80	25	2000
C2B	80	25	2000
C3B	80	25	2000
C4B	80	25	2000
C1C	80	25	2000
C2C	80	25	2000
C3C	80	25	2000
C4C	80	25	2000
C1D	25	80	2000
C2D	25	80	2000
C3D	25	80	2000
C4D	25	80	2000

Table A.12 Beam properties (F6-4S3B)

Beam		Depth (cm)	Width (cm)	Bottom Reinf. (mm ²)	Top Reinf. (mm ²)
B101	LEFT	50	20	200	413
	RIGHT	50	20	265	535
B102	LEFT	50	20	394	606
	RIGHT	50	20	387	594
B103	LEFT	50	20	323	561
	RIGHT	50	20	323	561
B201	LEFT	50	20	232	477
	RIGHT	50	20	265	542
B202	LEFT	50	20	419	639
	RIGHT	50	20	400	619
B203	LEFT	50	20	335	561
	RIGHT	50	20	355	561
B301	LEFT	50	20	213	432
	RIGHT	50	20	219	445
B302	LEFT	50	20	387	594
	RIGHT	50	20	368	568
B303	LEFT	50	20	284	561
	RIGHT	50	20	310	561
B401	LEFT	50	20	116	239
	RIGHT	50	20	181	368
B402	LEFT	50	20	355	561
	RIGHT	50	20	335	561
B403	LEFT	50	20	245	497
	RIGHT	50	20	239	484

A.7 F7-4S3B

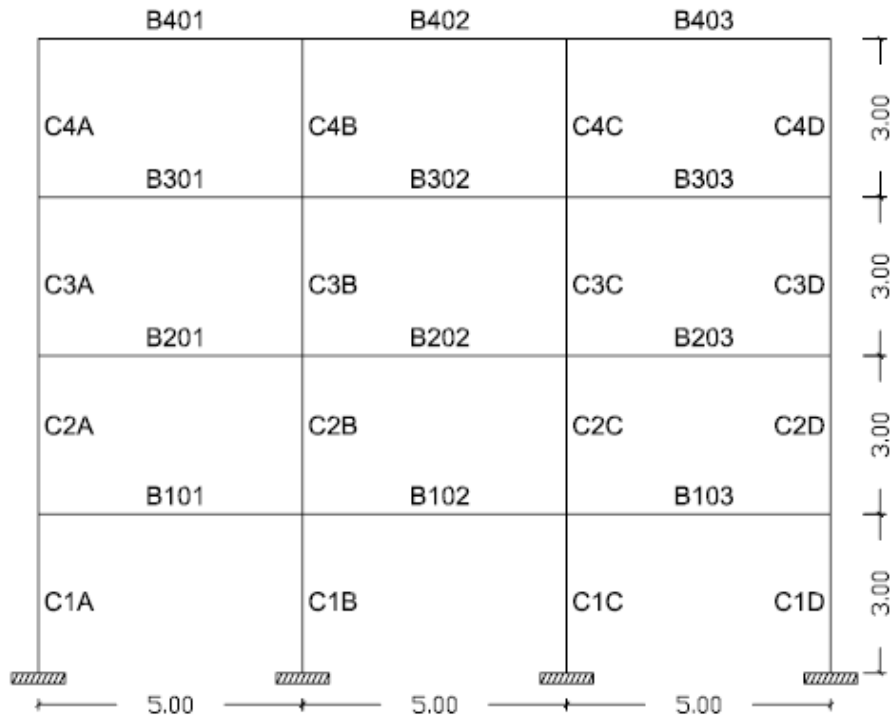


Figure A.7 Frame F7-4S3B

Table A.13 Column properties (F7-4S3B)

Column	Depth (cm)	Width (cm)	Reinf. Area (mm ²)
C1A	50	50	2500
C2A	50	50	2500
C3A	50	50	2500
C4A	50	50	2500
C1B	50	50	2500
C2B	50	50	2500
C3B	50	50	2500
C4B	50	50	2500
C1C	50	50	2500
C2C	50	50	2500
C3C	50	50	2500
C4C	50	50	2500
C1D	50	50	2500
C2D	50	50	2500
C3D	50	50	2500
C4D	50	50	2500

Table A.14 Beam properties (F7-4S3B)

Beam		Depth (cm)	Width (cm)	Bottom Reinf. (mm ²)	Top Reinf. (mm ²)
B101	LEFT	55	25	432	806
	RIGHT	55	25	432	800
B102	LEFT	55	25	432	761
	RIGHT	55	25	432	761
B103	LEFT	55	25	432	794
	RIGHT	55	25	432	800
B201	LEFT	55	25	432	806
	RIGHT	55	25	432	800
B202	LEFT	55	25	432	761
	RIGHT	55	25	432	761
B203	LEFT	55	25	432	794
	RIGHT	55	25	432	800
B301	LEFT	55	25	426	665
	RIGHT	55	25	406	632
B302	LEFT	55	25	406	632
	RIGHT	55	25	406	632
B303	LEFT	55	25	406	626
	RIGHT	55	25	426	658
B401	LEFT	55	25	277	432
	RIGHT	55	25	297	458
B402	LEFT	55	25	290	445
	RIGHT	55	25	290	445
B403	LEFT	55	25	297	458
	RIGHT	55	25	271	432

A.8 F8-5S4B

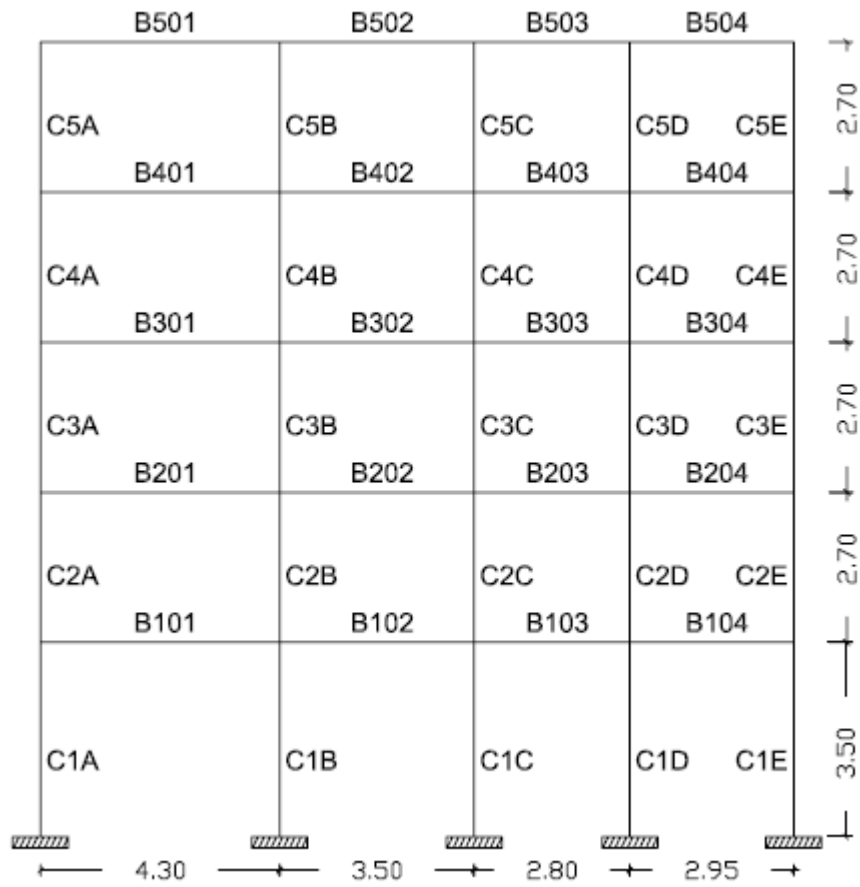


Figure A.8 Frame F8-5S4B

Table A.15 Column properties (F8-5S4B)

Column	Depth (cm)	Width (cm)	Reinf. Area (mm ²)
C1A	30	70	2100
C2A	30	70	2100
C3A	30	70	2100
C4A	30	70	2100
C5A	30	70	2100
C1B	30	70	2100
C2B	30	70	2100
C3B	30	70	2100
C4B	30	70	2100
C5B	30	70	2100
C1C	30	70	2100
C2C	30	70	2100
C3C	30	70	2100
C4C	30	70	2100
C5C	30	70	2100
C1D	30	70	2100
C2D	30	70	2100
C3D	30	70	2100
C4D	30	70	2100
C5D	30	70	2100
C1E	70	35	2450
C2E	70	35	2450
C3E	70	35	2450
C4E	70	35	2450
C5E	70	35	2450

Table A.16 Beam properties (F8-5S4B)

Beam		Depth (cm)	Width (cm)	Bottom Reinf. (mm ²)	Top Reinf. (mm ²)
B101	LEFT	60	20	677	806
	RIGHT	60	20	465	716
B102	LEFT	60	20	458	677
	RIGHT	60	20	510	677
B103	LEFT	60	20	587	677
	RIGHT	60	20	510	677
B104	LEFT	60	20	677	787
	RIGHT	60	20	1116	1335
B201	LEFT	60	20	561	774
	RIGHT	60	20	439	677
B202	LEFT	60	20	477	677
	RIGHT	60	20	490	677
B203	LEFT	60	20	600	677
	RIGHT	60	20	587	677
B204	LEFT	60	20	677	697
	RIGHT	60	20	871	1110
B301	LEFT	60	20	432	677
	RIGHT	60	20	368	677
B302	LEFT	60	20	361	677
	RIGHT	60	20	368	677
B303	LEFT	60	20	458	677
	RIGHT	60	20	465	658
B304	LEFT	60	20	535	677
	RIGHT	60	20	677	877
B401	LEFT	60	20	342	677
	RIGHT	60	20	277	568
B402	LEFT	60	20	277	568
	RIGHT	60	20	265	535
B403	LEFT	60	20	290	555
	RIGHT	60	20	323	510
B404	LEFT	60	20	303	458
	RIGHT	60	20	458	677
B501	LEFT	60	20	181	361
	RIGHT	60	20	181	368
B502	LEFT	60	20	181	368
	RIGHT	60	20	148	303
B503	LEFT	60	20	155	310
	RIGHT	60	20	142	284
B504	LEFT	60	20	110	213
	RIGHT	60	20	219	445

A.9 F9-5S3B

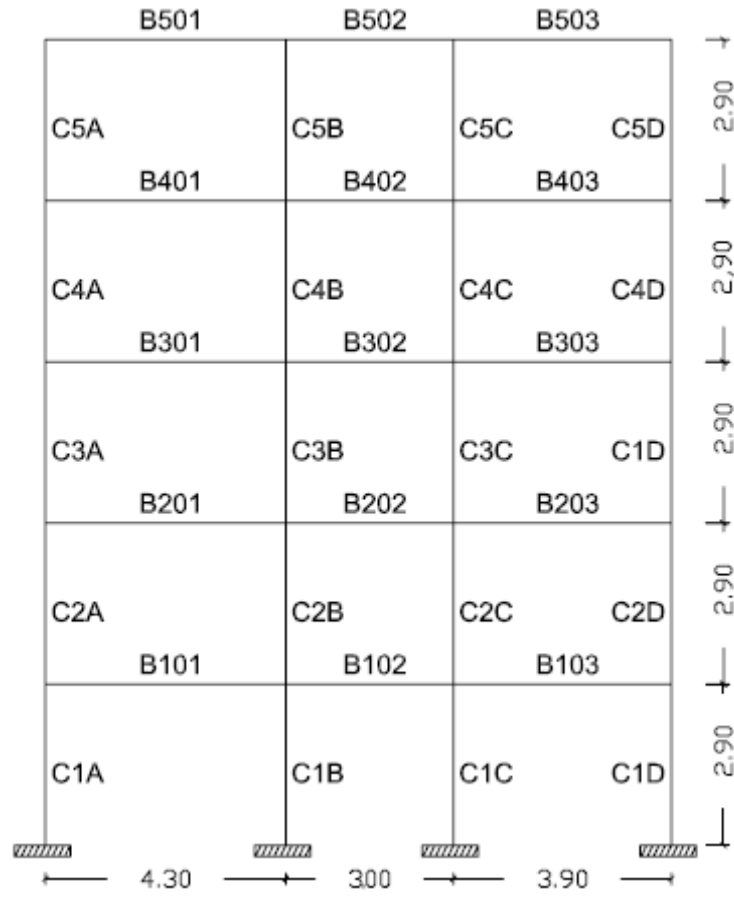


Figure A.9 Frame F9-5S3B

Table A.17 Column properties (F9-5S3B)

Column	Depth (cm)	Width (cm)	Reinf. Area (mm ²)
C1A	25	60	1500
C2A	25	50	1250
C3A	25	50	1250
C4A	25	50	1250
C5A	25	50	1250
C1B	25	60	1500
C2B	25	50	1250
C3B	25	50	1250
C4B	25	50	1250
C5B	25	50	1250
C1C	60	25	1500
C2C	50	25	1250
C3C	50	25	1250
C4C	50	25	1250
C5C	50	25	1250
C1D	60	25	1500
C2D	50	25	1250
C3D	50	25	1250
C4D	50	25	1250
C5D	50	25	1250

Table A.18 Beam properties (F9-5S3B)

Beam		Depth (cm)	Width (cm)	Bottom Reinf. (mm ²)	Top Reinf. (mm ²)
B101	LEFT	55	20	548	619
	RIGHT	55	20	303	613
B102	LEFT	55	20	471	619
	RIGHT	55	20	716	955
B103	LEFT	50	20	652	890
	RIGHT	50	20	619	677
B201	LEFT	55	20	561	645
	RIGHT	55	20	348	561
B202	LEFT	55	20	535	671
	RIGHT	55	20	690	955
B203	LEFT	50	20	652	884
	RIGHT	50	20	574	755
B301	LEFT	55	20	445	561
	RIGHT	55	20	297	561
B302	LEFT	55	20	406	561
	RIGHT	55	20	561	800
B303	LEFT	50	20	561	735
	RIGHT	50	20	561	632
B401	LEFT	55	20	277	561
	RIGHT	55	20	232	471
B402	LEFT	55	20	265	535
	RIGHT	55	20	406	561
B403	LEFT	50	20	413	561
	RIGHT	50	20	342	561
B501	LEFT	55	20	135	271
	RIGHT	55	20	155	310
B502	LEFT	55	20	148	297
	RIGHT	55	20	194	394
B503	LEFT	50	20	187	381
	RIGHT	50	20	135	271

A.10 F10-5S4B

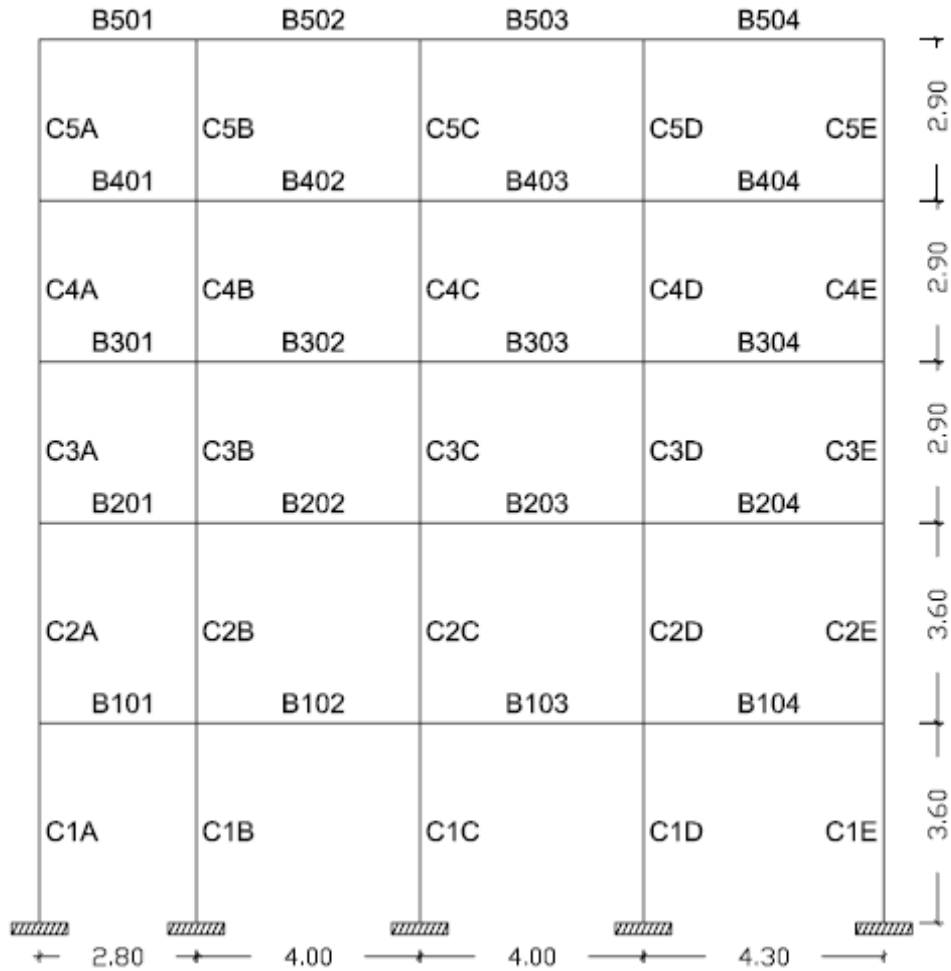


Figure A.10 Frame F10-5S4B

Table A.19 Column properties (F10-5S4B)

Column	Depth (cm)	Width (cm)	Reinf. Area (mm ²)
C1A	50	50	2500
C2A	50	50	2500
C3A	50	50	2500
C4A	50	50	2500
C5A	50	50	2500
C1B	50	50	2500
C2B	50	50	2500
C3B	50	50	2500
C4B	50	50	2500
C5B	50	50	2500
C1C	40	70	2800
C2C	40	70	2800
C3C	40	70	2800
C4C	40	70	2800
C5C	40	70	2800
C1D	70	30	2100
C2D	70	30	2100
C3D	70	30	2100
C4D	70	30	2100
C5D	70	30	2100
C1E	60	30	1800
C2E	60	30	1800
C3E	60	30	1800
C4E	60	30	1800
C5E	60	30	1800

Table A.20 Beam properties (F10-5S4B)

Beam		Depth (cm)	Width (cm)	Bottom Reinf. (mm ²)	Top Reinf. (mm ²)
B101	LEFT	60	20	1206	1413
	RIGHT	60	20	1039	1258
B102	LEFT	60	20	677	1077
	RIGHT	60	20	677	1071
B103	LEFT	60	20	677	1135
	RIGHT	60	20	710	1265
B104	LEFT	60	20	723	1361
	RIGHT	60	20	768	1374
B201	LEFT	60	20	1019	1277
	RIGHT	60	20	955	1097
B202	LEFT	60	20	677	1090
	RIGHT	60	20	677	1084
B203	LEFT	60	20	677	1116
	RIGHT	60	20	677	1200
B204	LEFT	60	20	677	1219
	RIGHT	60	20	677	1303
B301	LEFT	60	20	677	929
	RIGHT	60	20	677	748
B302	LEFT	60	20	581	910
	RIGHT	60	20	581	903
B303	LEFT	60	20	581	910
	RIGHT	60	20	606	948
B304	LEFT	60	20	587	923
	RIGHT	60	20	652	1032
B401	LEFT	60	20	432	677
	RIGHT	60	20	497	594
B402	LEFT	60	20	458	710
	RIGHT	60	20	458	716
B403	LEFT	60	20	452	703
	RIGHT	60	20	458	710
B404	LEFT	60	20	426	677
	RIGHT	60	20	503	781
B501	LEFT	60	20	187	374
	RIGHT	60	20	129	258
B502	LEFT	60	20	284	581
	RIGHT	60	20	297	606
B503	LEFT	60	20	284	574
	RIGHT	60	20	284	581
B504	LEFT	60	20	277	568
	RIGHT	60	20	303	613

A.11 F11-5S3B

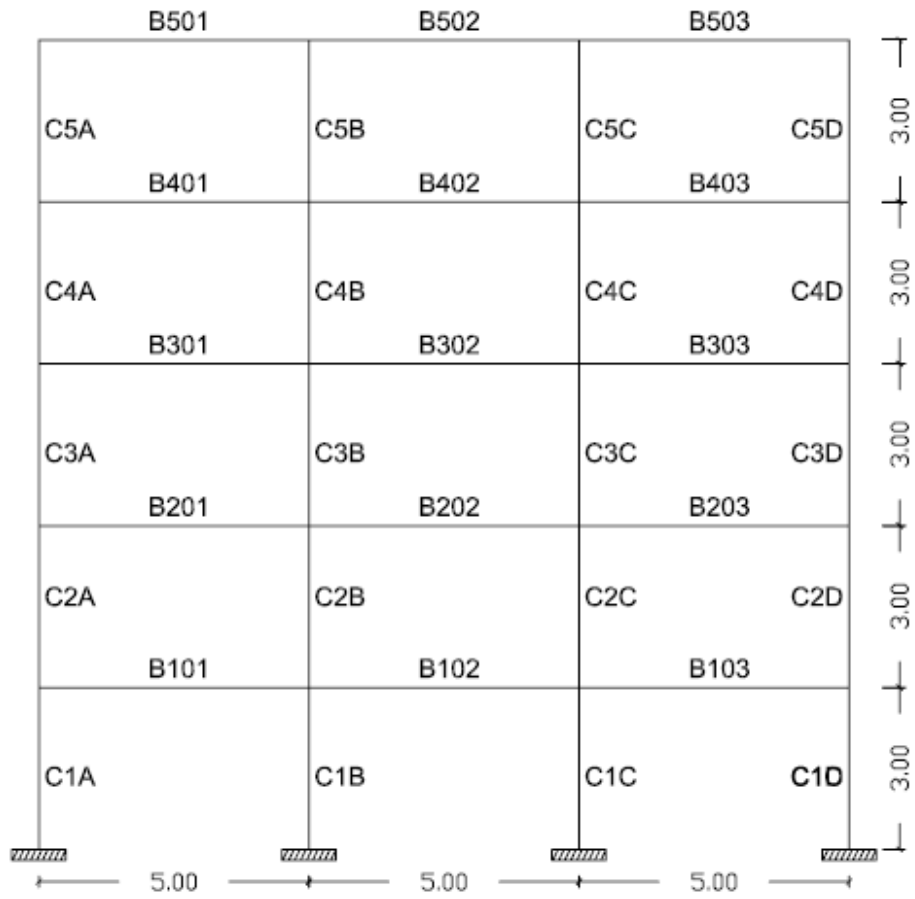


Figure A.11 Frame F11-5S3B

Table A.21 Column properties (F11-5S3B)

Column	Depth (cm)	Width (cm)	Reinf. Area (mm²)
C1A	45	45	3510
C2A	45	45	2026
C3A	45	45	2026
C4A	40	40	1903
C5A	40	40	1600
C1B	45	45	2148
C2B	45	45	2026
C3B	45	45	2026
C4B	40	40	1600
C5B	40	40	1600
C1C	45	45	2148
C2C	45	45	2026
C3C	45	45	2026
C4C	40	40	1600
C5C	40	40	1600
C1D	45	45	3510
C2D	45	45	2026
C3D	45	45	2026
C4D	40	40	1903
C5D	40	40	1600

Table A.22 Beam properties (F11-5S3B)

Beam		Depth (cm)	Width (cm)	Bottom Reinf. (mm ²)	Top Reinf. (mm ²)
B101	LEFT	50	30	890	1742
	RIGHT	50	30	845	1742
B102	LEFT	50	30	845	1645
	RIGHT	50	30	845	1645
B103	LEFT	50	30	845	1742
	RIGHT	50	30	890	1742
B201	LEFT	50	30	871	1832
	RIGHT	50	30	845	1735
B202	LEFT	50	30	845	1710
	RIGHT	50	30	845	1710
B203	LEFT	50	30	845	1735
	RIGHT	50	30	871	1832
B301	LEFT	50	30	845	1594
	RIGHT	50	30	845	1503
B302	LEFT	50	30	845	1497
	RIGHT	50	30	845	1497
B303	LEFT	50	30	845	1503
	RIGHT	50	30	845	1594
B401	LEFT	50	30	813	1258
	RIGHT	50	30	761	1174
B402	LEFT	50	30	774	1194
	RIGHT	50	30	774	1194
B403	LEFT	50	30	761	1174
	RIGHT	50	30	813	1258
B501	LEFT	50	30	432	845
	RIGHT	50	30	529	845
B502	LEFT	50	30	542	845
	RIGHT	50	30	542	845
B503	LEFT	50	30	529	845
	RIGHT	50	30	432	845

A.12 F12-6S4B

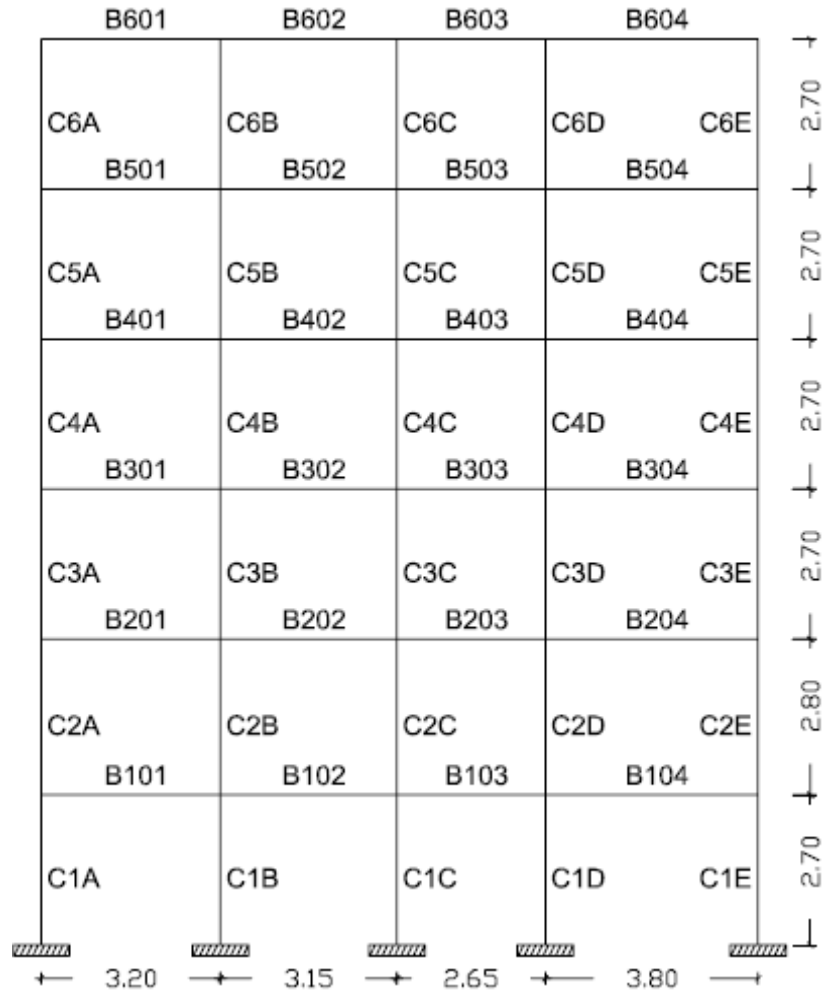


Figure A.12 Frame F12-6S4B

Table A.23 Column properties (F12-6S4B)

Column	Depth (cm)	Width (cm)	Reinf. Area (mm ²)
C1A	25	80	2000
C2A	25	80	2000
C3A	25	80	2000
C4A	25	80	2000
C5A	25	80	2000
C6A	25	80	2000
C1B	70	25	1750
C2B	70	25	1750
C3B	70	25	1750
C4B	70	25	1750
C5B	70	25	1750
C6B	70	25	1750
C1C	25	60	1500
C2C	25	60	1500
C3C	25	60	1500
C4C	25	60	1500
C5C	25	60	1500
C6C	25	60	1500
C1D	50	50	2500
C2D	50	50	2500
C3D	50	50	2500
C4D	50	50	2500
C5D	50	50	2500
C6D	50	50	2500
C1E	25	60	1500
C2E	25	60	1500
C3E	25	60	1500
C4E	25	60	1500
C5E	25	60	1500
C6E	25	60	1500

Table A.24 Beam properties (F12-6S4B)

Beam		Depth (cm)	Width (cm)	Bottom Reinf. (mm ²)	Top Reinf. (mm ²)
B101	LEFT	60	20	781	845
	RIGHT	60	20	845	1019
B102	LEFT	60	20	845	948
	RIGHT	60	20	329	594
B103	LEFT	60	20	323	516
	RIGHT	60	20	845	1000
B104	LEFT	60	20	658	968
	RIGHT	60	20	535	800
B201	LEFT	60	20	781	845
	RIGHT	60	20	845	1019
B202	LEFT	60	20	845	981
	RIGHT	60	20	387	652
B203	LEFT	60	20	374	535
	RIGHT	60	20	845	1019
B204	LEFT	60	20	658	968
	RIGHT	60	20	535	845
B301	LEFT	60	20	626	832
	RIGHT	60	20	845	845
B302	LEFT	60	20	845	865
	RIGHT	60	20	342	600
B303	LEFT	60	20	310	458
	RIGHT	60	20	761	903
B304	LEFT	60	20	548	845
	RIGHT	60	20	535	768
B401	LEFT	60	20	439	665
	RIGHT	60	20	671	806
B402	LEFT	60	20	671	845
	RIGHT	60	20	258	510
B403	LEFT	60	20	226	361
	RIGHT	60	20	542	845
B404	LEFT	60	20	445	845
	RIGHT	60	20	310	632
B501	LEFT	60	20	226	458
	RIGHT	60	20	394	503
B502	LEFT	60	20	432	697
	RIGHT	60	20	200	400
B503	LEFT	60	20	123	252
	RIGHT	60	20	355	729
B504	LEFT	60	20	329	665
	RIGHT	60	20	232	477
B601	LEFT	60	20	97	194
	RIGHT	60	20	116	239
B602	LEFT	60	20	213	432
	RIGHT	60	20	123	245
B603	LEFT	60	20	58	116
	RIGHT	60	20	226	465
B604	LEFT	60	20	219	439
	RIGHT	60	20	110	213

A.13 F13-6S3B

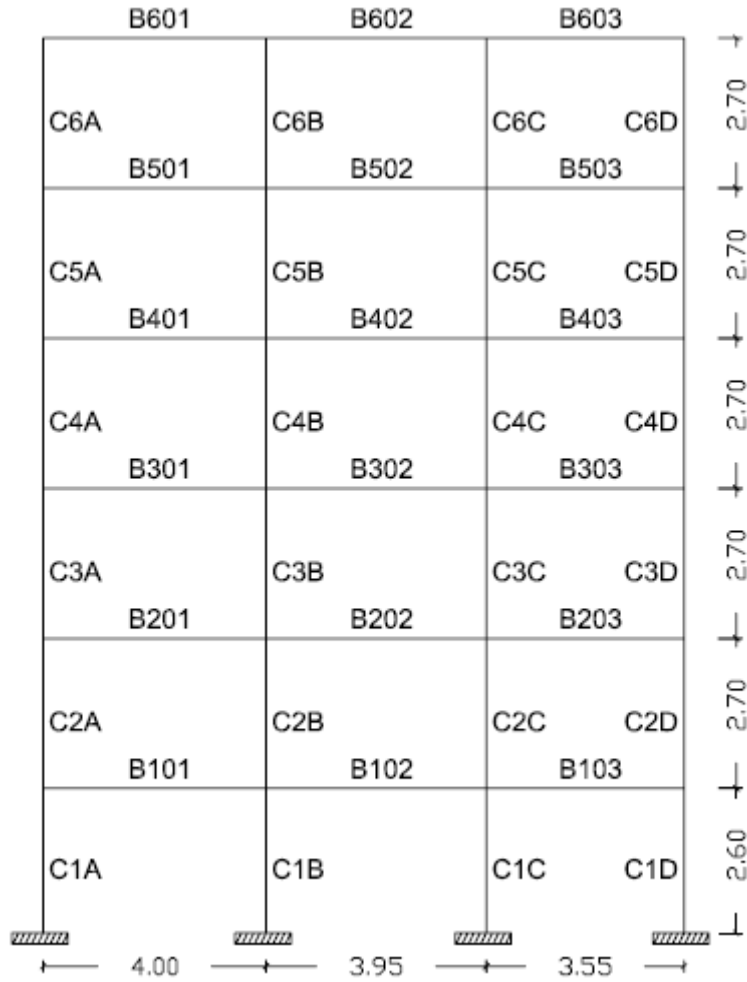


Figure A.13 Frame F13-6S3B

Table A.25 Column properties (F13-6S3B)

Column	Depth (cm)	Width (cm)	Reinf. Area (mm ²)
C1A	60	25	1500
C2A	60	25	1500
C3A	60	25	1500
C4A	60	25	1500
C5A	60	25	1500
C6A	60	25	1500
C1B	60	25	1500
C2B	60	25	1500
C3B	60	25	1500
C4B	60	25	1500
C5B	60	25	1500
C6B	60	25	1500
C1C	60	25	1500
C2C	60	25	1500
C3C	60	25	1500
C4C	60	25	1500
C5C	60	25	1500
C6C	60	25	1500
C1D	40	25	1000
C2D	40	25	1000
C3D	40	25	1000
C4D	40	25	1000
C5D	40	25	1000
C6D	40	25	1000

Table A.26 Beam properties (F13-6S3B)

Beam		Depth (cm)	Width (cm)	Bottom Reinf. (mm ²)	Top Reinf. (mm ²)
B101	LEFT	50	20	1006	1452
	RIGHT	50	20	897	1361
B102	LEFT	50	25	1103	1548
	RIGHT	50	25	1090	1568
B103	LEFT	50	20	890	1265
	RIGHT	50	20	871	1142
B201	LEFT	50	20	1142	1652
	RIGHT	50	20	1058	1503
B202	LEFT	50	25	1310	1755
	RIGHT	50	25	1284	1787
B203	LEFT	50	20	1045	1387
	RIGHT	50	20	981	1310
B301	LEFT	50	20	968	1490
	RIGHT	50	20	929	1329
B302	LEFT	50	25	1155	1581
	RIGHT	50	25	1129	1619
B303	LEFT	50	20	903	1213
	RIGHT	50	20	839	1174
B401	LEFT	50	20	697	1206
	RIGHT	50	20	690	1052
B402	LEFT	50	25	871	1271
	RIGHT	50	25	845	1316
B403	LEFT	50	20	665	942
	RIGHT	50	20	600	942
B501	LEFT	50	20	555	871
	RIGHT	50	20	542	735
B502	LEFT	50	25	703	903
	RIGHT	50	25	665	955
B503	LEFT	50	20	516	626
	RIGHT	50	20	432	671
B601	LEFT	50	20	342	561
	RIGHT	50	20	303	561
B602	LEFT	50	25	355	703
	RIGHT	50	25	381	703
B603	LEFT	50	20	245	497
	RIGHT	50	20	213	439

A.14 F14-6S3B

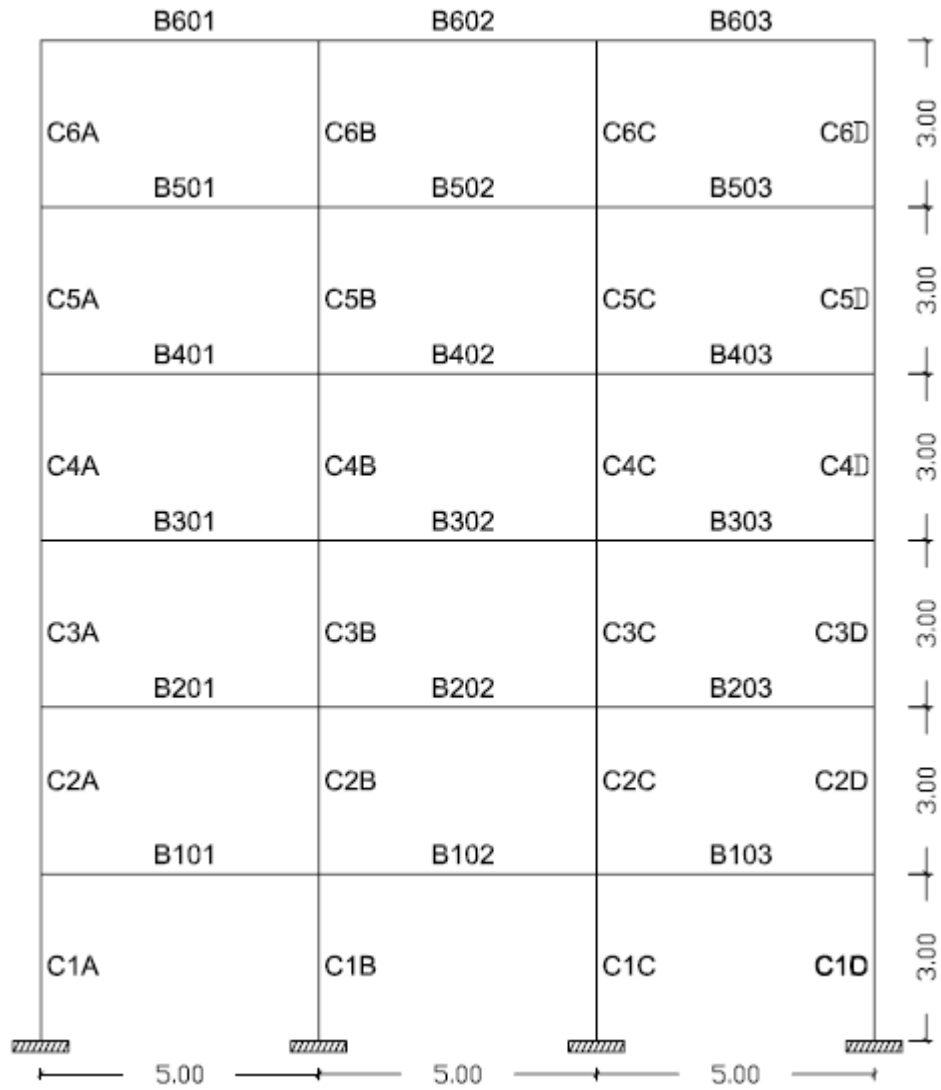


Figure A.14 Frame F14-6S3B

Table A.27 Column properties (F14-6S3B)

Column	Depth (cm)	Width (cm)	Reinf. Area (mm²)
C1A	50	50	2500
C2A	50	50	2500
C3A	50	50	2500
C4A	50	50	2500
C5A	50	50	2500
C6A	50	50	2500
C1B	50	50	2500
C2B	50	50	2500
C3B	50	50	2500
C4B	50	50	2500
C5B	50	50	2500
C6B	50	50	2500
C1C	50	50	2500
C2C	50	50	2500
C3C	50	50	2500
C4C	50	50	2500
C5C	50	50	2500
C6C	50	50	2500
C1D	50	50	2500
C2D	50	50	2500
C3D	50	50	2500
C4D	50	50	2500
C5D	50	50	2500
C6D	50	50	2500

Table A.28 Beam properties (F14-6S3B)

Beam		Depth (cm)	Width (cm)	Bottom Reinf. (mm ²)	Top Reinf. (mm ²)
B101	LEFT	60	25	671	1213
	RIGHT	60	25	555	1155
B102	LEFT	60	25	516	1090
	RIGHT	60	25	516	1090
B103	LEFT	60	25	548	1148
	RIGHT	60	25	658	1206
B201	LEFT	60	25	703	1310
	RIGHT	60	25	639	1206
B202	LEFT	60	25	587	1187
	RIGHT	60	25	587	1181
B203	LEFT	60	25	632	1200
	RIGHT	60	25	703	1303
B301	LEFT	60	25	574	1187
	RIGHT	60	25	535	1065
B302	LEFT	60	25	510	1084
	RIGHT	60	25	510	1077
B303	LEFT	60	25	535	1065
	RIGHT	60	25	568	1181
B401	LEFT	60	25	471	987
	RIGHT	60	25	445	865
B402	LEFT	60	25	445	903
	RIGHT	60	25	445	903
B403	LEFT	60	25	445	858
	RIGHT	60	25	465	981
B501	LEFT	60	25	445	742
	RIGHT	60	25	400	619
B502	LEFT	60	25	445	690
	RIGHT	60	25	445	690
B503	LEFT	60	25	400	619
	RIGHT	60	25	445	735
B601	LEFT	60	25	284	445
	RIGHT	60	25	277	445
B602	LEFT	60	25	303	465
	RIGHT	60	25	303	465
B603	LEFT	60	25	271	445
	RIGHT	60	25	284	445

A.15 F15-7S3B

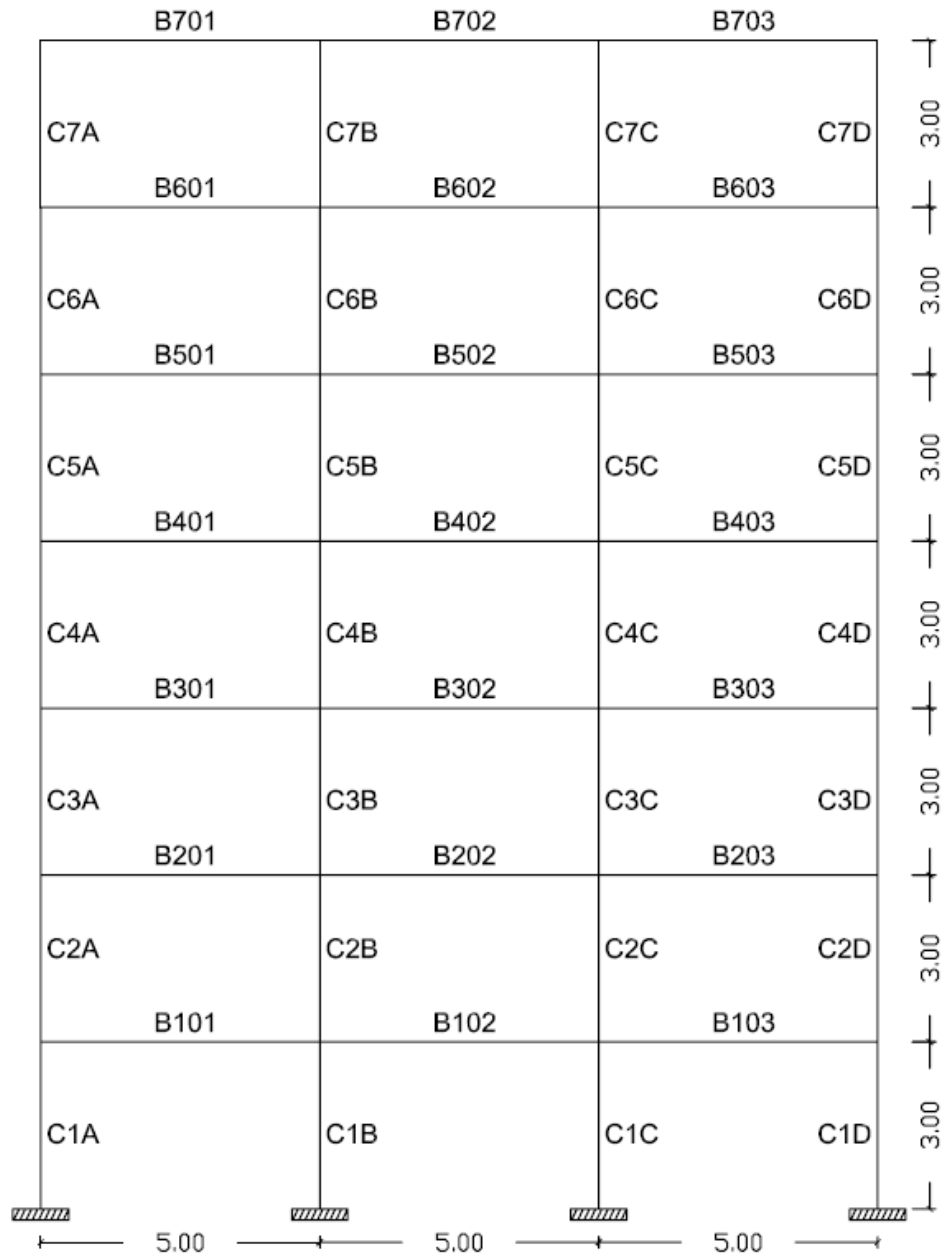


Figure A.15 Frame F15-7S3B

Table A.29 Column properties (F15-7S3B)

Column	Depth (cm)	Width (cm)	Reinf. Area (mm ²)
C1A	50	50	3161
C2A	50	50	2503
C3A	50	50	2503
C4A	45	45	2026
C5A	45	45	2026
C6A	40	40	1897
C7A	40	40	1600
C1B	50	50	2503
C2B	50	50	2503
C3B	50	50	2503
C4B	45	45	2026
C5B	45	45	2026
C6B	40	40	1600
C7B	40	40	1600
C1C	50	50	2503
C2C	50	50	2503
C3C	50	50	2503
C4C	45	45	2026
C5C	45	45	2026
C6C	40	40	1600
C7C	40	40	1600
C1D	50	50	3161
C2D	50	50	2503
C3D	50	50	2503
C4D	45	45	2026
C5D	45	45	2026
C6D	40	40	1897
C7D	40	40	1600

Table A.30 Beam properties (F15-7S3B)

Beam		Depth (cm)	Width (cm)	Bottom Reinf. (mm ²)	Top Reinf. (mm ²)
B101	LEFT	55	30	942	1632
	RIGHT	55	30	942	1581
B102	LEFT	55	30	942	1529
	RIGHT	55	30	942	1529
B103	LEFT	55	30	942	1581
	RIGHT	55	30	942	1632
B201	LEFT	55	30	942	1819
	RIGHT	55	30	942	1645
B202	LEFT	55	30	942	1677
	RIGHT	55	30	942	1677
B203	LEFT	55	30	942	1645
	RIGHT	55	30	942	1819
B301	LEFT	55	30	942	1768
	RIGHT	55	30	942	1542
B302	LEFT	55	30	942	1600
	RIGHT	55	30	942	1600
B303	LEFT	55	30	942	1542
	RIGHT	55	30	942	1768
B401	LEFT	50	30	845	1735
	RIGHT	50	30	845	1510
B402	LEFT	50	30	845	1594
	RIGHT	50	30	845	1594
B403	LEFT	50	30	845	1510
	RIGHT	50	30	845	1735
B501	LEFT	50	30	845	1523
	RIGHT	50	30	845	1310
B502	LEFT	50	30	845	1400
	RIGHT	50	30	845	1400
B503	LEFT	50	30	845	1310
	RIGHT	50	30	845	1523
B601	LEFT	50	30	794	1226
	RIGHT	50	30	671	1032
B602	LEFT	50	30	735	1142
	RIGHT	50	30	735	1142
B603	LEFT	50	30	671	1032
	RIGHT	50	30	794	1226
B701	LEFT	50	30	439	845
	RIGHT	50	30	477	845
B702	LEFT	50	30	523	845
	RIGHT	50	30	523	845
B703	LEFT	50	30	477	845
	RIGHT	50	30	439	845

A.16 F16-9S3B

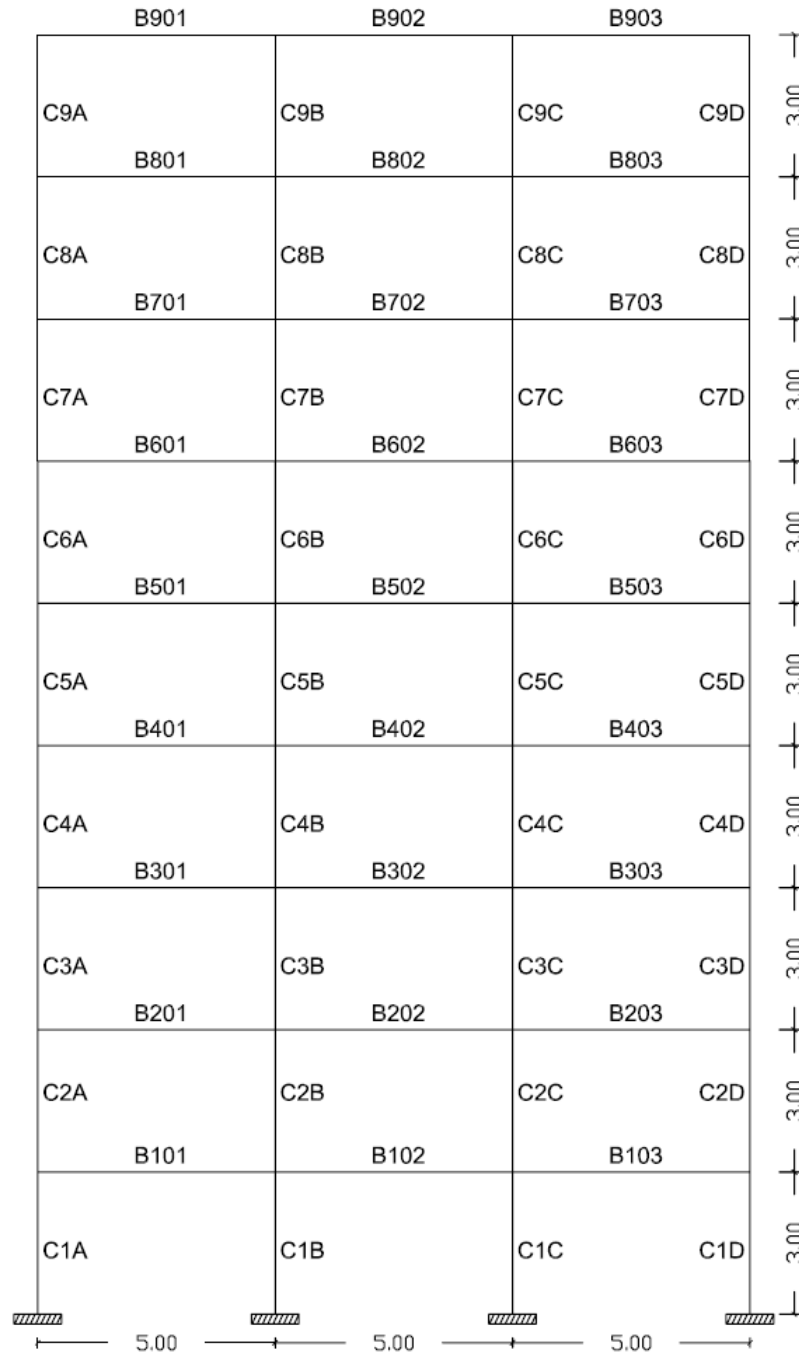


Figure A.16 Frame F16-9S3B

Table A.31 Column properties (F16-9S3B)

Column	Depth (cm)	Width (cm)	Reinf. Area (mm ²)
C1A	55	55	3026
C2A	55	55	3026
C3A	55	55	3026
C4A	50	50	2503
C5A	50	50	2503
C6A	50	50	2503
C7A	45	45	2026
C8A	45	45	2026
C9A	45	45	2026
C1B	55	55	3026
C2B	55	55	3026
C3B	55	55	3026
C4B	50	50	2503
C5B	50	50	2503
C6B	50	50	2503
C7B	45	45	2026
C8B	45	45	2026
C9B	45	45	2026
C1C	55	55	3026
C2C	55	55	3026
C3C	55	55	3026
C4C	50	50	2503
C5C	50	50	2503
C6C	50	50	2503
C7C	45	45	2026
C8C	45	45	2026
C9C	45	45	2026
C1D	55	55	3026
C2D	55	55	3026
C3D	55	55	3026
C4D	50	50	2503
C5D	50	50	2503
C6D	50	50	2503
C7D	45	45	2026
C8D	45	45	2026
C9D	45	45	2026

Table A.32 Beam properties (F16-9S3B)

Beam		Depth (cm)	Width (cm)	Bottom Reinf. (mm ²)	Top Reinf. (mm ²)
B101	LEFT	60	30	1032	1561
	RIGHT	60	30	1019	1477
B102	LEFT	60	30	948	1458
	RIGHT	60	30	948	1458
B103	LEFT	60	30	1019	1477
	RIGHT	60	30	1032	1561
B201	LEFT	60	30	1032	1800
	RIGHT	60	30	1032	1568
B202	LEFT	60	30	1032	1645
	RIGHT	60	30	1032	1645
B203	LEFT	60	30	1032	1568
	RIGHT	60	30	1032	1800
B301	LEFT	60	30	1032	1819
	RIGHT	60	30	1032	1510
B302	LEFT	60	30	1032	1619
	RIGHT	60	30	1032	1619
B303	LEFT	60	30	1032	1510
	RIGHT	60	30	1032	1819
B401	LEFT	55	30	942	1839
	RIGHT	55	30	942	1503
B402	LEFT	55	30	942	1658
	RIGHT	55	30	942	1658
B403	LEFT	55	30	942	1503
	RIGHT	55	30	942	1839
B501	LEFT	55	30	942	1761
	RIGHT	55	30	942	1361
B502	LEFT	55	30	942	1568
	RIGHT	55	30	942	1568
B503	LEFT	55	30	942	1361
	RIGHT	55	30	942	1761
B601	LEFT	55	30	942	1619
	RIGHT	55	30	865	1213
B602	LEFT	55	30	916	1419
	RIGHT	55	30	916	1419
B603	LEFT	55	30	865	1213
	RIGHT	55	30	942	1619
B701	LEFT	50	30	845	1490
	RIGHT	50	30	742	1148
B702	LEFT	50	30	845	1348
	RIGHT	50	30	845	1348
B703	LEFT	50	30	742	1148
	RIGHT	50	30	845	1490
B801	LEFT	50	30	813	1265
	RIGHT	50	30	574	877
B802	LEFT	50	30	723	1116
	RIGHT	50	30	723	1116
B803	LEFT	50	30	574	877
	RIGHT	50	30	813	1265
B901	LEFT	50	30	497	845
	RIGHT	50	30	419	845
B902	LEFT	50	30	516	845
	RIGHT	50	30	516	845
B903	LEFT	50	30	419	845
	RIGHT	50	30	497	845